A Coplanar Waveguide UWB Antenna With Notch Filter

by

Qianqian Wang
B.Eng., University of Victoria, 2012

A Thesis Submitted in Partial Fulfillment of the
Requirements for the Degree of

MASTER OF APPLIED SCIENCE

in the Department of Electrical and Computer Engineering
University of Victoria, British Columbia

A Coplanar Waveguide UWB Antenna With Notch Filter

by

Qianqian Wang
B.Eng., University of Victoria, 2012

Supervisory Committee

Dr. Jens Bornemann, Supervisor
(Department of Electrical and Computer Engineering)

Dr. Poman So, Departmental Member
(Department of Electrical and Computer Engineering)

ABSTRACT

Due to the release of 3.1-10.6 GHz band, UWB systems have a rapidly progressive development. They have been widely employed in short-range communication applications and large-bandwidth handheld devices. As part of the system, the UWB antenna plays an extremely important role. Due to the trend towards integrated printed circuits, co-planar waveguide technology is a feasible solution for designing the UWB antenna.

This thesis focuses on designing a UWB co-planar waveguide antenna with a band-stop filter. This band-stop filter offers rejection to unwanted frequencies in the range of the operating band in order to avoid unnecessary interference from other communication applications and improve its own systems performance. In addition, it can divide the whole wide band into a few sub-bands. This will create more flexibility for practical applications.

The professional full-wave field solver software package CST Microwave Studio is used as the analysis tool to obtain the performances of this antenna. It operates from 3.1 GHz to 10.6 GHz with a VSWR < 2 in the pass bands, and a VSWR > 2 in the stop bands. The selected frequencies demonstrate nearly omni-directional characteristics in radiation patterns. Comparing with other published UWB antenna designs, relatively reasonable group delay results are achieved. Measurements on a fabricated prototype validate the design approach.

Contents

List of Tables

List of Figures

List of Acronyms

AUT Antenna Under Test

BSF Band-stop Filter

CPW Co-planar Waveguide

CST Computer Simulation Technology

DBR Dual-behavior Resonator

DGB Defected Ground Plane

DSR Dual-spiral-shaped Slot Resonator

EBG Electromagnetic Band-gap

FCC Federal Communications Commission

HDTV High-definition TV

HIPERLAN High Performance Local Area Network

IEEE Institute of Electrical and Electronics Engineers

LPI Low Probability of Interception and Detection

MESFET Metal-semiconductor Field Effect Transistor

MMIC Monolithic Microwave Integrated Circuit

NBI Narrow-band Interferences

PC Personal Computer

PCB Printed Circuit Board

PDA Personal Digital Assistant

SIW Substrate Integrated Waveguide

SNR Signal-to-noise Ratio

STB Set-top Box

TEM Transverse ElectroMagnetic

UWB Ultra Wideband

VSWR Voltage Standing Wave Ratio

Wi-Fi Wireless Fidelity

WLAN Wireless Local Area Network

WPAN Wireless Personal Area Network

ACKNOWLEDGEMENTS

This thesis is the accomplishment of two years of research and experiment whereby I have been helped and supported by many people. Here and now, I am honored to express my appreciation to all of them.

The first person I would like to thank is my supervisor, Prof. Jens Bornemann. Under these years learning from Prof. Jens Bornemann, I have found he is knowledgeable, compassionate and friendly. I owe him a great deal of appreciation for his tireless guidance through the research, for his patience and support.

I would like to thank Farzaneh Taringou for her help in understanding CST simulation software and modeling of the proposed UWB antenna. Special thanks to Lisa Locke for being there when I needed her advice. I would also like to thank Mr. Ian Wood for performing CST simulation results on the proposed notch filter as part to confirm its validation. The work would not have been accomplished without the help from my fellow colleagues and friends. I appreciate them all for many discussions and having strong confidence in me.

Last, but not lease, my truehearted appreciation goes to my family for their caring, understanding and encouragement throughout my research.

Chapter 1

Introduction

The rapid development of modern telecommunication systems has dramatically increased the interest in enlarging the transmission bandwidth. As a result, components and systems for ultra wideband (UWB) technology have been performing a very imperative role in the telecommunication research community. Designing and testing a UWB application is at the forefront of research and development in this area. Within such a system, the UWB antenna is an important component because its transmitting and receiving properties are different from those for conventional narrowband operation. Many UWB antennas have been developed. TEM horns can be used for localized equipment, whereas printed-circuit antennas are more practical for mobile communication [1].

With the release of the 3.1-10.6 GHz band for UWB communication, a number of diversified UWB applications are invented, such as imaging systems, ground penetrating surveillance systems, vehicular radar systems, communications, and measurements systems, etc. Portable handhelds for short-range and large bandwidth communica-

tion will be involved in future UWB systems. The implementation of UWB antennas in printed-circuit technologies within a relatively small area is more than necessary. Nowadays, a variety of UWB antennas with either microstrip, e.g. [2]-[11] or coplanar waveguide feeds, e.g [12]-[27], and in combined technologies, e.g. [28][29] have been designed, mainly for the 3.1-10.6 GHz band, and for high frequency ranges, e.g. [30], and lower frequency ranges, e.g. [31], as well.

In addition, these UWB antennas need a band-rejection filter to avoid interference with existing wireless networks such as IEEE 802.11a in USA (5.15-5.35 GHz, 5.725-5.825 GHz) and HIPERLAN/2 in Europe (5.15-5.35 GHz, 5.47-5.725 GHz) [32]-[35]. To avoid adding new circuits to the communication system, band-notching techniques can be applied directly to various UWB planar antennas. One possibility is to load the UWB antenna with two SIW resonators in the ground plane, their center frequency being at the peak of the stop band.

1.1 Purpose of Thesis

Coplanar waveguide technology provides a great deal of advantages for the fabrication of printed-circuit UWB antennas. This technology only requires both the ground plane and antenna patch on the same side of the substrate, whereas microstrip technology applied to these antennas requires metallization patterns on both sides of the substrate. In this case, easier fabrication can be achieved with coplanar waveguide technology. Furthermore, UWB antennas with coplanar waveguide technology can provide wideband characteristics, and bidirectional radiation patterns similar to a microstrip feed.

The purpose of this thesis is to design a coplanar UWB antenna with a band-stop filter and use some commercially available electromagnetic field solvers to simulate this antenna's characteristics and performance. Through the design process, the finite-integration full wave solver CST Microwave Studio is employed for analysis purpose and for final optimization according to the voltage-standing wave ratio and radiation pattern behaviors. To validate the results, CST simulation results are analyzed first, and then a fabricated sample antenna is measured. It verifies that the simulated results agree well with the measured ones.

1.2 Contributions

The contributions of this research are twofold:

First, a new printed-circuit co-planar waveguide band-stop filter in substrate waveguide technology is presented. Its performance demonstrates that it is more suitable than other structures published so far.

Second, a printed-circuit UWB antenna in coplanar technology combined with a band-stop filter has a contribution of avoiding the interference from other wireless communication networks. It divides the entire band into multiple sub-bands. It makes this antenna application more practical than other designs published so far.

1.3 Thesis Overview

Chapter 2 of this thesis is an introduction to UWB development and provides basic knowledge about UWB antenna design. Every sub-section of Chapter 2 contains information based on one or two references. The major content is quite similar to these references, with changes only in wordings and phrases. This chapter introduces history and fundamentals of UWB technology. It offers background information and presents UWB applications.

Chapter 3 gives detailed information about research in different structures of a band-stop filter. And it shows the comparison of all simulated results of these structures. After these results are compared, it illustrates the reasons for choosing substrate integrated waveguide technology (SIW) for this band-stop filter. In addition, it provides the detailed mathematical calculation and design parameters of using SIW technology.

Chapter 4 presents a new printed-circuit UWB antenna in CPW technology combined with the above SIW band-stop filter. The first part shows the simulation results of this CPW UWB antenna alone in CST. Next, after the band-stop filter is integrated with the antenna, the entire antenna simulation results are presented. A comparison of the simulation results between the antenna alone and the combined application is demonstrated as well. Finally, experimental results demonstrate the validity of the design process.

Chapter 5 summarizes the most important accomplishments throughout the thesis.

Chapter 2

Fundamentals of Ultra Wideband Technology

Ultra Wideband technology has come to be realized since the 1960s. It is defined through utilizing carrier-free, impulse, baseband, time domain, nonsinusoidal and large-relative-bandwidth radio/radar signals. The benefits of carrier-free are that a transmitting signal does not need the analog modulating stage, and a receiving signal does not need the analog demodulating stage. Because of this, the mixing stage in a tranceiver is not necessary any more. This will reduce the design complexity of the analog circuit. The basic concept of developing ultra wideband is to transmit and receive a number of extremely short pulses at ultra low power, besides being extremely compact and inexpensive [36]. The duration of one pulse is typically a few tens of picoseconds to a few nanoseconds. These pulses represent one or a few cycles of an RF carrier waveform. As a result, the resulting waveforms can achieve extremely broadband signals. Due to the difficulty of determining the actual RF fundamental frequency for an extremely short pulse, the term carrier-free is used [37]. The FCC has

recently authorized Ultra-Wideband (UWB) communication between 3.1 GHz and 10.6 GHz; it has a bandwidth equal to or larger than 20% of the center frequency, or has a bandwidth equal to or greater than 500 MHz [38]. Moreover, it allows UWB devices to share the spectrum with existing radio services as long as emission restrictions, in the form of a spectral mask, are met. Its power spectral density emission limit for UWB transmitters is -41.3 dBm/MHz, equal to 75 nanowatts/MHz [39]. It indicates that the UWB signal provides very low power spectral density, which causes the maximum transmitting power to be a few milliwatts. It guarantees that these spectral power densities are well below a receiver noise level.

Advantages of UWB technology are:

- The FCC requires that the transmitting power for UWB systems is -41.3 dBm/MHz. It puts them in the category of unintentional radiators, such as TVs and computer monitors. This power limitation restricts UWB systems to stay below the noise floor of a typical narrowband receiver. With this regulation, UWB systems are able to coexist with current radio services with minimal or no interference [39].

- It provides a large bandwidth in UWB systems so that the channel capacity is improved. Channel capacity, or data rate in a digital system, is defined as the maximum amount of information being able to be transmitted per second over a communication channel. There is a channel capacity of a UWB system since Hartley-Shannon's capacity formula depends on the system's bandwidth. It is given by

$$C = B \cdot log_2(1 + SNR), \tag{2.1}$$

where C is the maximum channel capacity, B indicates the system bandwidth,

and the SNR is the signal-to-noise ratio. From the above equation, channel capacity linearly increases with the bandwidth. Since UWB signals occupy several gigahertz of bandwidth, it leads the data rate to be gigabits per second. This makes UWB systems a perfect candidate for short-range, high-data-rate wireless applications such as wireless personal area networks (WPANs) [39].

- Eqn 2.1 also shows that the channel capacity logarithmically depends on signal-to-noise ratio (SNR). It implies that UWB communications systems are able to work in harsh communication channels with low SNRs and still provide a large channel capacity due to their large bandwidth [39].

- Since UWB communications systems have low average power transmission, it is extremely difficult to detect and intercept their signals. Furthermore, UWB pulses are time modulated with unique codes for each transceiver pair. The time modulation of very narrow pulses makes UWB systems more secure to transmit because detecting a picosecond pulse, without knowing when it will come, is nearly impossible. Thus, UWB systems can achieve high security, low probability of interception and detection communications. This is a mandatory attribute for military operations [39].

2.1 Development of Ultra Wideband Technology and Antennas

2.1.1 History of Ultra Wideband Technology

In the late 1950's, an effort was made to develop a phased array radar system in the Lincoln Laboratory. This radar system employed two Butler Hybrid Phasing Matrices which were an interconnection of 3 dB branch line couplers to form a 2-N port network. Due to the demand of understanding the wideband properties of this network, studies were deployed to investigate the properties of the four-port interconnection of quarter-wave TEM-mode lines forming the branch line coupler. Such studies did not exist at that time. It began with the analysis of a general microwave 2-N port as a bi-conjugate network. The impulse response of this network was a pulse train and equally spaced [36]. From this point in time, ultra wideband (UWB) became a new branch of research in the field of time-domain electromagnetics [40]. At the same time, Oliver invented a sampling oscilloscope, and he used avalanche transistors and tunnel diodes to generate the short pulses [36]. The impulse response of the above networks could be monitored and measured. From this point, the development of short pulse radar and communications systems had begun. In the late 1960s, Ross and Robbins at the Sperry Research Center implemented a few radar and communication applications by using this impulse response method [41]. In 1973, the first UWB communications application was invented as a short-pulse receiver by Ross.

Through the late 1980s, this ultra wideband technology was named baseband, carrier-free or impulse generation technology until approximately 1989, when the U.S. Department of Defense announced it as "ultra wideband". By that time, the

UBW theory had existed for 30 years. Therefore, quite a few techniques and many applications about it had been developed. In addition, over 50 patents had been awarded to Sperry for his contributions in the fields of UWB pulse generation and reception methods, and applications such as communications, radar, automobile collision avoidance radar, positioning systems, liquid level sensing and altimetry [42].

Prior to 1994, researches and development in UWB technology, especially in the field of impulse communications, were regulated by the U.S. Government. Since 1994, the U.S. government loosened the classification restrictions on the UWB fields, so a number of works could be accomplished [42].

2.1.2 Development of Ultra Wideband Antenna

The first proposal of ultra-wideband antennas presented the idea of narrowband frequency domain radio. In 1898, the concept of "syntony" was introduced by Oliver Lodge. This idea was to tune a transmitter and a receiver to the same frequency in order to maximize the receiving signal [43]. Using this idea, he came up with a variety of "capacity areas", and these capacity areas were later called antennas. Lodge made a significant contribution in the antenna development because he invented spherical dipoles, square plate dipoles, bi-conical dipoles, and triangular or "bow-tie" dipoles. Figure 2.1 (a) shows Lodge's triangular bow-tie antenna, and Figure 2.1 (b) describes Lodge's fifth figure of a biconical antenna which is used in a transmitter-receiver link [1].

Since higher frequencies and shorter waves became more and more popular in the 1930s, Lodge's design was replaced by a "thin-wire" quarter-wave antenna. After television was invented, the research focused on its signal transmission. The interest in antennas with higher bandwidth, which could carry video signals, was increased [1].

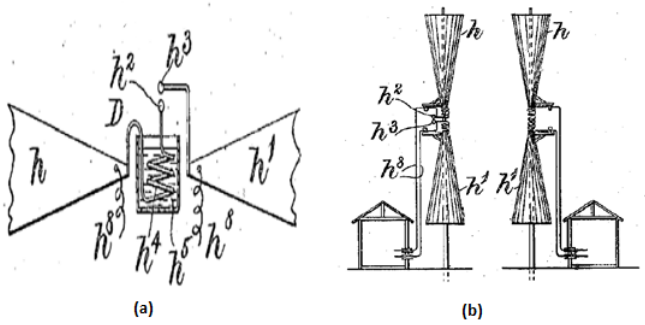

Figure 2.1: (a) Lodge's Triangular Bow-Tie Antenna [43] (b) Lodge's Bi-Conical Antenna [43]

Due to this interest, the bi-conical antenna in Figure 2.2 (a) and conical monopole in Figure 2.2 (b) were rediscovered by Carter in 1939 [44].

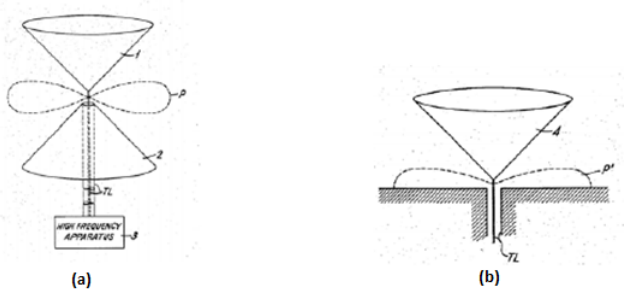

Figure 2.2: (a) Carter's Bi-Conical Antenna [44] (b) Carter's Conical Monopole [44]

He improved Lodge's original design by incorporating a tapered feed to his antennas [45]. A few years later, conical waveguides and feed structures in conjunction with a spherical dipole were invented by Schelkunoff (Figure 2.3). However, this design was not very practical and it was not turned into commercial usage [1].

In the 1930's, Lindenblad invented a coaxial horn element. Figure 2.4 (a) shows this element in cross-section. It was the most prominent UWB antenna at that period. He modified the idea of a sleeve dipole element by adding a gradual impedance transformation to make it more broad banded [1]. In addition, he used these horn elements to build a turnstile array (Figure 2.4 (b)) which was chosen for experiments in

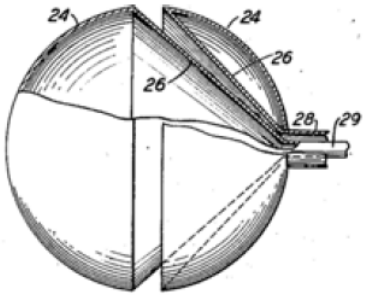

Figure 2.3: Schelkunoff's Spherical Dipole [1]

television transmission. This wideband antenna was quite a solution because multiple channels were required to broadcast at the same location. It was located at the top of the Empire State Building in New York City and used the folded dipoles to transmit the audio portion of the television signal [1].

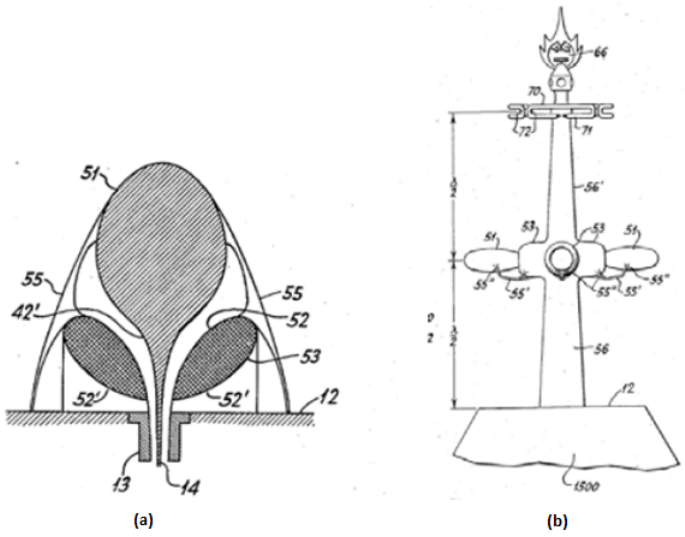

Figure 2.4: (a) Lindenblad's Element [1] (b) Lindenblad's Turnstile Array [1]

Furthermore, the concept of constructing antennas from coaxial transitions was developed by other researchers. Brillouin presented the idea of coaxial horns, both omni-directional in Figure 2.5 (a) and directional in Figure 2.5 (b) [46].

Other more traditional horn designs were invented at the same period of time.

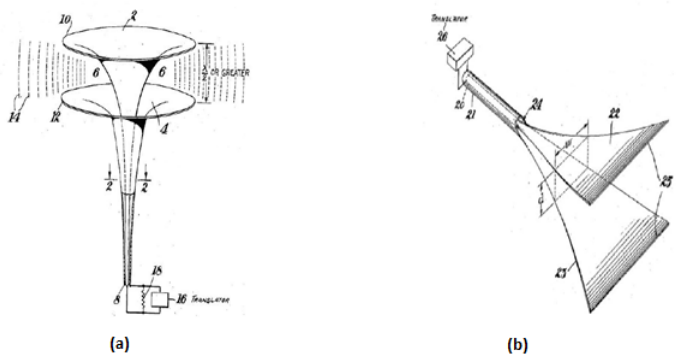

Figure 2.5: (a) Brillouin's Omni-Directional Coxial Horn [46] (b) Brillouin's Directional Coaxial Horn [46]

King developed a conical horn (Figure 2.6 (a)) and Katzin built a rectangular horn as shown Figure 2.6 (b) [47][48].

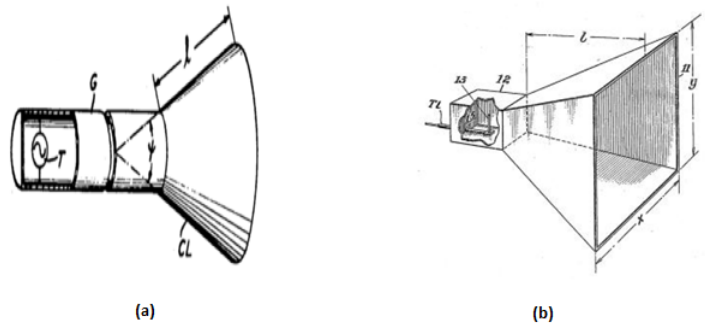

Figure 2.6: (a) King's Conical Horn [47] (b) Katzin's Rectangular Horn [48]

Even though these existing antennas provided outstanding performance, new design ideas continued to be investigated. Since broadband receivers were used commonly, antenna engineers focused more on inexpensive, easily fabricated designs. For example, Masters modified the triangular dipole design and built an inverted one which was called a "diamond dipole" later by antenna engineers (Figure 2.7) [49][50].

Recently, a variety of more sophisticated antennas has been developed. Stohr came up with the ellipsoidal monopoles (Figure 2.8 (a)) and dipoles (Figure 2.8 (b)) [51]. Later on, Lalezari invented a broadband notch antenna (Figure 2.9 (a)), and

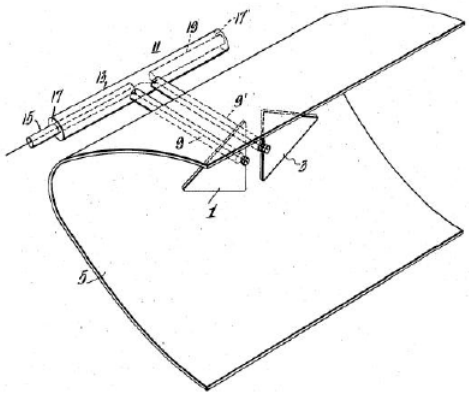

Figure 2.7: Master's Diamond Dipole [1]

Thomas et. al. developed a planar circular element dipole (Figure 2.9 (b)). The advantages of this antenna are that it is small in size, easily manufactured, and is easily placed in an array.

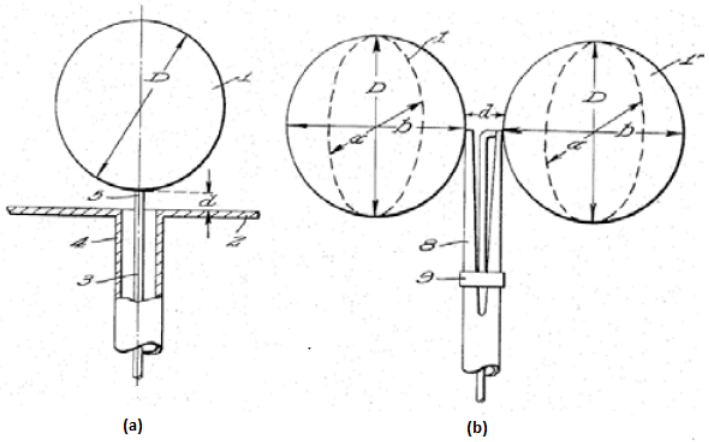

Figure 2.8: (a) Stohr's Ellipsoidal Monopole [1] (b) Stohr's Ellipsoidal Dipole [1]

Due to the new concept of magnetic UWB, which uses slot resonators, this type of antenna has been developed significantly. Marie built a modified slot antenna (Figure 2.10) by varying the width of the slot-line in order to improve its bandwidth.

Another improved magnetic antenna shown in Figure 2.11 was implemented by Harmuth, who used the concept of the large current radiator in his design [52]. Since

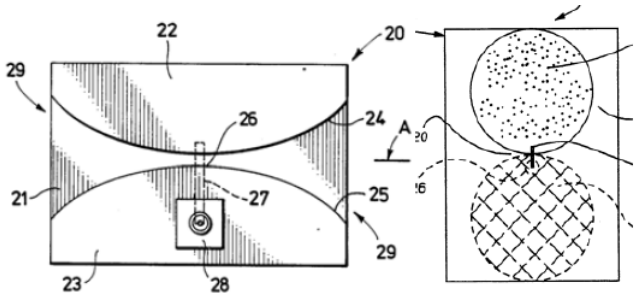

Figure 2.9: (a) Lalezaris' Broadband Notch Antenna [1] (b) Thomas et al's Circular Element Dipole [1]

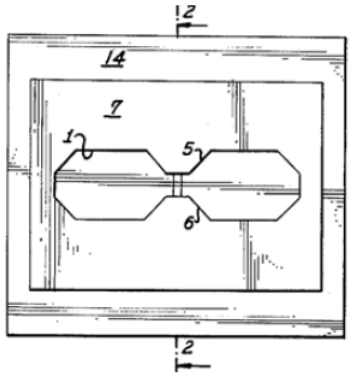

Figure 2.10: Marie's Wide Band Slot Antenna [1]

the radiation was from both sides of the antenna, a lossy ground plane was employed to confine undesired resonances [1]. However, by doing this, the efficiency and performance of large current radiators were confined. Pioneer researchers started trying different structures to achieve better performance. Barnes' UWB magnetic slot antenna (Figure 2.12) was one of the best designs. Since there was an appropriately chosen taper for the slot-line, it provided excellent broadband matching and performance. It was used in the first generation through-wall radar, the Radar Vision 1000 in The Time Domain Corporation [1].

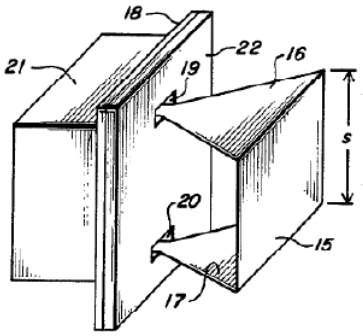

Figure 2.11: Harmuth's Large Current Radiator [1]

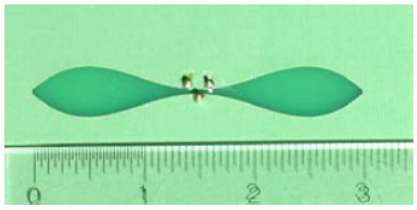

Figure 2.12: Barne's UWB Slot Antenna [1]

2.2 Ultra Wideband Antenna Design Principle

2.2.1 Antenna Definition

An antenna is a necessary part of any communication system. It converts guided electromagnetic energy in a transmission line to radiated electromagnetic energy in free space, as shown in Figure 2.13.

When an antenna works as part of a receiver, it collects incident electromagnetic waves and transforms them into signals. Furthermore, an antenna ideally picks up signals in a particular direction or frequency and suppresses the rest. As a result, the antenna should serve as a directional device. And according to design requirement, it should have different shapes, such as a piece of conducting wire, an aperture, a patch, a reflector, a lens, an assembly of elements and so on [54]. In addition, an antenna can be treated as an impedance transformer, which couples between an input or line

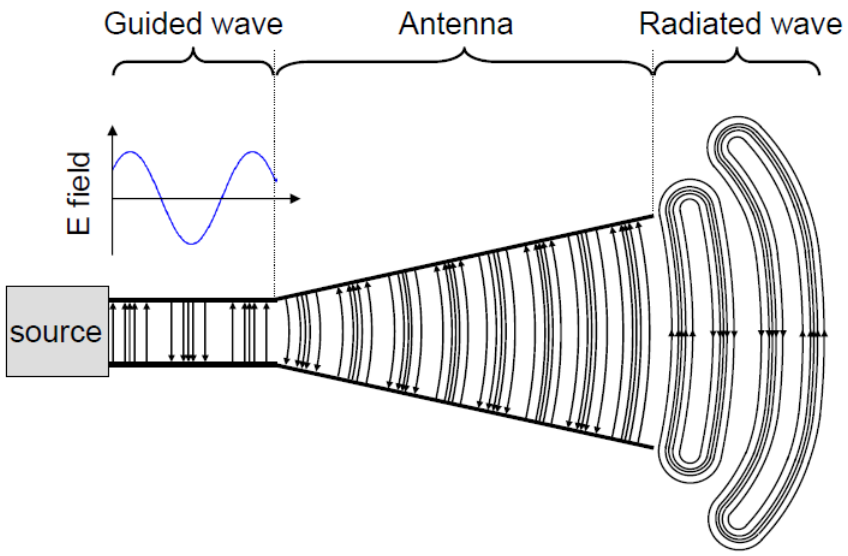

Figure 2.13: Antenna Principle [53]

impedance and the impedance of free space [55]. A sophisticated antenna design is able to meet the system specifications and improve overall performance.

2.2.2 Important Antenna Parameters

The performance and the characteristics of an antenna depend on a variety of parameters including radiation pattern, directivity, gain, input impedance etc.

1. *Radiation Pattern*

   Radiation pattern is a mathematical function or graphical representation of the radiation properties of an antenna. It can indicate the field strength and radiation intensity. It is always measured in the far-field region because the spatial distribution is independent on radial distance. The radiation pattern in the far-field region is a function of a particular position along the path or surface of constant radius and is represented as a two dimensional or three dimensional graph. Figure 2.14 demonstrates a radiation pattern example of a Hertzian

dipole, where θ and ϕ are two variables in the spherical co-ordinate system.

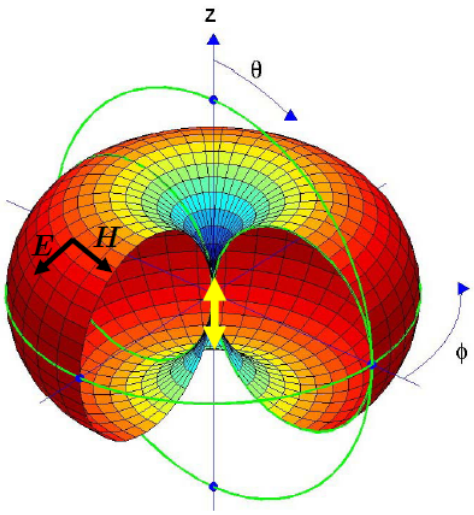

Figure 2.14: Antenna Radiation Pattern [53]

A few plots of variable θ and ϕ for a range of frequencies can provide all the field radiation information [54]. θ and ϕ are the directions of a spherical co-ordinate system. The relationship between a spherical co-ordinate system and a Cartesian co-ordinate system is illustrated in Figure 2.15 and given by

$$x = r \sin\theta \cos\phi, \tag{2.2a}$$

$$y = r \sin\theta \sin\phi, \tag{2.2b}$$

$$z = r \cos\theta. \tag{2.2c}$$

The major E-plane and H-plane patterns of an antenna indicate its behavior. In this thesis, the E-plane includes the electric-field vector in y-z plane of the spherical co-ordinate system in Figure 2.16 (a), whereas the H-plane includes the same field vector in the x-y plane in Figure 2.16 (b).

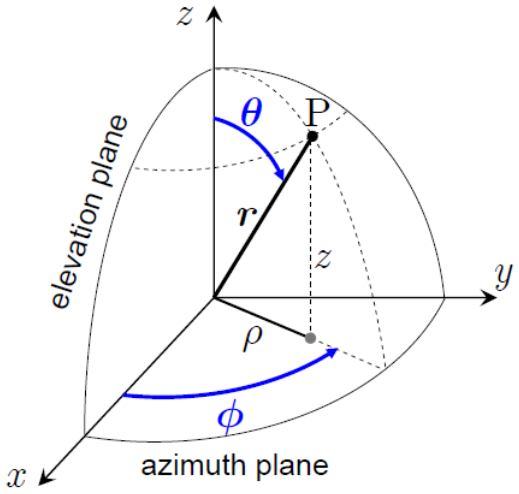

Figure 2.15: Co-ordinate System Transformation Between Cartesian and Spherical Coordinates [53]

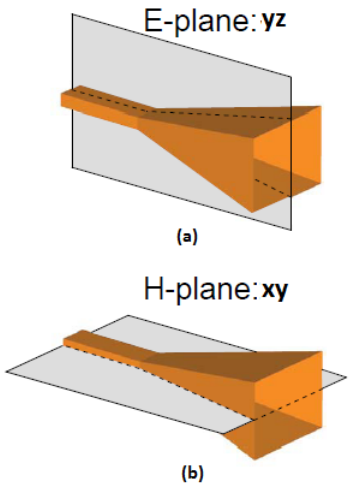

Figure 2.16: Radiation Plane [53]

There are three commonly used radiation patterns shown in Figure 2.17. They are isotropic, directional, and omnidirectional patterns. Note that the isotropic radiator is used only as the theoretical stardard to measure directivity in deciBel over isotropic (dBi).

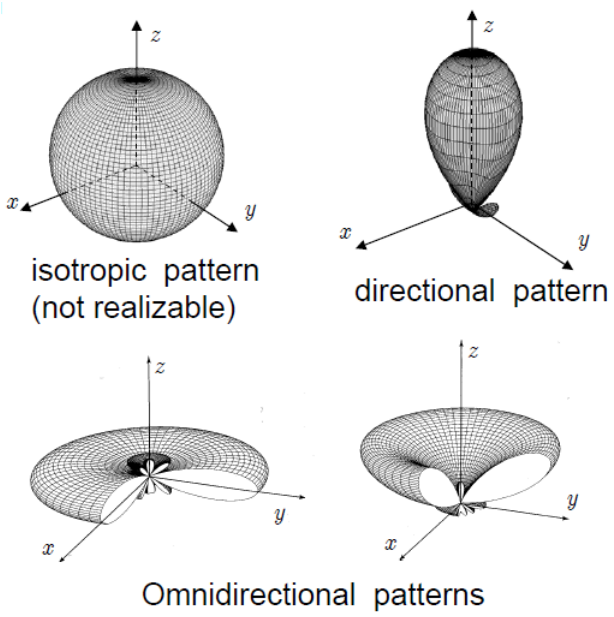

Figure 2.17: Common Radiation Patterns [53]

2. *Directivity*

   The directivity D is the ratio of the radiation intensity U in a given direction to the radiation intensity average U_0 over all directions (Figure 2.18). The directivity is given by

$$D(\theta, \phi) = \frac{U(\theta, \phi)}{U_0} = \frac{4\pi U(\theta, \phi)}{P_{rad}}, \tag{2.3}$$

   where P_{rad} is the radiated power.

3. *Gain*

   Antenna gain is defined as

$$G(\theta, \phi) = \frac{4\pi U(\theta, \phi)}{P_{in}} = \frac{4\pi U(\theta, \phi)}{P_{rad} + P_{loss}}, \tag{2.4}$$

   where P_{in} is the input power to the antenna of which only the radiated power

P_{rad} is radiated while P_{loss} is absorbed. In general, the overall efficiency of the antenna is given by

$$e_0 = e_{cd}(1 - |\Gamma|^2), \tag{2.5}$$

where e_{cd} is the antenna efficiency, and Γ is the reflection coefficient,

$$|\Gamma| = \frac{VSWR - 1}{VSWR + 1}, \tag{2.6}$$

where VSWR is the voltage standing wave ratio.

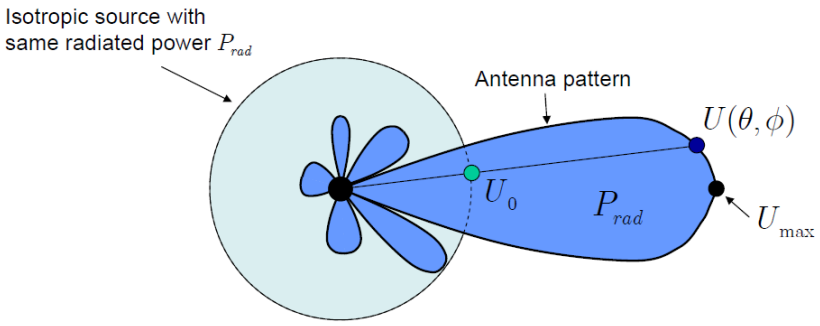

Figure 2.18: Antenna Directivity [53]

4. *Input Impdeance*

The input impedance of an antenna is presented at its terminals. The value of the input impedance is the ratio of the voltage and current across terminals a and b in Figure 2.19 (a) for the transmitting mode and Figure 2.19 (b) for the receiving mode.

It also can be written as

$$Z_A = R_A + jX_A = R_L + R_{rad} + jX_A, \tag{2.7}$$

where X_A is the antenna reactance, R_L is the loss resistance and R_{rad} is the

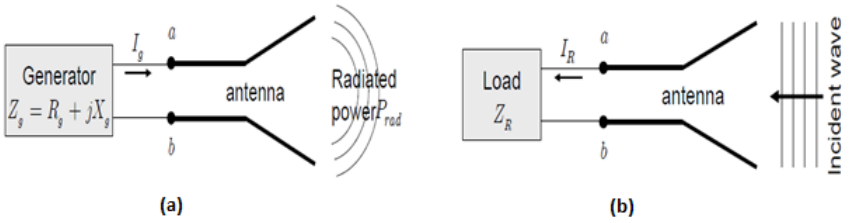

Figure 2.19: (a) Antenna Transmitting Mode (b) Antenna Receiving Mode [53]

radiation resistance. Therefore, the radiated power is defined as

$$P_{rad} = \frac{1}{2}|I_g|^2 R_{rad}. \tag{2.8}$$

Conjugate impedance matching is required to yield the maximum power for transmitting and receiving. According to the Thevenin equivalent circuit for the transmitting mode in Figure 2.19 (a), the conjugate impedance matching is

$$R_{rad} + R_L = R_g, \tag{2.9a}$$

$$X_A = -X_g. \tag{2.9b}$$

Then the maximum power delivered to the antenna is

$$P_g = P_{rad} + P_L = \frac{|V_g^2|}{8R_g}, \tag{2.10a}$$

$$P_{rad} = \frac{|V_g|^2}{8}\frac{R_{rad}}{(R_{rad} + R_L)^2}, \tag{2.10b}$$

$$P_L = \frac{|V_g|^2}{8}\frac{R_L}{(R_{rad} + R_L)^2}. \tag{2.10c}$$

Moreover, according to the Thevenin equivalent circuit for the receiving mode

in 2.19 (b), the conjugate impedance matching is

$$R_{rad} + R_L = R_R, \tag{2.11a}$$

$$X_A = -X_R. \tag{2.11b}$$

The maximum power received at the load of the antenna is

$$P_R = \frac{|V_R|^2}{2}|\frac{R_R}{4(R_{rad}+R_L)^2}| = \frac{|V_R|^2}{8}|\frac{1}{R_{rad}+R_L}| = \frac{|V_R|^2}{8R_R}, \tag{2.12a}$$

$$P_{rad} = \frac{|V_g|^2}{8}\frac{R_{rad}}{(R_{rad}+R_L)^2}, \tag{2.12b}$$

$$P_L = \frac{|V_g|^2}{8}\frac{R_L}{(R_{rad}+R_L)^2}. \tag{2.12c}$$

2.2.3 Requirements of Ultra Wideband Antennas

UWB communication techniques have received a great amount of attention from both academia and industry in the past few years because of the high merit of their advantages. All wireless systems and applications including UWB designs need a means of transferring energy or signals from the apparatus, which is an antenna, to free space in the form of electromagnetic waves or vice versa. An antenna has been recognized as a critical element of a successful design of any wireless device since wireless systems are highly dependent on their antenna characteristics. Based on that, UWB antennas have become an important and active area of research and have presented antenna engineers with major design challenges [56]. Antennas play crucial roles in either conventional wireless or UWB wireless systems. Due to the strong commercial demand of ultra-wideband systems, their antenna designs have

been regaining interest in recent years. However, designing a UWB antenna presents more challenges than designing a conventional one because a UWB antenna is required to receive all frequencies in the wide band at the same time. As a result, the behavior and performance of a UWB antenna should be consistent and predictable across the entire bandwidth [55].

The main challenge is the extremely wide bandwidth. A UWB antenna is fundamentally different from a narrow band antenna since its frequency bandwidth is ultra wide. The FCC requires a UWB antenna to be capable of providing an absolute wide frequency band of at least 500MHz. It should perform consistently across the entire frequency bandwidth. This requires that the antenna radiation pattern, gain and impedance matching must be stable over the whole bandwidth [54]. In some cases, since other narrow band devices and services occupy a portion of this ultra wide band, a UWB antenna should be able to yield the band-rejection features to prevent the interference from those devices and services [57][58].

The second challenge is that the directivity of an antenna is either directional or omni-directional, depending on application. If it is a mobile or a hand-held device, an omni-directional radiation pattern is required. On the other hand, if it is a radar system or a high gain directional system, a directional radiation pattern is required [54].

The third challenge is the size of a UWB antenna. Due to the usage of a suitable antenna in a mobile or a portable device, it must be compatable with integration on a printed circuit board (PCB).

The fourth challenge is to achieve good time domain performance for a UWB antenna. Unlike a conventional system transmitting information by a carrier wave, a UWB system directly employs extremely short pulses for data transmission. In other

words, the ultra-wide frequency band should be occupied [54]. Due to this enormous operating bandwidth, a crucial impact on the transmitted and received waveforms is imposed by the UWB antenna. A good time domain performance, such as minimizing pulse distortion, is a primary requirement of a suitable UWB antenna because the signal waveform is the carrier of useful data information [54].

2.3 Ultra Wideband Applications

Ultra wideband technology, well-known for its high data throughput, low probability of interception and detection, multipath immunity, precision ranging and location, has been considered for a diversity of applications which include both wireless communications and radar systems [42].

First, UWB technology provides a solution for the band-width, cost, power consumption, and physical size requirements for consumer electronic devices. By using this technology, Personal Computers (PCs) are able to connect to all their wireless PC peripherals such as personal digital recorders, MP3 recorders and players, digital cameras, etc., as seen in Figure 2.20.

Second, with UWB technology, high-definition TVs (HDTVs), set-top boxes (STBs), gaming systems, personal digital assistants (PDAs), and cell phones are able to connect to each other in a wireless personal area network (WPAN) in a digital home as shown in Figure 2.21.

Third, due to the high data rate characteristic, UWB systems are able to collect, propagate or exchange information in a very short time period. As a result, higher accuracy for short-range UWB positioning and tracking systems can be achieved. For example, with the advanced tracking mechanism in [42], precisely determining

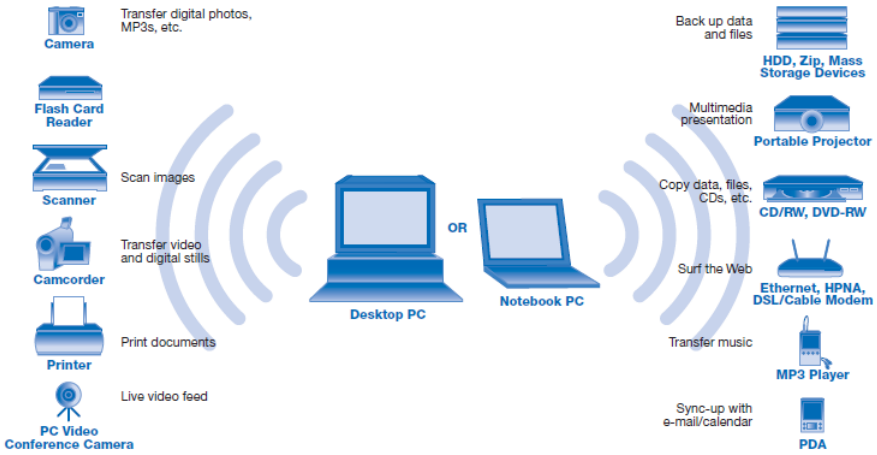

Figure 2.20: PC and Its Peraphicals (c.f.Appendix)

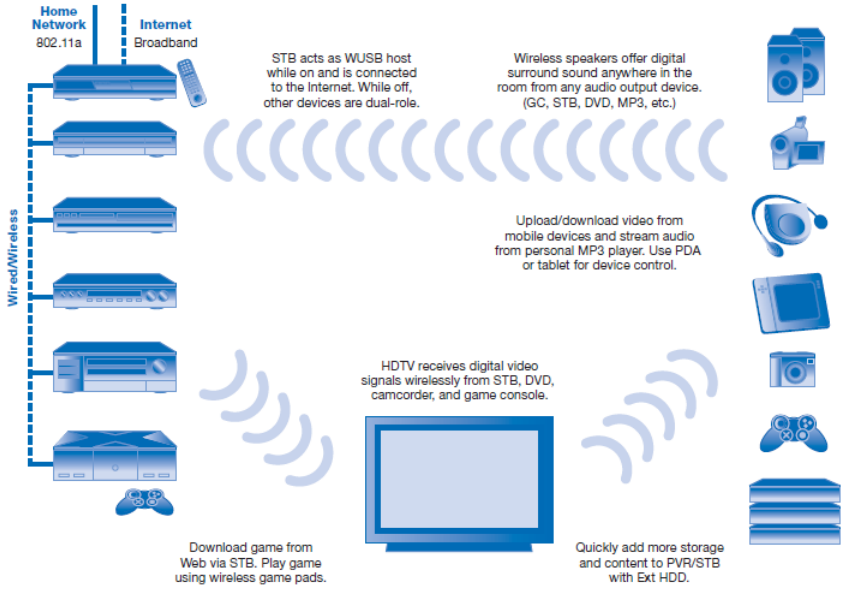

Figure 2.21: WPAN (c.f.Appendix)

the position of a moving object in a short-range environment can be accomplished within an accuracy of a few centimeters [54]. In addition, UWB sensors as that in [42] for indoor asset tracking have thrived in commercial systems [59].

Fourth, numerous UWB sensors can compose a large sensor network within a geographical area. These sensors can be either static or carried by a moving body.

When they are applied for securing homes, tracking and monitoring, or mobile, these sensors can be installed on soldiers, firemen, automobiles, or robots in military and emergency response situations [60]. UWB systems have operated in a variety of difficult situations in order to provide faster and more accurate communications. For example, they are used to search for people or objects in a collapsed building after an earthquake, children lost in a playground, injured athletes in remote places, fire fighters in a burning building and so on [54].

Fifth, UWB applications also include radar systems. It was originally applied in military services and later for commercial usage. For example, the Hummingbird system is a radar application for the U.S. Naval Air Systems Command and is shown in [42]. It utilizes the high data rate characteristic to determine the altitude precisely, and avoid collision [42].

Another application of short range radar operating in the X-band region of the spectrum is also presented in [42]. This radar was deployed for the U.S. Army Missile Command as a low probability of interception and detection (LPI/D), anti-jam, radar proximity sensor for caliber, small caliber and submunition applications. This system has a center frequency of 10 GHz with a 2.5 GHz operating band. This application was specially designed for short range (less than 6 feet), and the resolution distance of these UWB sensors was 6 inches. Due to its average output power of less than 85 nanowatts, this radar was capable of detecting a -4 dB per m^2 target in a range of approximately 15 feet with a small, micro-strip patch antenna [42]. The usage of UWB is everywhere, such as mobile phones, medical applications, satellite communications, etc.

Chapter 3

Coplanar Waveguide Notch Filters

3.1 Introduction to CPW Technology

The CPW was invented by Wen in 1969 [65]. This structure includes a strip of metallic film deposited on the top of a dielectric substrate with two ground planes at each side of the strip as shown in Figure 3.1. The original idea was that the thickness of the substrate be infinite. However, that cannot be practically implemented. Thus, the thickness of the substrate becomes finite and needs to be large enough so that all the electric and magnetic fields can taper to zero inside the substrate. In addition, the width of the ground plane should be as small as possible if the CPW is mounted in monolithic microwave integrated circuits (MMICs).

The electric and magnetic field distribution of the CPW structure are shown in Figure 3.2. It demonstrates that not all the fields are contained in the dielectric substrate. Some of them are in the substrate, and the others are in open air. It causes the analysis of the CPW structure to be quasi-static. The full-wave analysis of the CPW is involved to investigate the phase velocity and characteristic impedance

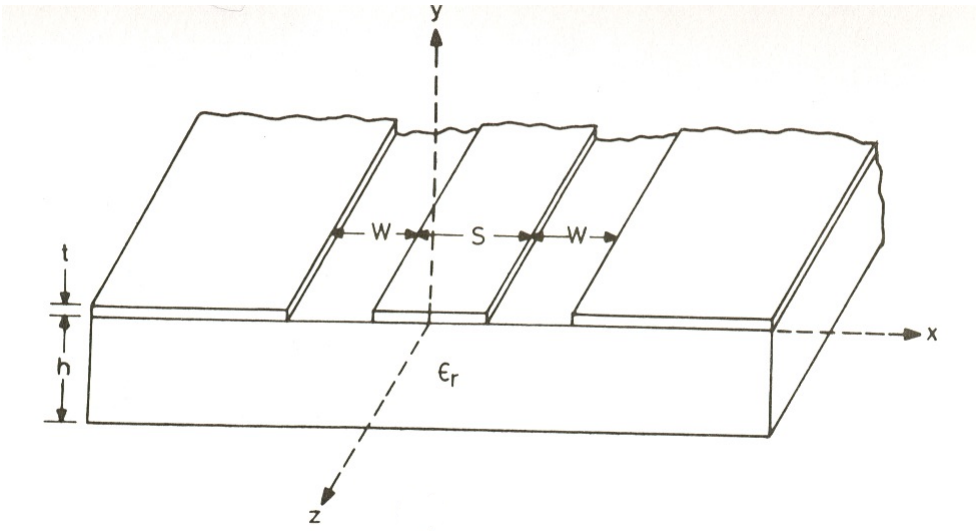

Figure 3.1: General CPW Structure [65]

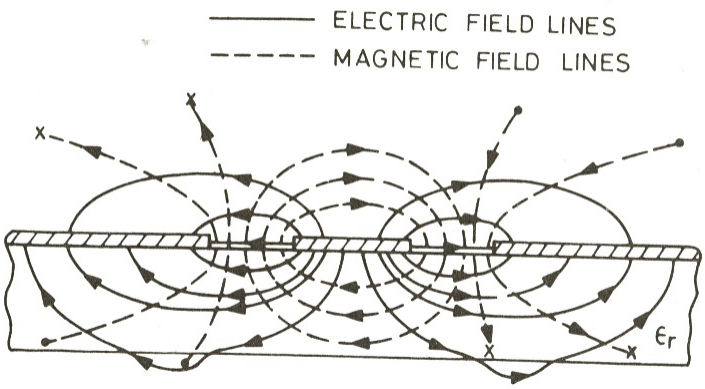

Figure 3.2: Electric and Magnetic Fields in CPW [65]

associated with frequencies. The quasi-static formulas for calculating the effective dielectric constant (ε_{re}), the phase velocity (υ_{ph}), and the characteristic impedance (Z_{0cp}) are given by [65]

$$\varepsilon_{re} = 1 + \frac{\varepsilon_r - 1}{2} \frac{K(k_4)}{K'(k_4)} \frac{K'(k_3)}{K(k_3)}, \tag{3.1a}$$

$$\upsilon_{ph} = \frac{c}{\sqrt{\varepsilon_{re}}}, \tag{3.1b}$$

$$Z_{0cp} = \frac{30\pi}{\sqrt{\varepsilon_{re}}} \frac{K'(k_3)}{K(k_3)}, \tag{3.1c}$$

where

$$\frac{K(k)}{K'(k)} = \begin{cases} \frac{\pi}{ln[\frac{2(1+\sqrt{k})}{(1-\sqrt{k})}]} & \text{for } 0 \leq \text{k} \leq 0.707 \\ \frac{1}{\pi} ln[\frac{2(1+\sqrt{k})}{(1-\sqrt{k})}] & \text{for } 0.707 \leq \text{k} \leq 1 \end{cases}, \tag{3.2a}$$

$$k_3 = \frac{a}{b} \sqrt{\frac{1 - \frac{b^2}{c_0^2}}{1 - \frac{a^2}{c_0^2}}}, \tag{3.2b}$$

$$k_4 = \frac{sinh(\frac{\pi a}{2h})}{sinh(\frac{\pi b}{2h})} \sqrt{\frac{1 - \frac{sinh^2(\frac{\pi b}{2h})}{sinh^2(\frac{\pi c_0}{2h})}}{1 - \frac{sinh^2(\frac{\pi a}{2h})}{sinh^2(\frac{\pi c_0}{2h})}}}, \tag{3.2c}$$

and a, b, c_0 and h are depicted in Figure 3.3.

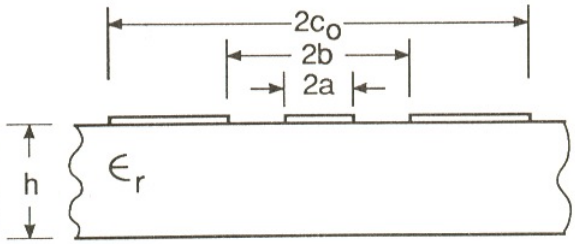

Figure 3.3: Cross-section Dimensions of The CPW Structure [65]

There are quite a few advantages to using CPW technology. First, from the circuit isolation perspective, this technology provides good isolation because there is always RF ground between metal traces. Second, since all metal layers are in the same plane, it saves time and expenses to only process one side of the substrate. Third, the CPW structure can be easily connected to active elements such as MESFETs because they are all coplanar in nature [65]. In comparison, microstrip technology requires metalic planes on both sides of the substrate. This causes difficulty for surface mounting of components. In addition, a larger portion of the field in microstrip technology is

contained in the substrate which causes increased losses. With these advantages, the antenna in this thesis adopts the CPW structure.

3.2 Introduction to Coplanar Waveguide Notch Filters

A UWB wireless system employs signals with a bandwidth spectrum of 3.1-10.6 GHz and transmits the signal at a high transmission speed of 100-480 Mbps. It enables transmission at a higher speed than conventional WLAN such as Wi-Fi at a speed of 54 Mbps. Due to the characteristic of low energy per pulse, UWB systems are subject to high level narrow-band interferences (NBI) even though UWB systems may enjoy a high spreading gain due to the large bandwidths. Specially, IEEE 802.11a systems operate around 5 GHz, which overlap the band of UWB signals regulated by the FCC, and will bring significant interference to UWB systems. If such interference is not suppressed properly, the UWB receiver will not function well. Thus, it is necessary to employ a band-stop filter to offer rejection ability in a band from 5 to 6 GHz. One solution to this specification is to design a notch filter after the receiving antenna to provide an appropriate rejection at the required frequency range [61]. There are numerous types of notch filters attached to antenna structures in modern wireless communication systems. However, the trend of designing such a filter and antenna is to utilize a planar waveguide structure in the UWB system because this filter in combination with this antenna should be small enough to build on small, low-profile integrated circuits in order to be compatible with portable electronic devices. The purpose of a planar design is to miniaturize the volume of the UWB antenna and filter. Furthermore, its two dimensional (2D) geometry makes the fabrication relatively easy.

As a result, Coplanar Waveguide (CPW) technology, as a kind of planar transmission line technology, is a good candidate for this design due to its high merits of low cost, compact-size, light weight, planar structure and easy integration with other components on a single printed circuit board [56]. This chapter focuses on research of a few CPW notch filter structures.

3.3 Notch Filter Structures in CPW

There are enormous numbers of topologies for designing fixed notch filters, such as open-circuit quarter-wavelength stubs, short-circuit half-wavelength stubs, and coupled resonators [62]. Due to the dimension requirement, different structures of a notch filter are designed. A few of these structures are researched because they are compact, inexpensive, and easy to fabricate. The following criteria are deemed acceptable for a reasonable notch filter in this application. The maxium attenuation at the notch peak should be greater than 20 dB, the 3 dB bandwidth of the filter should be less than 1 GHz, and it needs to be compatible with CPW technology.

3.3.1 Bent Resonators in the Ground Plane

This structure exploits bent resonators in the ground plane to notch off certain frequency bands in order to provide the characteristics of a band-reject filter. Two types of slot-line structures can be considered as these resonators.

One structure is to make one end of the slot-line open in the ground plane. According to transmission line theory, if one end of the line is open, the lengths of the resonators should be quarter-wavelength at the center frequency of the stop-band. These resonators are capacitively coupled to the main patch (Figure 3.4) [63].

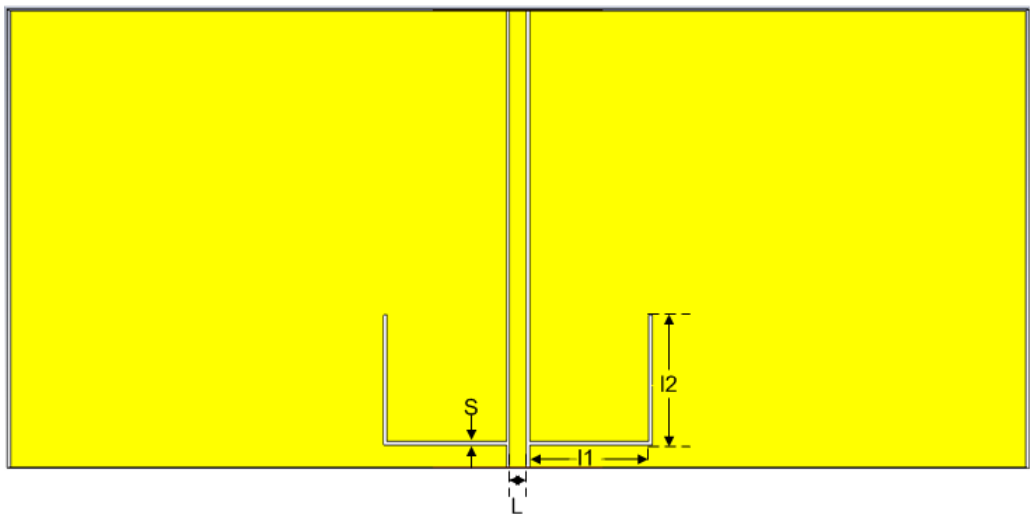

Figure 3.4: Bend Resonators With Open Structure

The length (l_1 and l_2) of each section is one eighth of the effective wavelength at 5 GHz. Two of them connecting like an L shape form a bent resonator. The substrate used here is RT/Duroid 6002 ($\varepsilon_r = 2.94$). The dimensions of L and S are 0.7 mm and 0.2 mm, respectively. This leads to a characteristic impedance of Z_0 equal 70.8 Ω. The effective wavelength λ_{eff} is given as

$$\lambda_{eff} = \frac{\lambda_{free}}{\sqrt{\varepsilon_{re}}} = \frac{c}{f_{center}\sqrt{\varepsilon_{re}}}, \tag{3.3}$$

where c is the speed of light in free space, f_{center} is the center frequency of the stop band, and ε_{re} is the substrate effective relative permittivity at this center frequency. The value of ε_{re} can be found from the CST simulation plot shown in Figure 3.5.

After λ_{eff} is found, l_1 and l_2 can be calculated. At this point, all the dimensions of this filter are available. It is designed and simulated with the full wave solver CST Microwave Studio whose time-domain option is better suited for UWB analysis than the frequency domain solver HFSS. Its frequency response is shown in Figure 3.6.

This figure demonstrates the S-parameter values across a frequency range of 0-

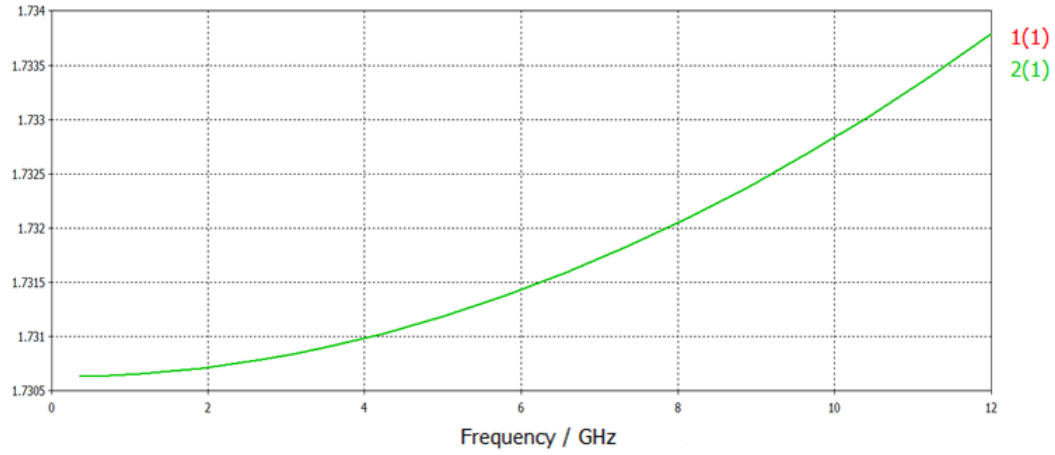

Figure 3.5: Effective Permittivity for The Bend Resonator With Open Structure

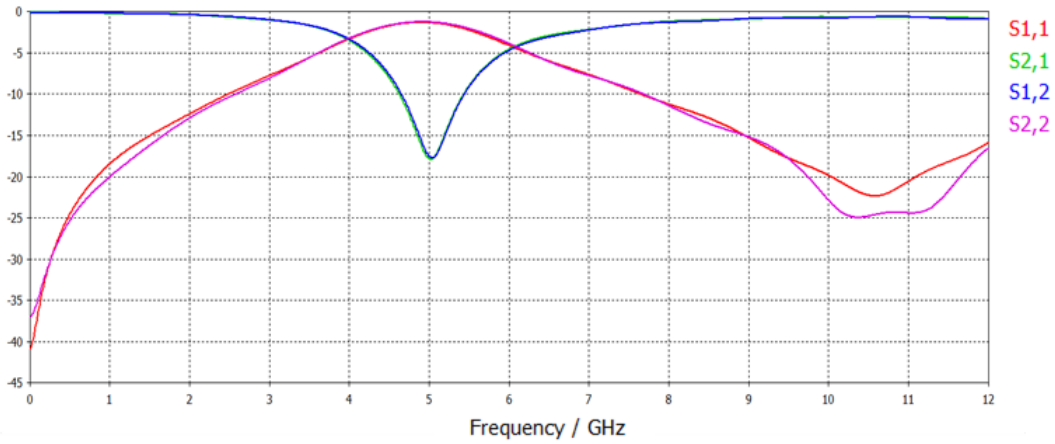

Figure 3.6: Frequency Response for The Bend Resonator With Open Structure

12 GHz. It has the deepest frequency notch at about 5 GHz. It proves that these two resonators function as a notch filter according to the theory. However, the 3 dB bandwidth is about 2 GHz, which is too wide for a narrow stop band. In addition, the insertion loss S_{21} and S_{12} are less than 20 dB at the center frequency. It does not provide a sharp notch performance. Hence, this structure is not practical for a filter which can offer a sharp narrow stop-band performance. The difference for S_{21} and S_{12} in Figure 3.6 is due to the fact that the structure is not symmetric horizontally, the meshing cells cannot be equally distributed in the structure for the simulation.

The other structure is to make both ends of the slot-line short in the ground plane. According to transmission line theory, if both ends of the line are short, the resonator lengths should be half-wavelength at the center frequency of the stop-band. These resonators are inductively coupled to the main patch (Figure 3.7).

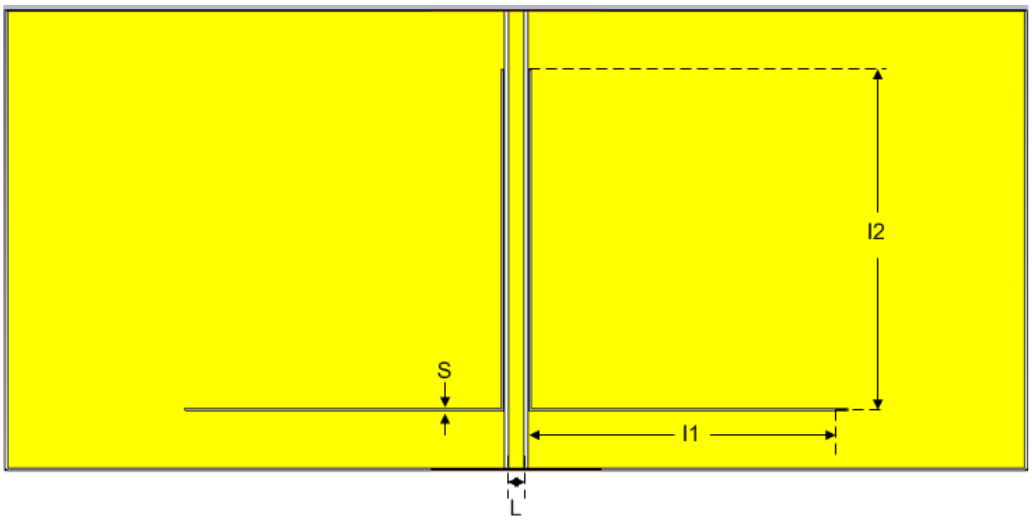

Figure 3.7: Bend Resonators With Short Structure

The two vertical stubs should be as close as possible to the slot lines in order to get the maximum inductive coupling. However, this distance is limited by fabrication parameters. The minimum allowed distance is 150 μm. The length (l_1 and l_2) of each stub for the resonator is a quarter of the effective wavelength at the notched center frequency. The way to calculate this effective wavelength is exactly the same as the one for the open stub structure. This filter is also designed and simulated with CST. Its frequency response is shown in Figure 3.8.

Even though the 3 dB bandwidth of this notched filter is improved dramatically, the S_{21} and S_{12} parameters become worse, and are even above -10 dB. As a result, it does not perform like a sharp notch filter. The difference for S_{21} and S_{12} in Figure

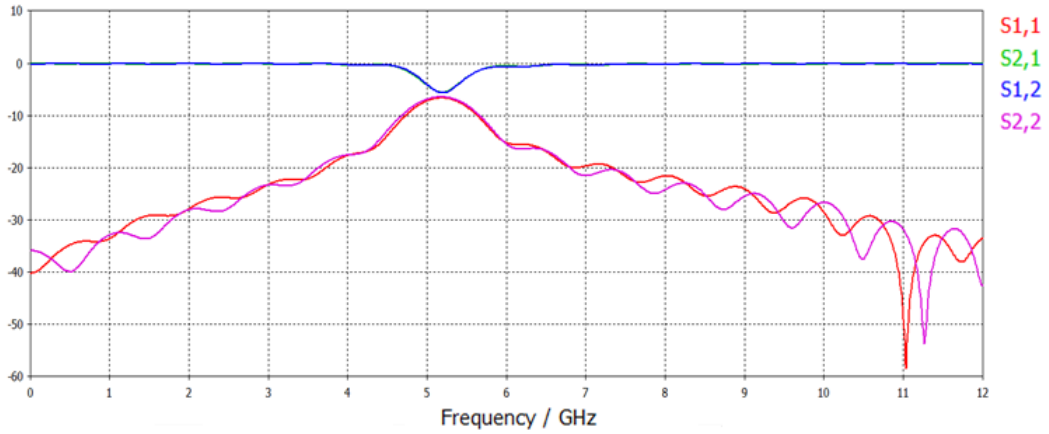

Figure 3.8: Frequency Response for The Bend Resonator With Short Structure

3.8 is due to the fact that the structure is not symmetric horizontally, the meshing cells cannot be equally distributed in the structure for the simulation. In conclusion, since these two structures are limited by the fabrication constraints of minimum 200 μm slotwidth, they do not provide a sharp notch and narrow 3 dB bandwidth.

3.3.2 Dual-Behavior Resonators in the Ground Plane

Dual-behavior resonators are based on open-ended stubs in parallel, building on a transmission line configuration shown in Figure 3.9. Each stub provides its own transmission zero depending on its basic resonant condition (Figure 3.10) [64].

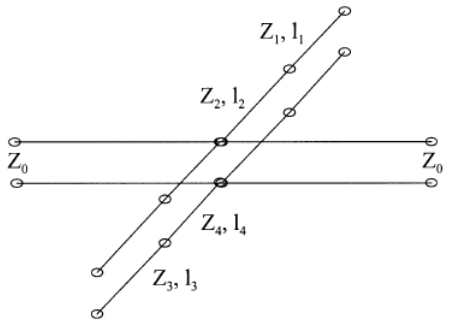

Figure 3.9: Ideal Transmission-line Scheme [64]

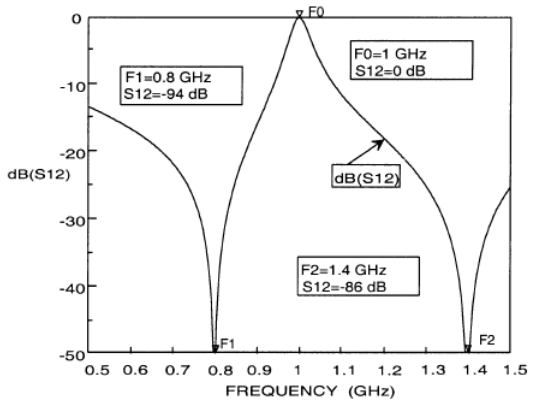

Figure 3.10: Transmission Zeros in DBR Structure [64]

This open-ended stub structure leads the transmission zeros to appear at frequencies for which length l associates with an odd multiple of a quarter wavelength at this frequency. At each branch, the stub can be decomposed into two cascaded transmission lines with different characteristic impedances [64]. The location of transmission zeros can be controlled by modifying those characteristic impedances. For example, the first transmission zero location can be controlled by adjusting the impedance ratio Γ in order to shift its location to either the positive side or the negative side of the center frequency. This impedance ratio Γ is given as

$$\Gamma = \frac{Z_{first\_section\_line}}{Z_{second\_section\_line}}. \tag{3.4}$$

If $\Gamma < 1$, then the frequency related to the transmission zero should shift to the right side of the center frequency. Otherwise, the frequency should shift to the left side of the center frequency [64].

Due to the S-parameter characteristics showing two transmission zeros in Figure 3.10, this method might be adopted to the coplanar waveguide structure when all open-ended stubs can be replaced by slot-lines (Figure 3.11).

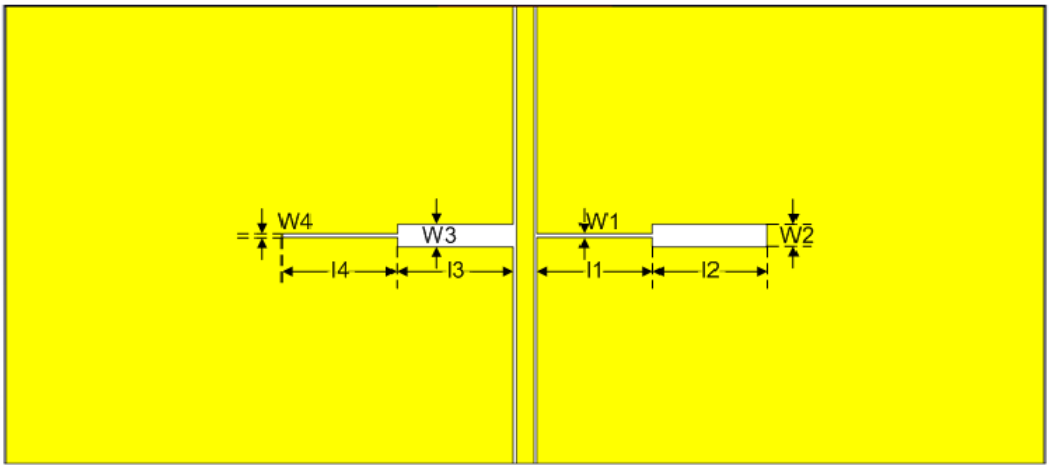

Figure 3.11: DBR Technology in CPW Structure

It shows two slot-lines in the ground plane acting like the open-ended stubs of the DBR structure. The widths (W_1 and W_3) of the narrower slot-line are 0.15 mm, and the wider ones (W_2 and W_4) are 1 mm. And the length (l_1, l_2, l_3 and l_4) of each slot-line is 1/8 of the wavelength at the center frequency of 5 GHz. The formula to calculate the slot-line impedance is given as [65]

$$\begin{aligned} Z_{0s} = 60 + 3.69sin[\frac{(\varepsilon_r - 2.22)\pi}{2.36}] + 133.5ln(10\varepsilon_r)\sqrt{\frac{w}{\lambda_0}} \\ +2.81[1 - 0.011\varepsilon_r(4.48 + ln\varepsilon_r)]\frac{w}{h}ln(\frac{100h}{\lambda_0}) \\ +131.1(1.028 - ln\varepsilon_r)\sqrt{\frac{h}{\lambda_0}} + 12.48(1 + 0.18ln\varepsilon_r) \\ \frac{\frac{w}{h}}{\sqrt{\varepsilon_r - 2.06 + 0.85(\frac{w}{h})^2}}, \end{aligned} \tag{3.5}$$

where w is the slot-line width, h is the substrate height, ε_r is the substrate permittivity, and λ_0 is the wavelength in free space for the center frequency. The impedance of these two slot-lines can be calculated with this formula. The narrower one is 94.197 Ω, and the wider one is 147.903 Ω. Therefore, the impedance ratio of the right side slot-line shown in Figure 3.11 is $\Gamma = \frac{94.197}{147.903} = 0.637 < 1$.

The frequency associated with this transmission zero should shift to the right side of the center frequency. And the left side of the overall slot-line has an impedance ratio greater than 1, so the frequency at this transmission zero should shift to the left side of the center frequency. However, the S parameter simulation results shown in Figure 3.12 do not show those two transmission zeros. The only transmission zero is at the center frequency of 5 GHz. Moreover, this transmission zero does not create a sharp notch. It only creates about 10 dB attenuation which is not efficient enough to filter out a strong interference signal. In addition, its 3 dB bandwidth is too wide to be used for a narrow band notch filter. Converting the DBR structure directly to coplanar waveguide cannot achieve a response suitable for a band-reject filter.

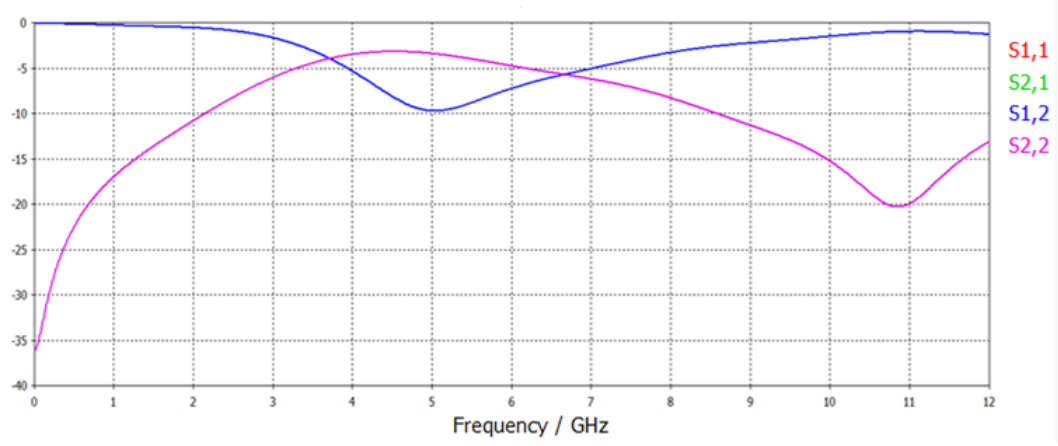

Figure 3.12: Frequency Response of The DBR Structure

However, a modified version of this DBR structure might provide improved performance (Figure 3.13). This modified version shows that the slot-lines in the ground plane of the coplanar waveguide filter are symmetric, and all dimensions remain as the previous one. Its simulated frequency response is shown in Figure 3.14, and indicates that the insertion loss S_{21} in the stop band is about -16 dB, and the 3 dB bandwidth is nearly 2 GHz, which is still too wide to be a narrow band notch filter.

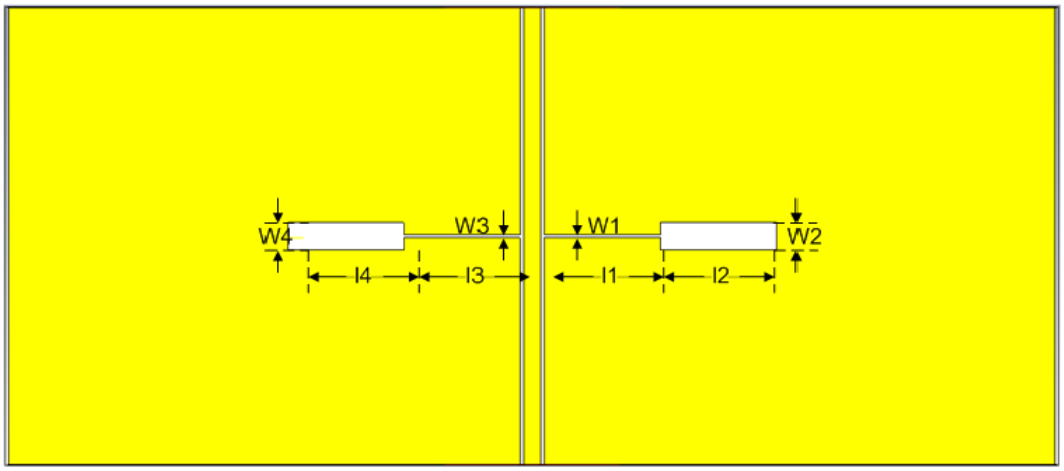

Figure 3.13: The Modified Version of The DBR Structure

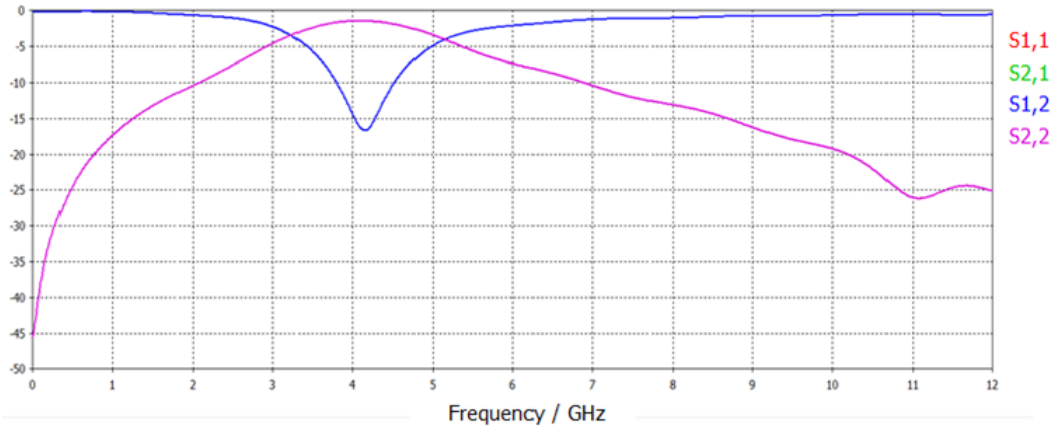

Figure 3.14: Frequency Response of The Modified DBR Structure

Any other same shaped slot-lines inserted in the ground should theoretically increase the insertion loss in the stop band. A coplanar waveguide filter with two slot-lines is illustrated in Figure 3.15. And its frequency response is shown in Figure 3.16.

It can be observed that the insertion loss has decreased to more than -20 dB, so that it improves the notch ability of this band-reject filter. However, its 3 dB bandwidth is still more than 2.5 GHz and is thus too wide to meet the requirement. This DBR technique is not suitable for CPW structures because it cannot provide the

3dB bandwidth in the stop band for less than 2 GHz with these confined dimensions.

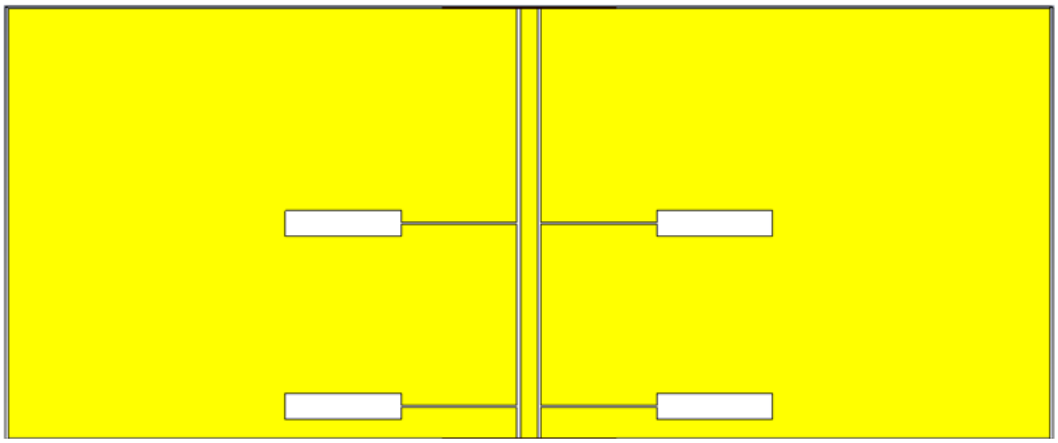

Figure 3.15: Two Slot-line DBR Structure

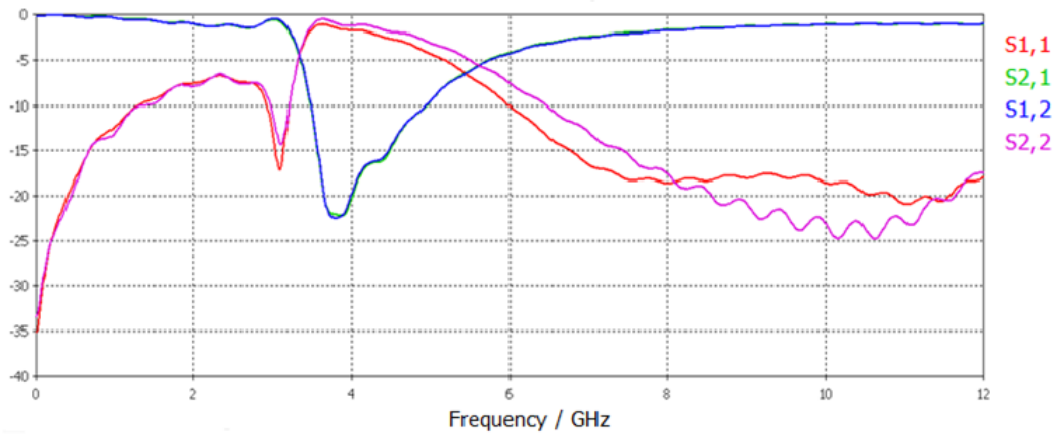

Figure 3.16: Frequency Response of Two Slot-line DBR Structure

3.3.3 Loaded EBG in the Ground Plane (Electromagnetic Band-gaps)

Electromagnetic band-gaps have caught recent attention in the microwave and millimeter-wave community because of their filtering properties or inhibition of signal propagation in certain directions [66]. These EBG structures can be etched in the ground

plane (Figure 3.17). Its equivalent circuit is illustrated in Figure 3.18.

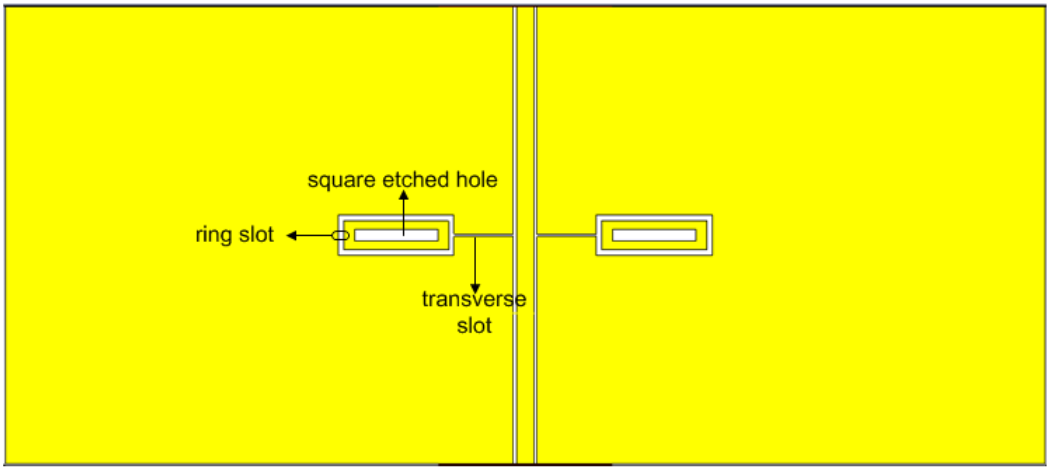

Figure 3.17: Loaded EBG Structure

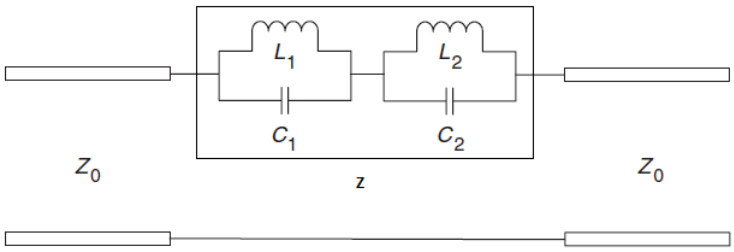

Figure 3.18: Equivalent Circuit of The Loaded EBG Structure [66]

This configuration demonstrates that L_1 in parallel with C_1 represents one loaded EBG and L_2 in parallel with C_2 represents the other loaded EBG. Z is the equivalent impedance value of the cascaded resonant circuit. It is given as [66]

$$Z = (j\omega C_1 + \frac{1}{j\omega L_1})^{-1} + (j\omega C_2 + \frac{1}{j\omega L_2})^{-1}, \tag{3.6}$$

where the subscripts '1' and '2' indicate the two different resonant circuits. However, in this case, they have the same values because the two EBGs have the same dimensions.

Figure 3.19 illustrates the frequency response of this band-reject filter with the EBG structure as obtained from a simulation with CST. It can be seen that it has an insertion loss of about 18 dB at the center frequency of the stop band. It is not sharp enough to reject the interference signals. In addition, its 3 dB bandwidth of the stop band is very large, more than 2.5 GHz. It causes the operating band to lose the optimal band utilization percentage. Hence, this EGB structure in the ground plane of a CPW is not a good solution for this band-reject filter.

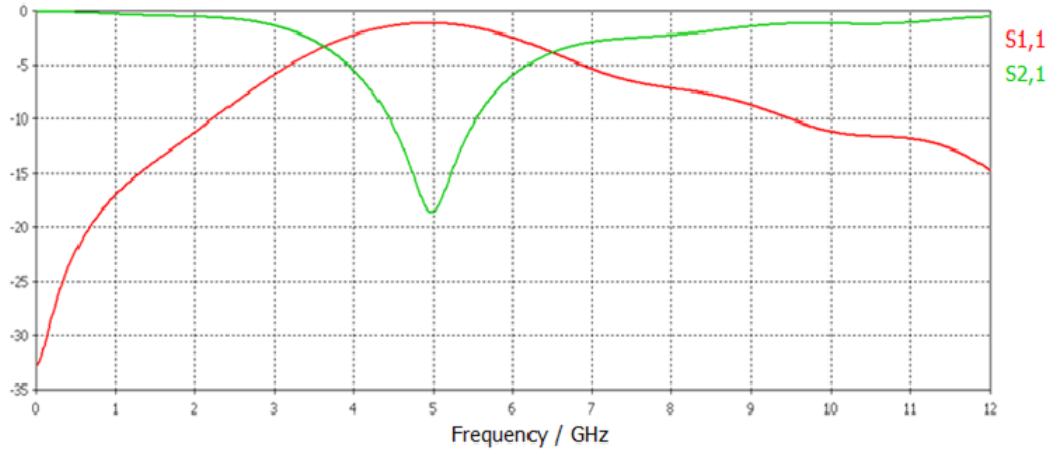

Figure 3.19: Frequency Response of The Loaded EBG Structure

3.3.4 Microwave Coplanar Waveguide BSF Realization By Short-ended Stubs

In this band-stop filter structure, short-ended stubs are placed in the center conductor of CPW. This new structure is intended to provide good performance of insertion loss. The total length of the short-ended stub is given as

$$L_{total} = \frac{c}{4\sqrt{\varepsilon_{re}} f_0}, \tag{3.7}$$

where c is the speed of light in free space, f_0 is the notched center frequency, and ε_{re} is the substrate effective relative permittivity.

This coplanar waveguide BSF with short-ended stubs is shown in Figure 3.20. Since the notched center frequency is 5 GHz, its quarter wavelength in a slot-line is 10.687 mm. Therefore, the initial values of length L_1 and L_2 in Figure 3.20 are 4 mm and 6 mm, respectively. The BSF's frequency response is illustrated in Figure 3.21.

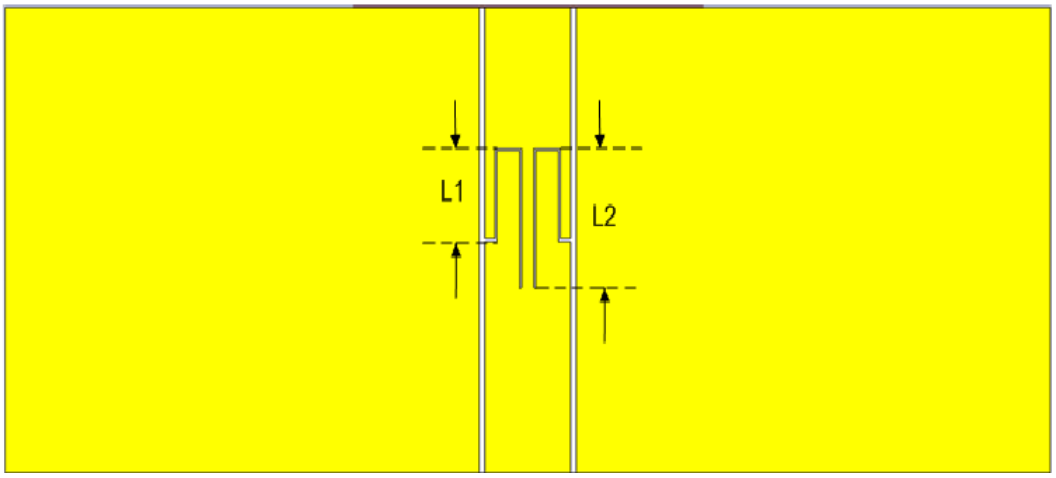

Figure 3.20: BSF With Short Stubs

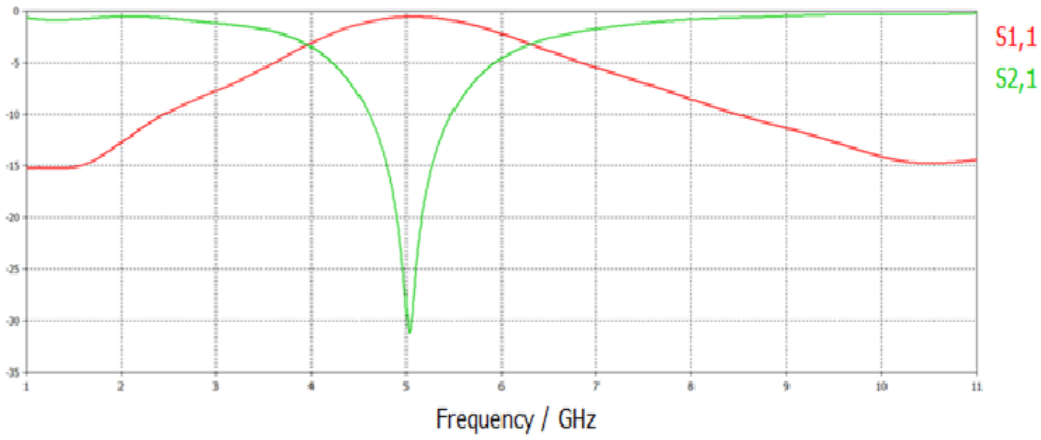

Figure 3.21: Frequency Response of The BSF With Short Stubs

It can be observed that this band-reject filter has a very deep notch at the center frequency, which means that this filter can provide a good notch performance

around 5 GHz. However, its 3 dB bandwidth is too wide to make an efficient band usage. Therefore, this structure is not practical to be exploited in the UWB antenna application.

3.3.5 CPW Band-stop Filter with Periodically Loaded Slot Resonators

In this section, a new dual-spiral-shaped slot resonator in a co-planar waveguide (CPW-DSR) is presented and its model is established in CST. This CPW-DSR is placed in the ground plane as a band-stop filter as shown in Figure 3.22.

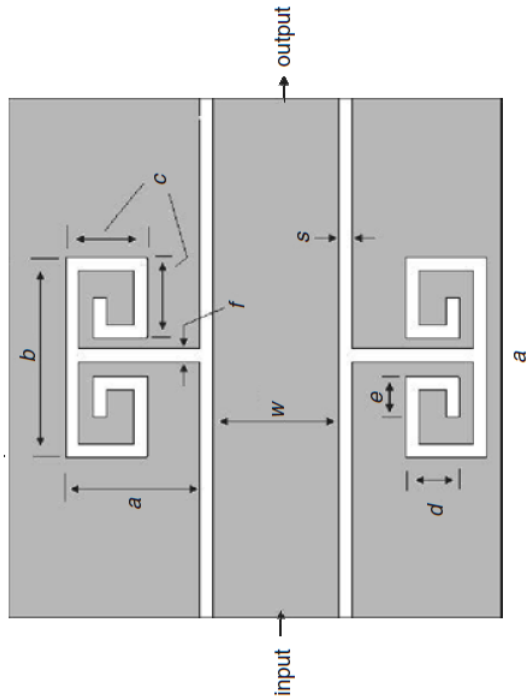

Figure 3.22: BSF With Periodically Loaded Slot Resonators [67]

Since the periodically loaded slots function as resonators and one end of the slot is open on the ground plane, the total length of one branch of the slot should be a quarter wavelength at the notched center frequency. In this case, the center frequency

is 5 GHz, so the quarter wavelength for the slot-line is about 10mm. Thus the initial values for a, b, c, d, e and f are 3.2 mm, 6 mm, 2.4 mm, 1 mm, 0.6 mm and 0.2 mm, respectively.

Its equivalent circuit is illustrated in Figure 3.23. It can be observed that resonator 1 and resonator 2 represent two periodically separately loaded slots.

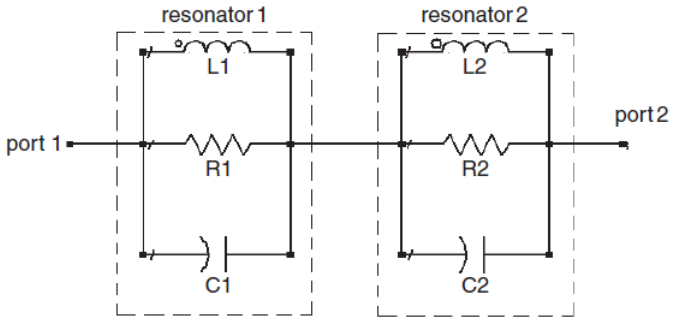

Figure 3.23: Equivalent Circuit of a BSF With Periodically Loaded Slot Resonators [67]

This filter structure can be readily modelled and simulated with CST software, and its frequency response is shown in Figure 3.24.

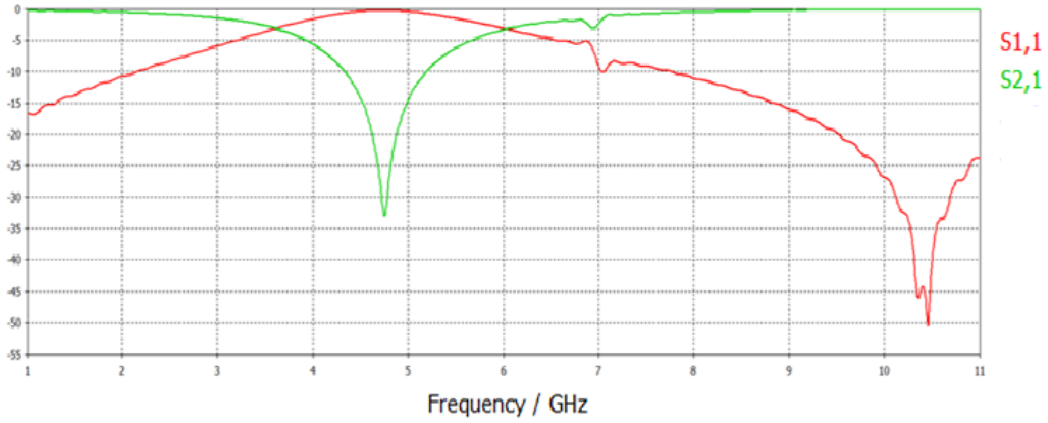

Figure 3.24: Frequency Response of a BSF With Periodically Loaded Slot Resonators

It can be observed that the attenuation S_{21} reaches about 32 dB. It signifies that this CPW-DSR structure can be exploited as an effective band-stop filter from the

insertion loss point of view. However, its 3 dB bandwidth is more than 2 GHz. Thus, this structure is not practical for the UWB antenna application.

3.3.6 CPW Band-stop Filter With Defected Ground Structure (DGS)

The cells of the defective ground structure (DGS) serve as resonators and are etched in the ground plane of the coplanar waveguide. As a new stop-band structure, it has attracted the interest of many researches since 1998 [68].

The first experimental structure of this type of stop-band filter includes two DGS cells, and either of them is etched in each side of the coplanar waveguide ground plane (Figure 3.25).

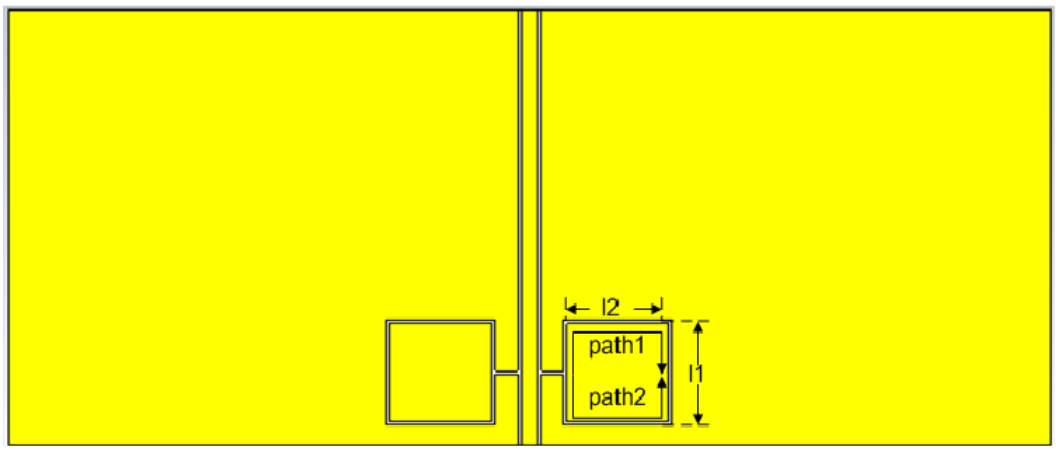

Figure 3.25: Band-stop Filter With DGS Structure

It can be observed that one edge of the DGS cell is connected to the open end of the ground plane, so the total length of each path should be a quarter wavelength in the slot-line at the center frequency of 5 GHz. The calculation of the quarter

wavelength of the slot-line is given as

$$L = \frac{c}{4\sqrt{\varepsilon_{re}} f_0}, \tag{3.8}$$

where f_0 is 5 GHz, c is the speed of light and ε_{re} is the substrate effective relative permittivity. From the above formula, the value of L can be derived and is approximately 10.7 mm. As a result, the values for l_1 and l_2 can be initialized with 5 mm each. After the dimensions of the DGS cells are set, this stop-band filter simulation can be run with CST software. Its frequency response is illustrated in Figure 3.26.

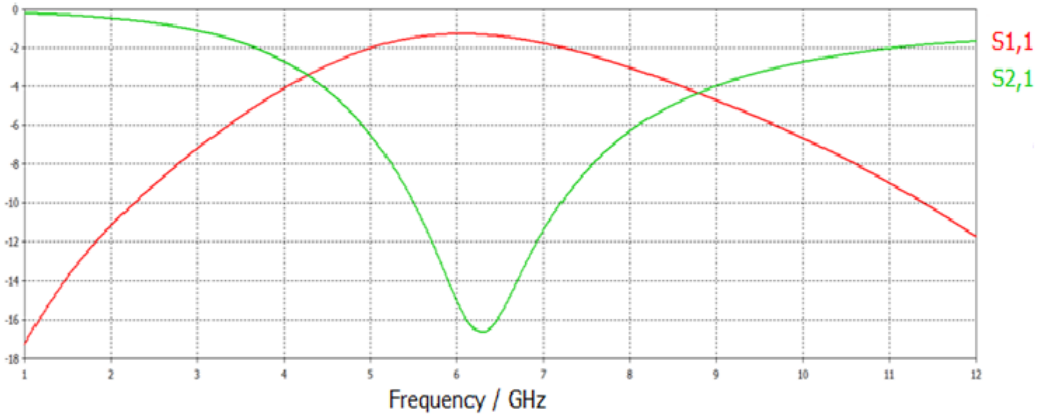

Figure 3.26: Frequency Response of A BSF With DGS Structure

No matter where the DGS cells are positioned in the ground plane, it only changes the notched center frequency to some extent, but the shape of the plots remain the same. Figure 3.26 demonstrates that the insertion loss (S_{21}) is greater than -18 dB and the 3 dB bandwidth is too wide. This structure cannot be used as an efficient stop-band filter. Nevertheless, this structure can be modified to provide better frequency response in theory. The following structures are the try-outs of the modified version for this type of band-stop filter.

The second structure has two DGS cells that cascade on each side of the ground

plane (Figure 3.27). The distance between two DGS cells in each side of the ground plane is around 0.155 mm. This is the minimum width that can be constructed by the local fabricator. The idea of having two DGS cells on one side of the ground plane is that the electromagnetic field is able to be coupled from the first DGS cell to the second one. This should provide higher insertion loss in the stop band. Its frequency response is shown in Figure 3.28.

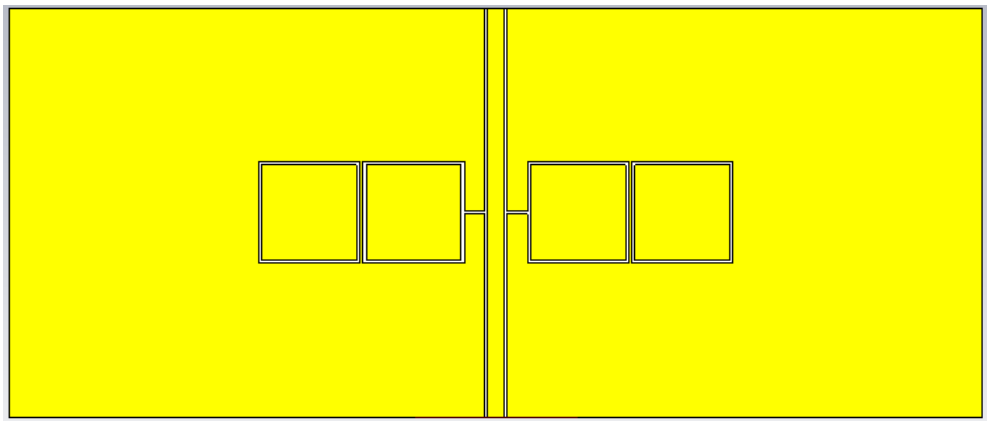

Figure 3.27: Band-stop Filter With DGS Coupling Structure

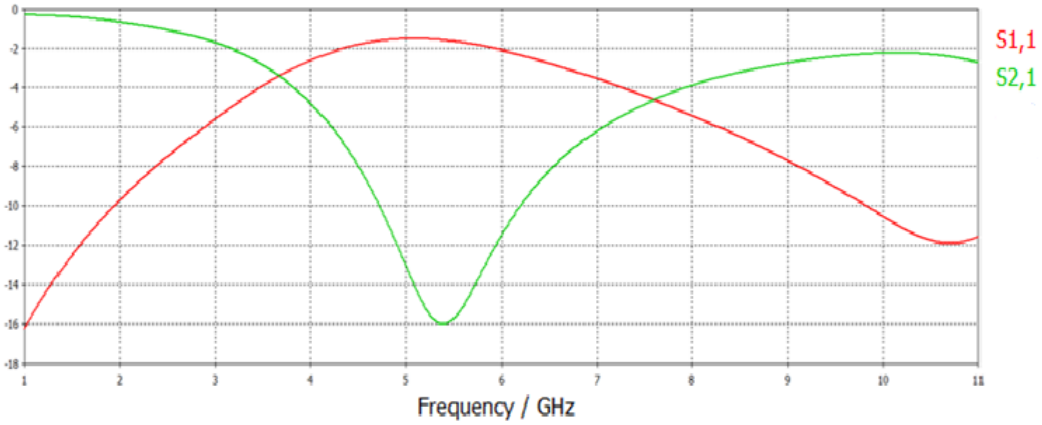

Figure 3.28: Frequency Response of a BSF With DGS Coupling Structure

It can be observed that the frequency response of this structure does not differ much from the previous structure. This can be attributed to the distance between

the two DGS cells in one side of the ground plane. It is too wide to yield a good coupling between two DGS cells but it is the most narrow width able to be provided by the manufacturer. Even though this structure is not suitable for a stop-band filter, it leads to another similarly shaped structure.

The new structure is not intended to create coupling between two DGS cells but to establish a path between two DGS cells (Figure 3.29). Initial values for l_1 and l_2 are given as 1 mm and 4 mm. Then the simulation of the above structure is run to obtain the frequency response of this stop-band filter (Figure 3.30).

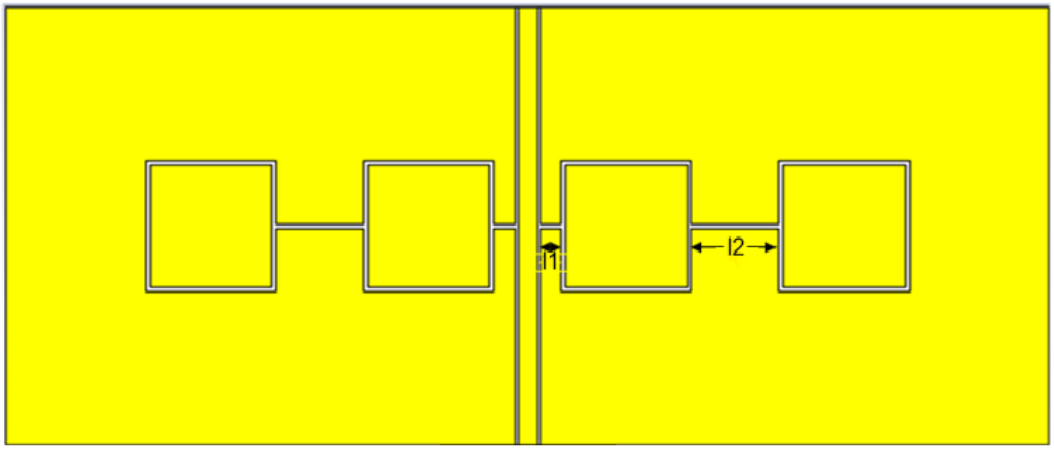

Figure 3.29: Band-stop Filter With DGS Through Structure

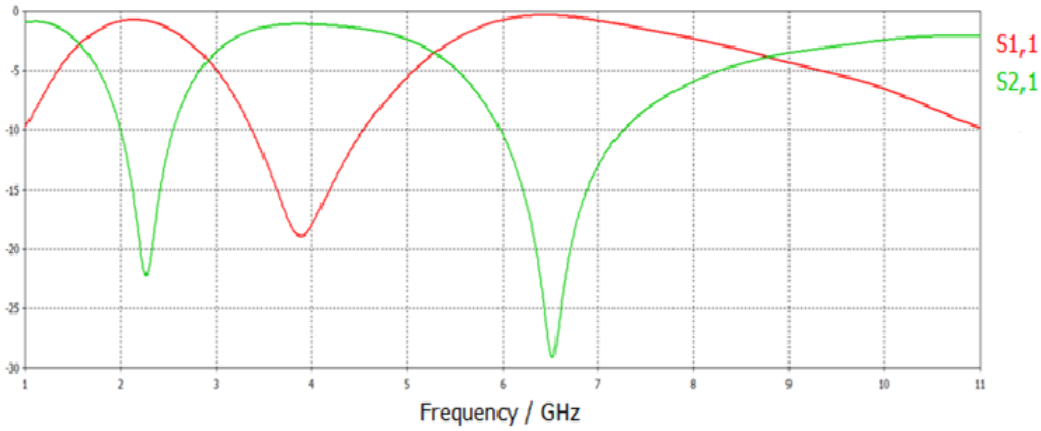

Figure 3.30: Frequency Response of A BSF With DGS Through Structure

It can be observed that there are two notches in the plot, and the second notch will reach as low as -28 dB. This provides an acceptable insertion loss as a sharp stop-band filter, but the 3 dB bandwidth is still too wide. l_1 and l_2 can be adjusted to attempt to narrow down the 3 dB bandwidth. However, doing this only causes the notched center point to move to the left or the right. Thus, this DGS cell structure in the ground plane is not suitable for a band-stop filter in this case.

3.3.7 Substrate-Integrated Waveguide (SIW) Resonator Structure

Substrate-Integrated Waveguide (SIW) has attracted the millimeter-wave researchers' attention since it is a reasonable compromise between planar integrated circuits and metallic waveguide technology [69]. According to Table 3.1, the Q factors of CPW and microstrip technologies are an order of magnitude lower than those of SIW. For the purpose of this work, though, it is expected that SIW will provide narrower 3 dB bandwidth and better attenuation in the stopband. Interfacing SIW with CPW is becoming more and more popular in millimeter-wave applications. Figure 3.31 shows the main SIW parameters. The transition between SIW and CPW is the key factor to get a good frequency response for many applications.

	CPW/Microstrip	**Integrated waveguide (SIW)**
Parameters	$h = 10\ mil$, $\varepsilon_r = 2.33$	$h = 10\ mil$, $\varepsilon_r = 2.33$
Unloaded Q Factor	42	462

Table 3.1: Q Factor Comparison Between CPW/Microstrip and SIW

a_{equ} is the equivalent waveguide width and is determined by the SIW's cutoff

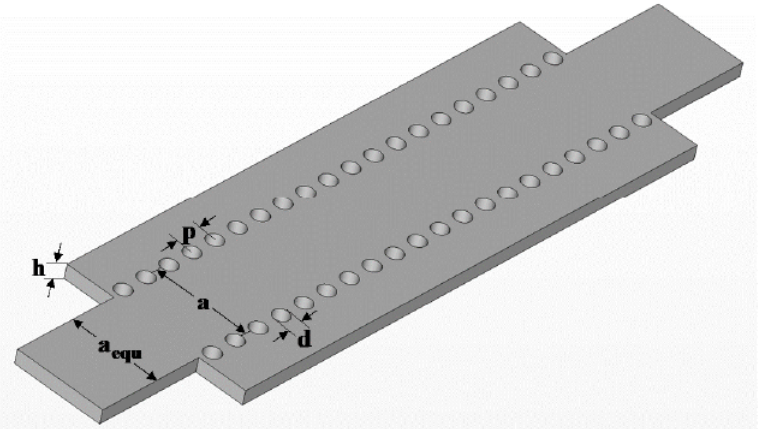

Figure 3.31: SIW Parameters [69]

frequency. It is given as

$$a_{equ} = \frac{c}{2f_c\sqrt{\varepsilon_r}}, \tag{3.9}$$

where f_c is the cut-off frequency and set to 4 GHz, c is the speed of light and ε_r is the substrate relative permittivity. After a_{equ} is obtained, the calculation of a is derived by [70]

$$a_{equ} = a[x_1 + \frac{x_2}{\frac{p}{d} + \frac{x_1+x_2-x_3}{x_3-x_1}}], \tag{3.10a}$$

$$x_1 = 1.0198 + \frac{0.3465}{(\frac{a}{p} - 1.0684)}, \tag{3.10b}$$

$$x_2 = -0.1183 - \frac{1.2729}{(\frac{a}{p} - 1.2010)}, \tag{3.10c}$$

$$x_3 = 1.0082 - \frac{0.9163}{(\frac{a}{p} + 0.2152)}, \tag{3.10d}$$

where p is the distance between two via-hole centers, and d is the diameter of one via-hole. The confinement for p and d is that d/p needs to be in range between 0.4 and 0.8 [71]. The best performance is when $d/p > 0.5$. In this case, the initial values for p and d are 1.4 mm and 1 mm, respectively. The value of a is 22.626 mm from the above formulas.

Since SIW is employed as the notch structure, it should be placed in the ground plane as a resonator with half wavelength. For the initial design, the center frequency of the resonator is picked as 6 GHz. And the guided wavelength is given as

$$\lambda_g = \frac{c}{\sqrt{\varepsilon_r}\sqrt{f^2 - f_c^2}}, \tag{3.11}$$

where c is the speed of light, ε_r is the permittivity of the dielectric, and f_c is the cutoff frequency. After calculation, the guided wavelength at 6 GHz is 39 mm, and the half wavelength is 19.5 mm. The structure of this stop-band filter with SIW resonator is shown in Figure 3.32. Note that due to the CPW-to-SIW transition, the resonance frequency will be shifted slightly downwards.

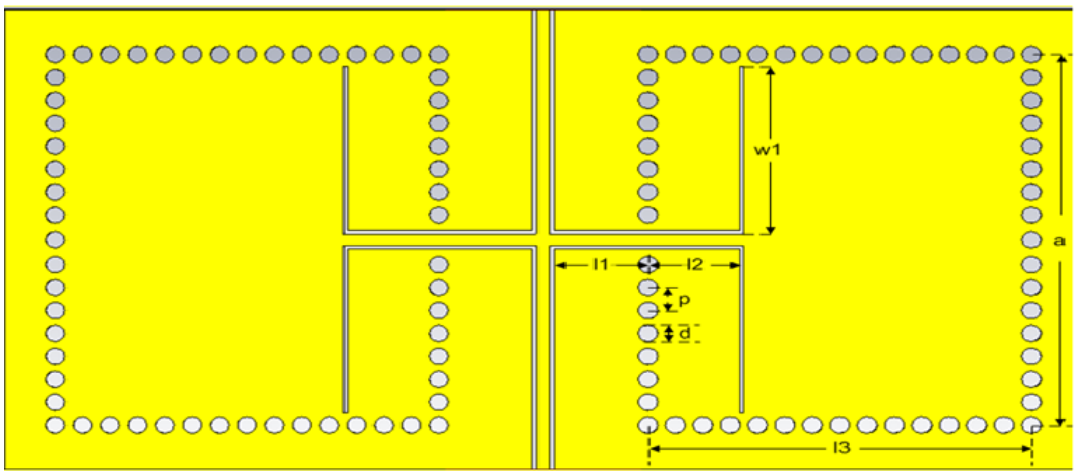

Figure 3.32: Band-stop Filter With SIW Initial Dimensions

It can be observed that there are other parameters in the structure except for p, d and a. They are l_1, l_2, l_3, and w_1. The initial values for them are given in Table 3.2. Then the simulation for the above structure with these initial values is run in CST to get its frequency response (Figure 3.33).

There is a sharp notch between 5 and 6 GHz shown in this figure. The peak

Symbol	Dimension (mm)	Symbol	Dimension (mm)
l_1	5	l_2	4.875
l_3	19.5	w_1	10

Table 3.2: Initial Dimensions for The SIW Structure

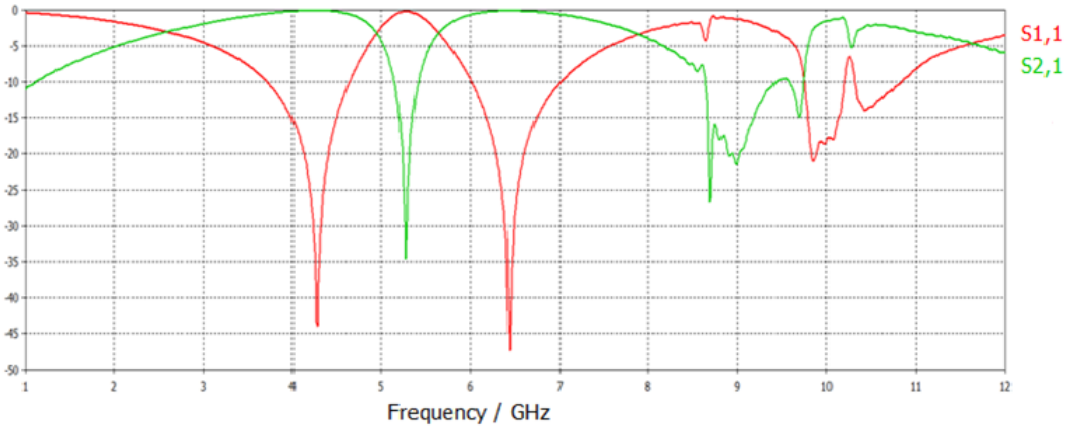

Figure 3.33: Frequency Response of A BSF With SIW Initial Dimensions

point of the insertion loss (S_{21}) is about 35 dB. And the 3 dB bandwidth of the stop band is very narrow. However, the plot indicates that the frequency response varies drastically beyond 8.5 GHz. The transition between the SIW and the CPW is a factor that may cause this problem. It is crucial to design a more efficient matching network for this transition.

The design of this new matching network does not have any design guidelines to follow. It only depends on the experimental results, which means that the design should provide the best frequency response of the notch filter with correct dimensions of this matching network. To start, the previous transition is divided into three sections as shown in Figure 3.34. Their dimensions are l1, l2, l3, w1, w2 and w3, respectively. The initial values for these new dimensions are provided in Table 3.3. With these initial values, the matching network is supposed to guide the waves more efficiently and provide better frequency response for this notch filter.

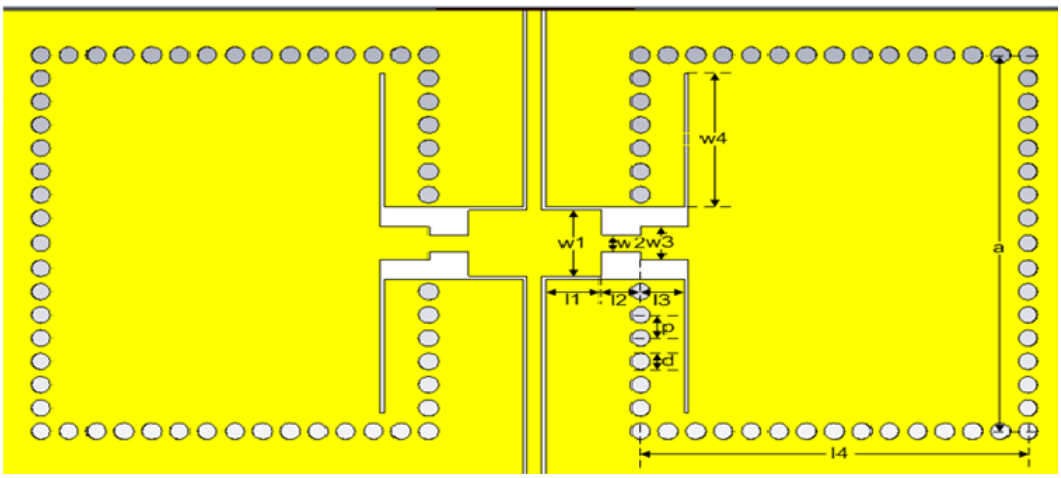

Figure 3.34: Band-stop Filter With SIW Structure of New Transition

Symbol	**Dimension (mm)**	**Symbol**	**Dimension (mm)**
l_1	4	w_1	2
l_2	3	w_2	1
l_3	4.875	w_3	1
l_4	19.5	w_4	10
a	1.4	d	1
p	22.626		

Table 3.3: Initial Dimensions for The SIW Structure With New Transition

The simulated response of this structure with these initial values is shown in Figure 3.35. It is observed that both S_{21} and S_{11} are improved for the new structure when the frequency goes above 8 GHz.

It is necessary to optimize all the dimensions of the new matching network to obtain the best frequency response of this notch filter. Table 3.4 gives the optimized dimensions. With these optimized dimensions, the frequency response of this stop-band filter structure is shown in Figure 3.36.

This demonstrates that there are two notches in the required band. One has an insertion loss about 40 dB, and the other has an insertion loss about 26 dB at 8.7 GHz. This is the second harmonic of the notch filter. Theorically, the length of

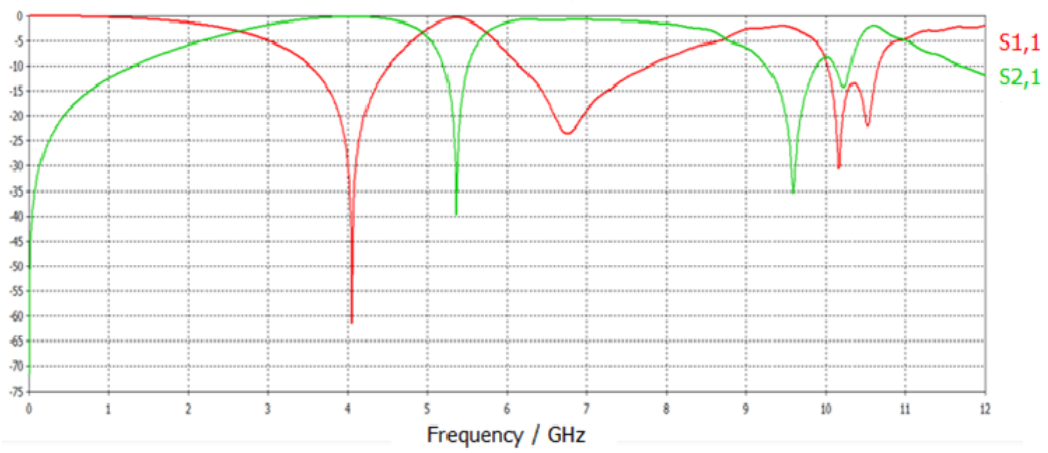

Figure 3.35: Frequency Response of A BSF With New SIW Transition Initial Dimensions

Symbol	Dimension (mm)	Symbol	Dimension (mm)
l_1	3	w_1	2
l_2	2	w_2	0.5
l_3	4.875	w_3	1
l_4	19.5	w_4	8
a	1.4	d	1
p	22.626		

Table 3.4: Optimized Dimensions for The SIW Structure With New Transition

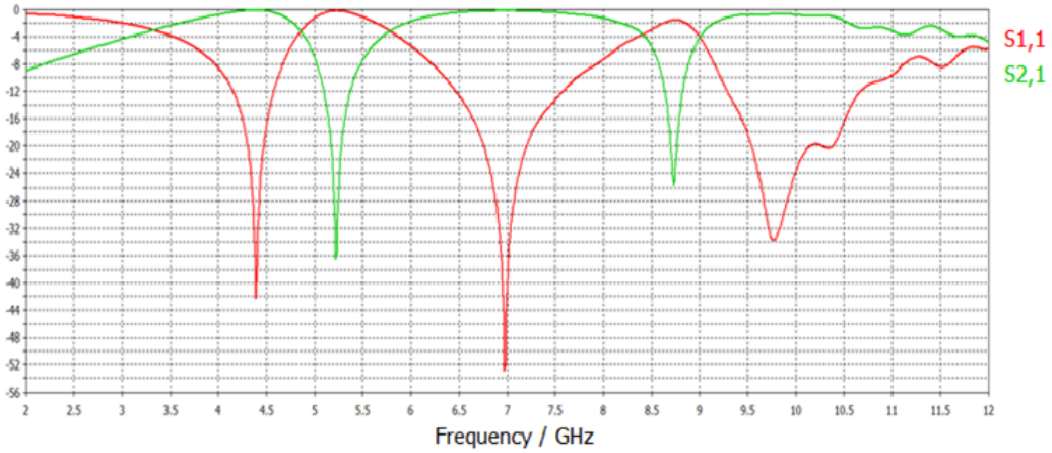

Figure 3.36: Frequency Response of A BSF With New SIW Transition Optimized Dimensions

the resonator in SIW structure is half wavelength at 6 GHz and full wavelength at 9.7 GHz. Due to CPW-to-SIW transition, the resonance frequencies will be shifted slighly downwards. It can be seen in Figure 3.36 that the first resonance is at 5.2 GHz and the second resonance is at 8.7 GHz. These two notches are sharp enough to eliminate unwanted signal interference. Moreover, the 3 dB bandwidth of these two notches is very narrow, less than 0.8 GHz, so that the band utilization rate of this band-stop filter is high. This SIW resonator structure can be exploited as a proper band-stop filter. Thus the research on the stop-filter model is completed.

Structure	**BW (GHz)**	**Loss at Notch (dB)**
Bent Resonators with Open Structure in the Ground Plane	2	17
Bent Resonators with Short Structure in the Ground Plane	1.2	5
Dual-Beharior Resonators in the Ground Plane	2.2	16
Short-Ended Stubs in the Main Patch	2.6	32
Periodically Loaded Slot Resonators in the Ground Plane	2.6	33
Defected Ground Structure	4	22
Substrate-Integrated Waveguide Resonators in the Ground Plane	0.8	26

Table 3.5: Structure Comparison

Table 3.5 compares the main characteristics of the band-reject filters investigated in this chapter. It is obvious that the SIW resonator provides the best option for the purpose of this research.

Chapter 4

UWB Antenna in Coplanar Waveguide (CPW) Technology

4.1 Coplanar Waveguide (CPW) UWB Antenna

Figure 4.1 shows a model of a CPW UWB antenna without the band-stop filter. The design follows an example in [72] and the dimensions of this antenna are given in Table 4.1. The main reason to choose this model is that all the previous filter designs include the CPW structure. This antenna is easy to integrate with those filters without designing an extra transition part.

Symbol	**Dimension (mm)**	**Symbol**	**Dimension (mm)**
l_1	0.7	w_1	20.3
l_2	0.2	w_2	23.1
l_3	23.5	w_3	16.3
l_4	29.1	w_4	38
l_5	34.1	w_5	40.5
ε_r	2.94	h	0.508

Table 4.1: Dimensions of The CPW Antenna

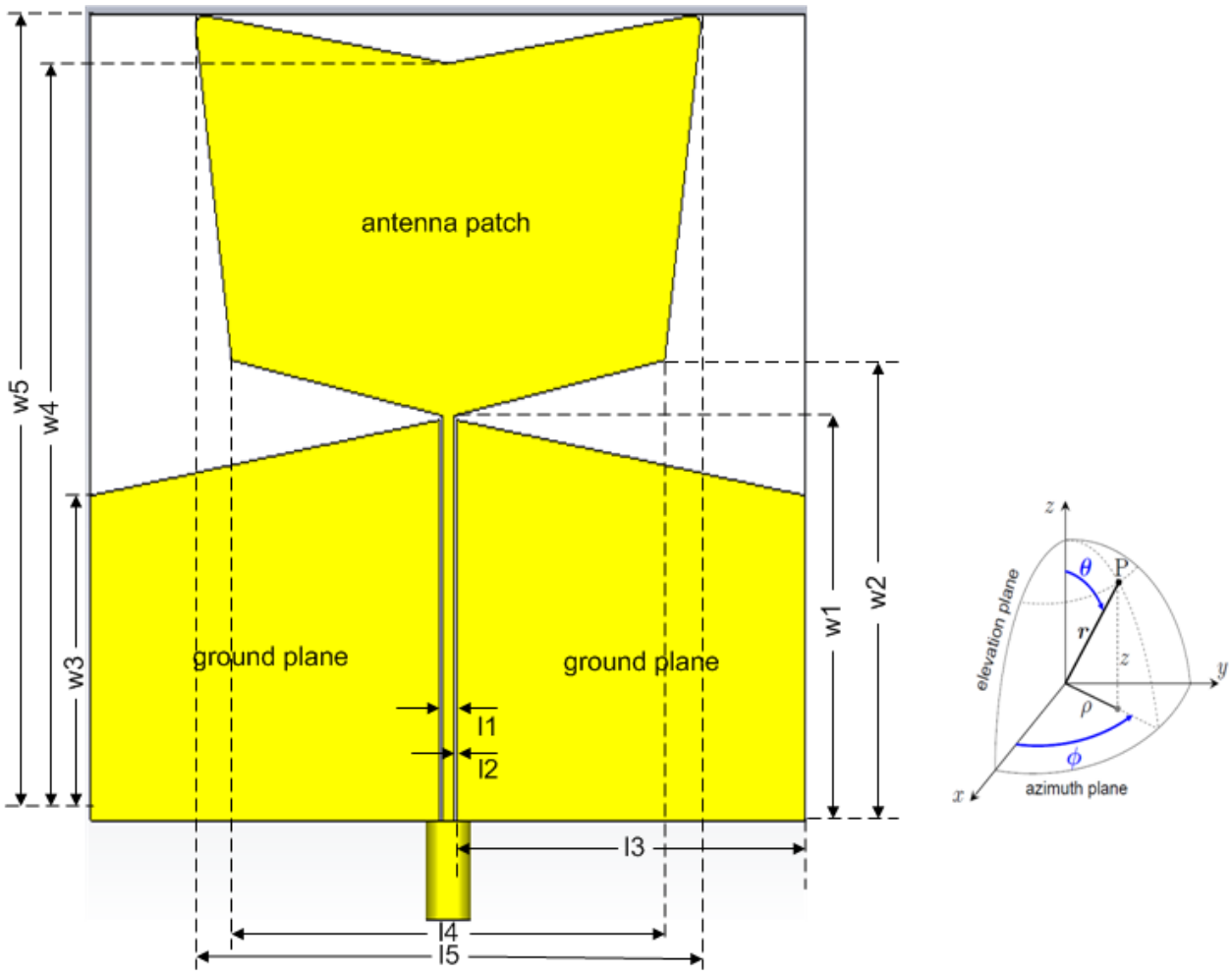

Figure 4.1: CPW UWB Antenna Without The Band-stop Filter [72]

CST software is employed to simulate this antenna's characteristics and performance. Figure 4.2 shows the input signal in the time-domain. Figure 4.3 indicates the amplitude of this signal and Figure 4.4 shows its phase. This input signal is generated at the end of the coaxial cable which has a 50 Ω impedance as shown in Figure 4.1.

Figure 4.5 illustrates the input reflection coefficient of this antenna. It can be observed that the input reflection cofficient (S_{11}) in the frequency band (3.1-10.6 GHz) is mostly below -10 dB. It indicates that this CPW antenna model is feasible

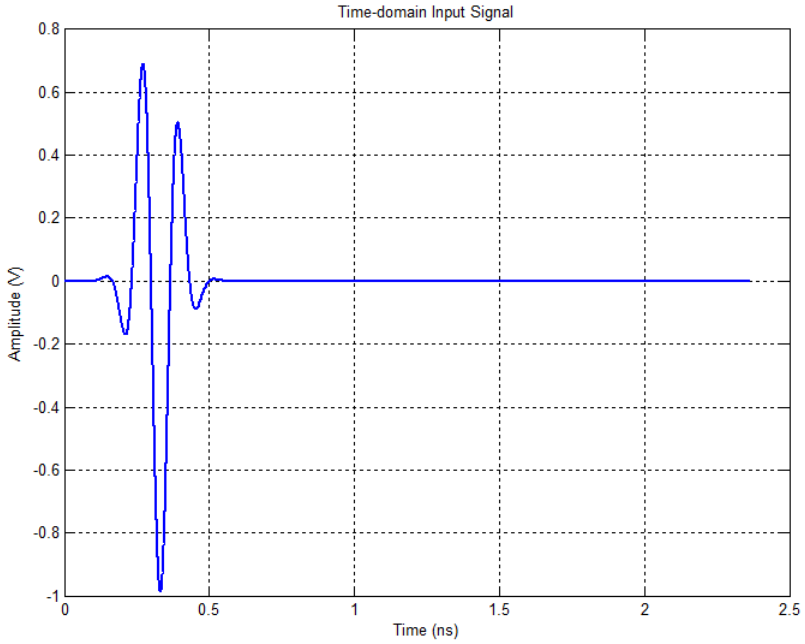

Figure 4.2: Input Time-domain Signal

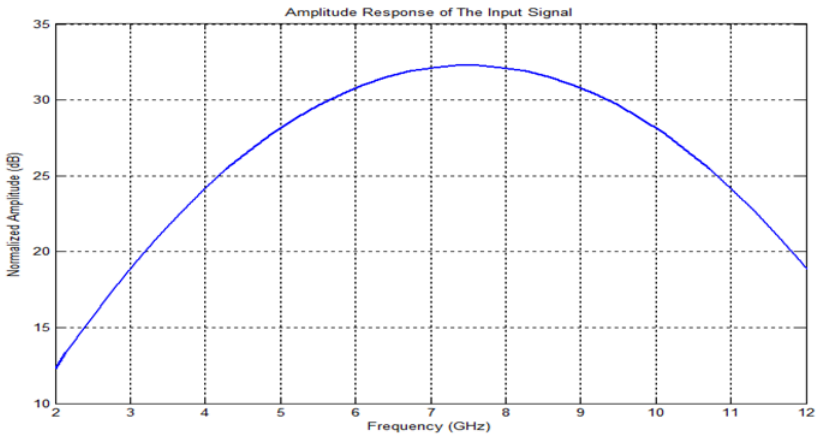

Figure 4.3: Amplitude of The Input Signal

as an UWB antenna.

In order to further investigate this antenna's performances, it is necessary to check its characteristics in the far-field. The minimum distance R in the far-field is determined by

$$R = \frac{2D^2}{\lambda}, \tag{4.1}$$

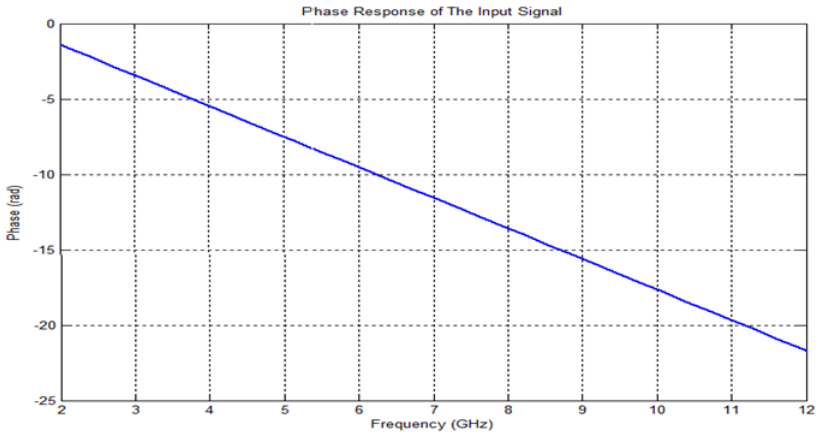

Figure 4.4: Phase of The Input Signal

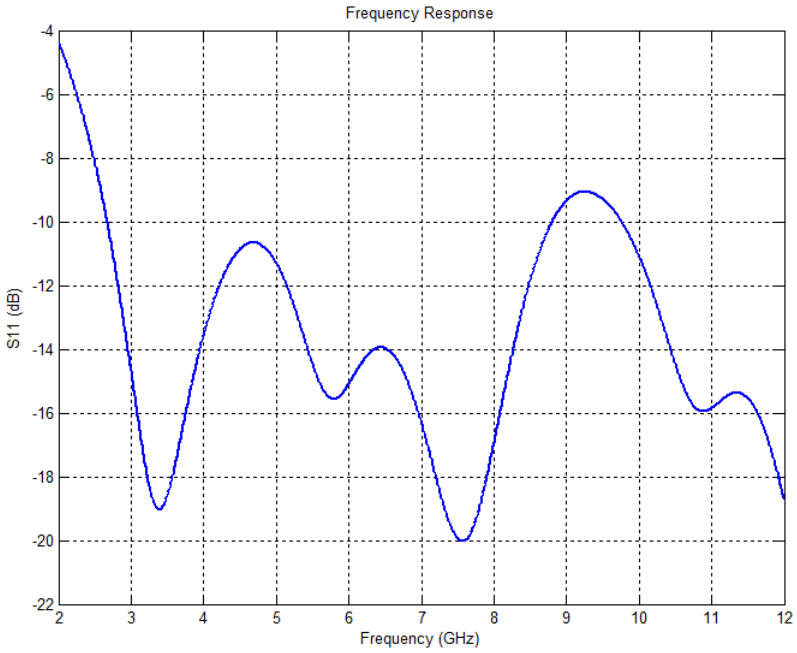

Figure 4.5: Return Loss of The UWB Antenna

where D is the largest dimension of the antenna and λ is the wavelength at the higher end of the band. The largest dimension of this proposed antenna is 62.8 mm (diagonal distance of a 48 x 40.5 mm^2 PCB). Two probes are deposited in the far-field at θ = 90^o, ϕ = 90^o and R = 316 mm as shown in Figure 4.1. The direction of one of

the probes is the θ direction, and the other is the ϕ direction. The electric field detected in the θ direction is called the co-polarization, and the electric filed detected at the ϕ direction is called the cross-polarization. Figure 4.6 shows the output signal in the time-domain for both directions. And Figure 4.7 and Figure 4.8 indicate the amplitude and the phase respectively, of this output signal in both directions.

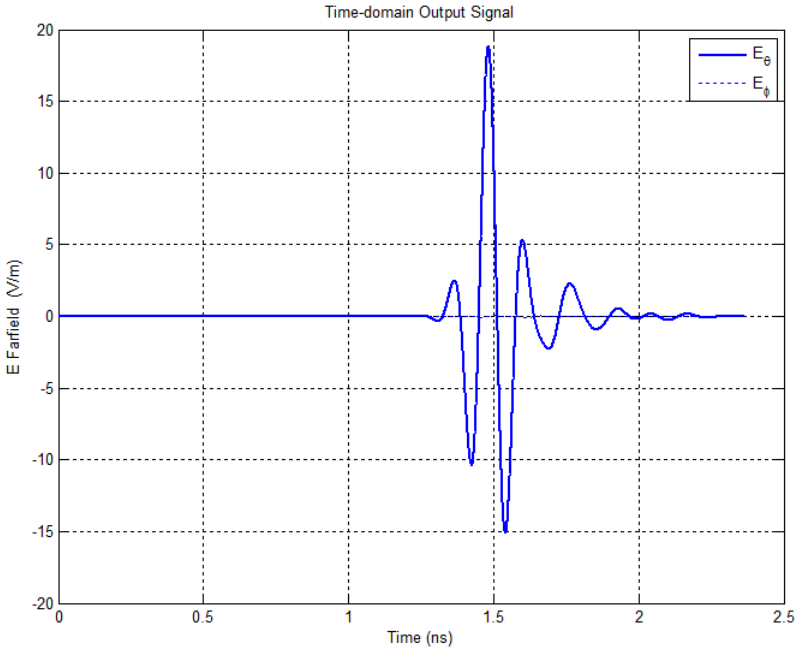

Figure 4.6: Time-domain Output Signal of The UWB Antenna (note that E_ϕ is below 0.06 V/m)

Besides these fundamental characteristics, the gain, radiation pattern and group delay in the far-field are other important parameters to evaluate an antenna's performance. Figure 4.9 shows the gain of this antenna in a distinct direction as well as in two planes. It depicts that the realized gain (at $\theta = 90^o$ and $\phi = 90^o$) decreases to below 0 dB at lower frequencies. However, the gain in the E-plane ($\phi = 90^o$ and varying θ) and in the H-plane ($\theta = 90^o$ and varying ϕ) remain positive all the time. It means that the gain of the antenna is positive in the two principle planes. However,

it is not always positive in the $\theta = 90^o$ and $\phi = 90^o$ direction (realized gain) as the direction of the beam maximum varies with frequency.

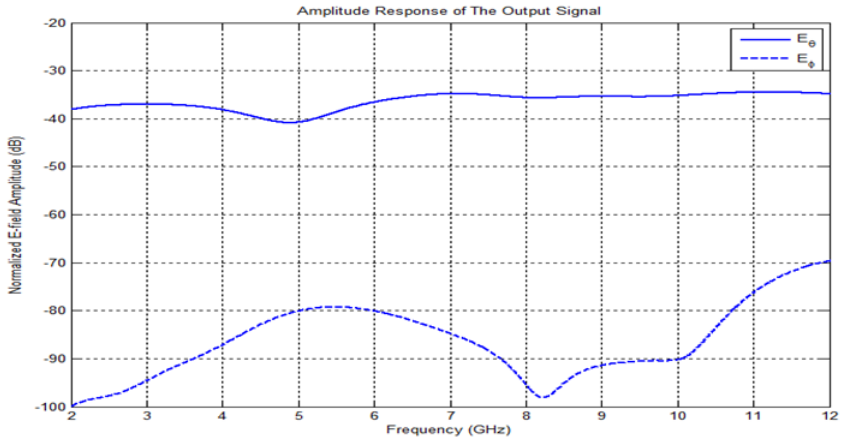

Figure 4.7: Output Signal Amplitude of The UWB Antenna

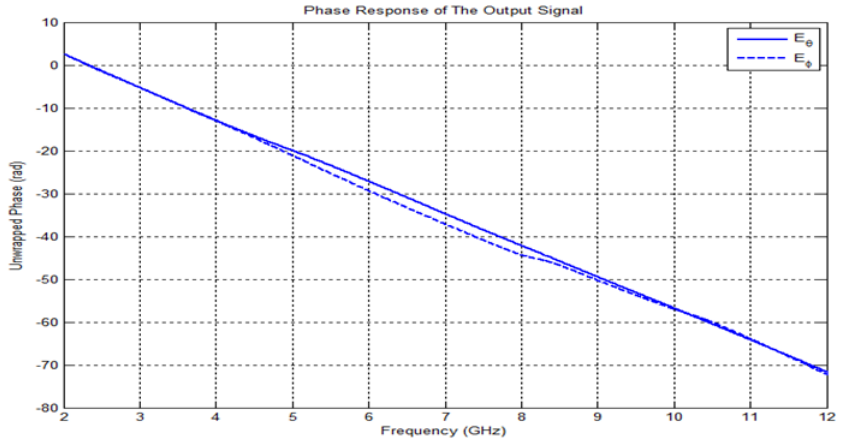

Figure 4.8: Output Signal Phase of The UWB Antenna

Next, Figure 4.10 (a) and Figure 4.10 (b) indicate the radiation patterns in the H-plane for both the co-polarization and the cross-polarization. And Figure 4.11 (a) and Figure 4.11 (b) illustrate the radiation patterns in the E-plane for both the polarizations.

These figures demonstrate that this antenna is omni-directional, and its radiation

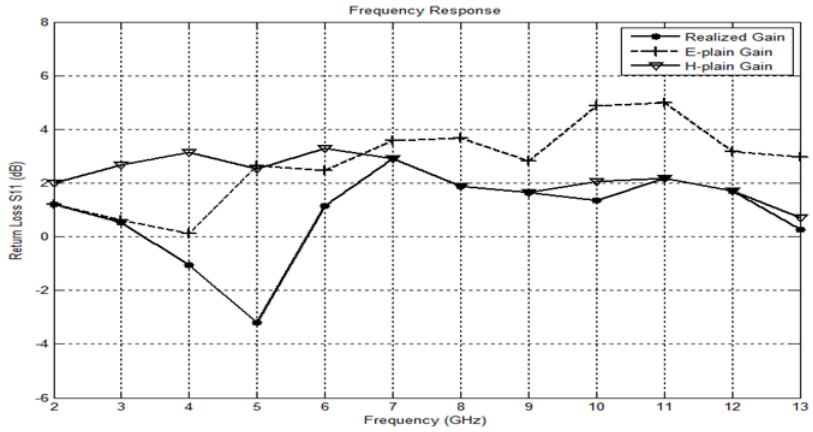

Figure 4.9: Gain of The UWB Antenna

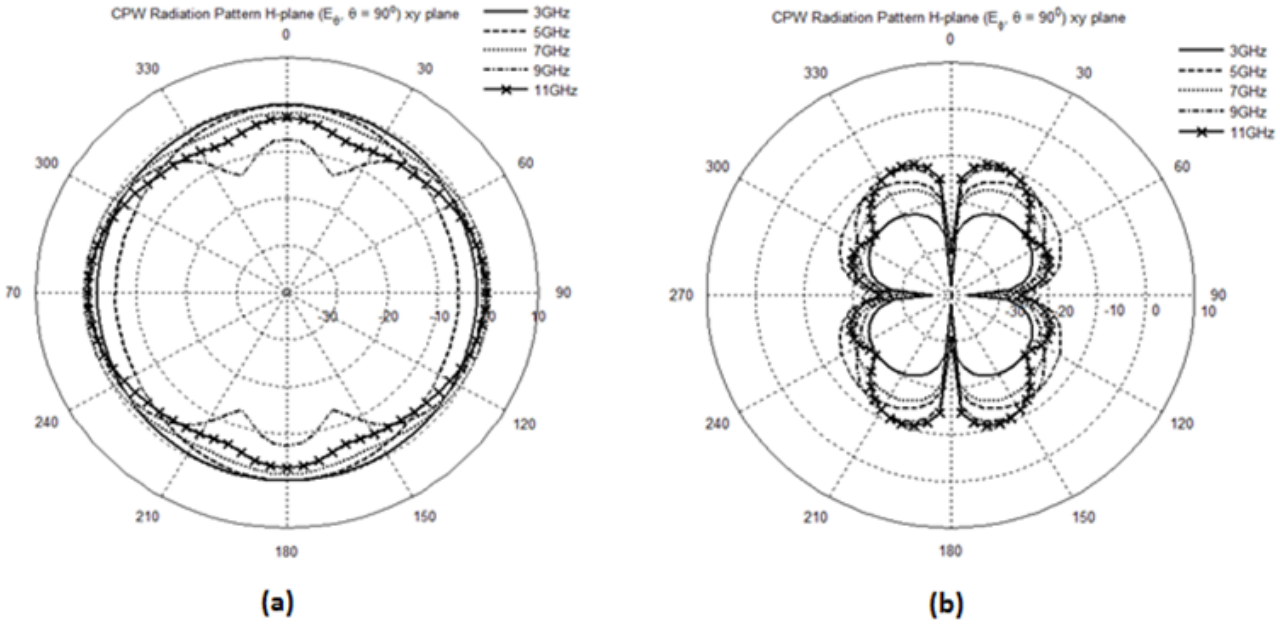

Figure 4.10: H-plane Radiation Patterns of The UWB Antenna; (a) Co-polarization, (b) Cross-polarization

in co-polarization direction is dominant in the lower frequency range (H-plane) and over the entire frequency range in the E-plane.

Another important attribute of this antenna is the group delay. Since this is an UWB antenna and it occupies a large bandwidth, it is necessary to make sure that the group delay across the entire band is nearly constant. Figure 4.12 illustrates

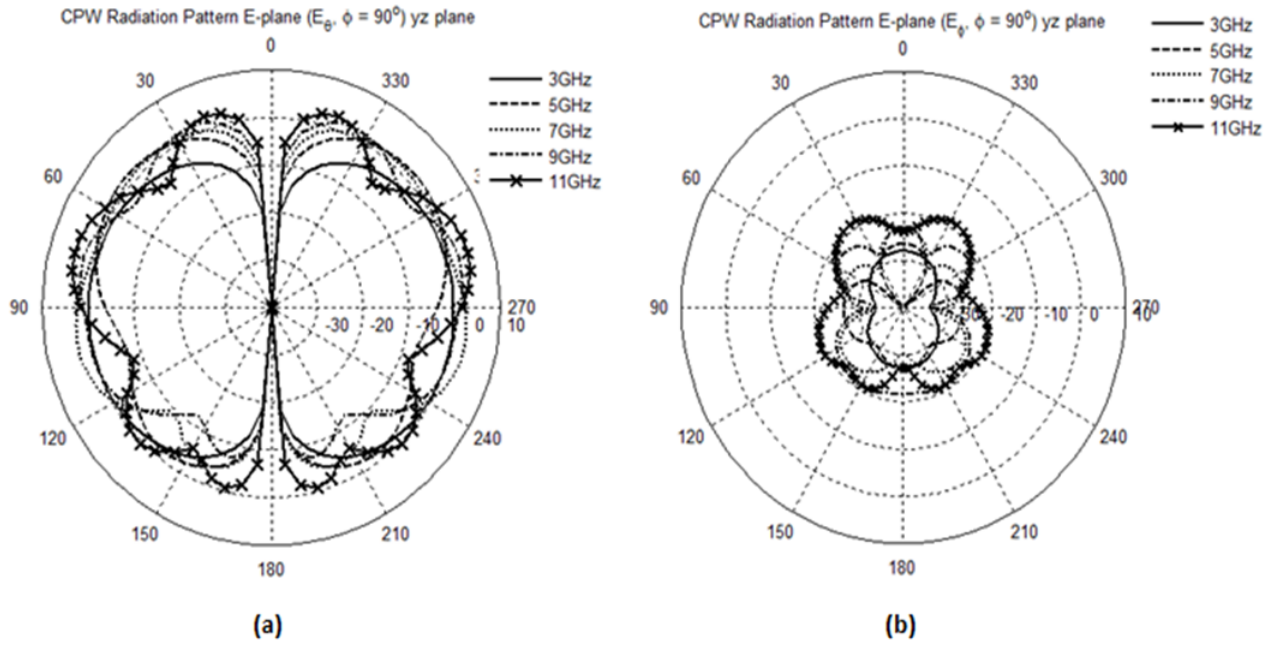

Figure 4.11: E-plane Radiation Pattern of The UWB Antenna; (a) Co-polarization, (b) Cross-polarization

the group delay in both the co-polarization and the cross-polarization directions. It can be observed that the variation of the group delay in the co-polarization direction is less than 200 ps, and that in the cross-polarization direction is less than 700 ps. Even though the variation of the group delay in the cross-polarization direction is much greater than the one in the co-polarization direction, the radiation in the co-polarization direction dominates the signal propagation. Thus, the variation of the group delay is 200 ps. It is a very small variation compared to other UWB antennas so that the group delay across the entire band can be considered virtually constant.

After all these parameters are simulated, it is concluded that this antenna is a valid design, and it can be exploited as a practical CPW UWB antenna.

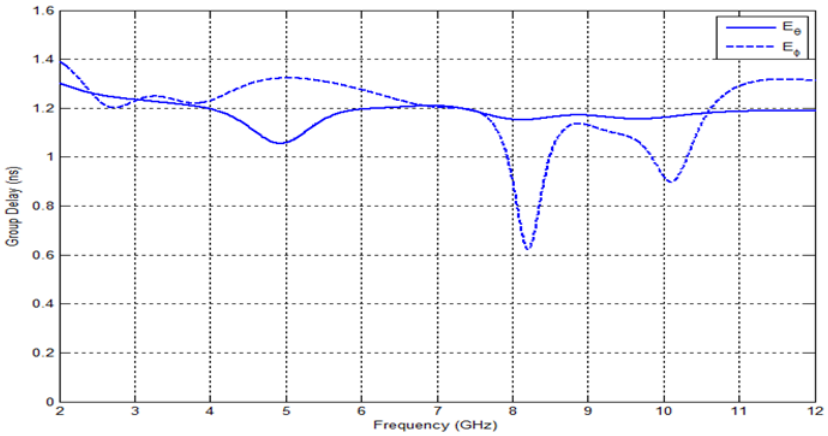

Figure 4.12: Group Delay of The UWB Antenna

4.2 Coplanar Waveguide (CPW) UWB Antenna With Band-stop Filter

4.2.1 Design of The CPW UWB Antenna With Band-stop Filter

Since the band-stop filter has been designed and a practical CPW UWB antenna model has been found, a CPW UWB antenna with band-stop filter should be theoretically the combination of these two parts. First, this combination is modeled in CST with the original dimensions in Table 4.2. It can be observed that the antenna width and the filter width can be combined to obtain the total width of the new structure.

Name	Dimension (mm)	Name	Dimension (mm)
$AntennaLength$	55.074	$AntennaWidth$	40.5
$FilterLength$	55.074	$FilterWidth$	28

Table 4.2: Dimensions of The UWB Antenna and The Filter

Figure 4.13 shows this combined structure, and it is the initial design of the CPW UWB antenna with the band-stop filter. The frequency response of this antenna is shown in Figure 4.14.

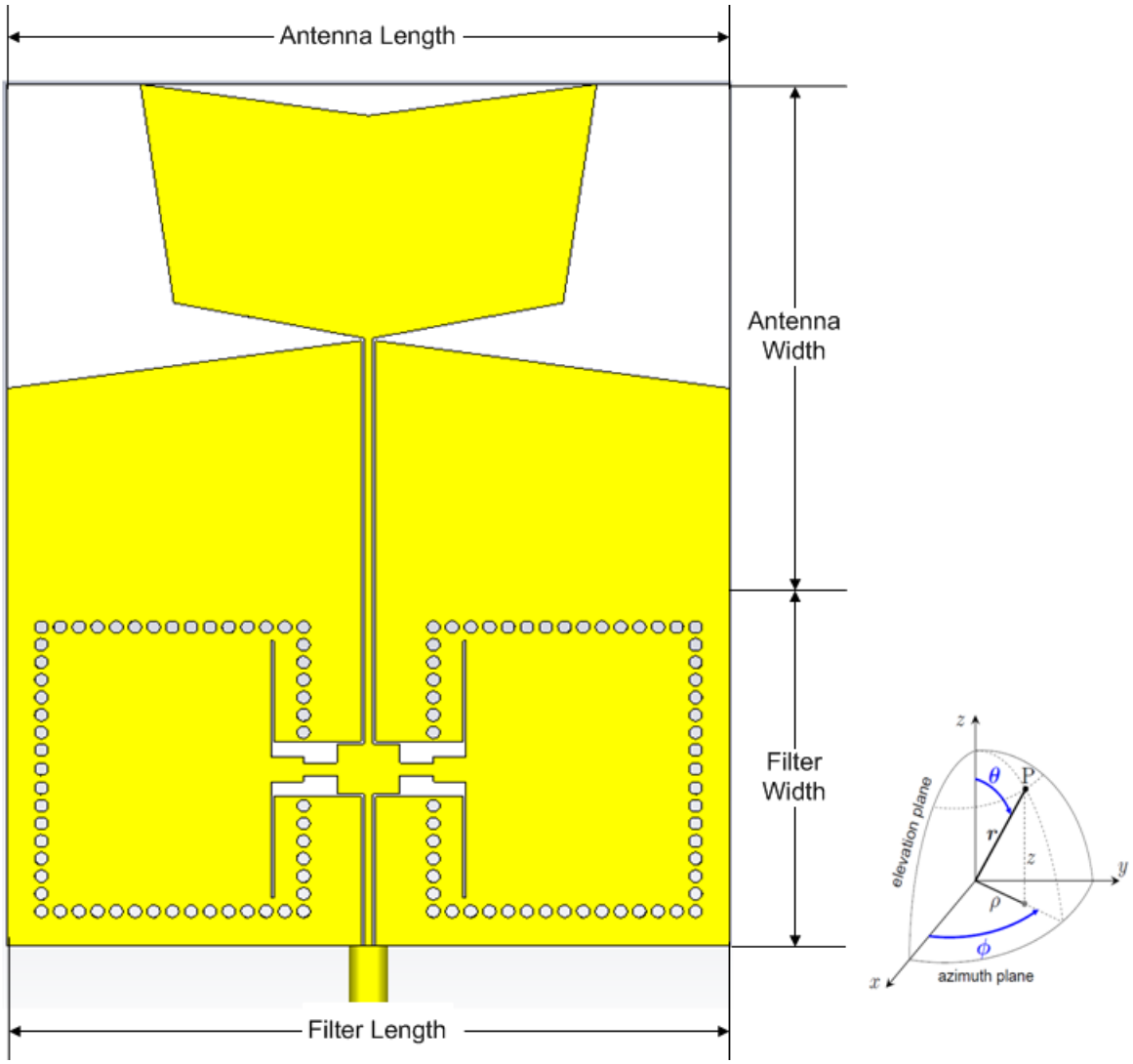

Figure 4.13: CPW UWB Antenna With Stop-band Filter

The frequency response depicts that the entire band from 3.1-10.6 GHz has been divided into three sub-bands. The first sub-band is from 4.1-4.6 GHz, the second one is from 6.6-8.2 GHz, and the third one is from 9.3-10.8 GHz. It proves that this CPW UWB antenna with stop-band filter performs according to theory. Next, it is

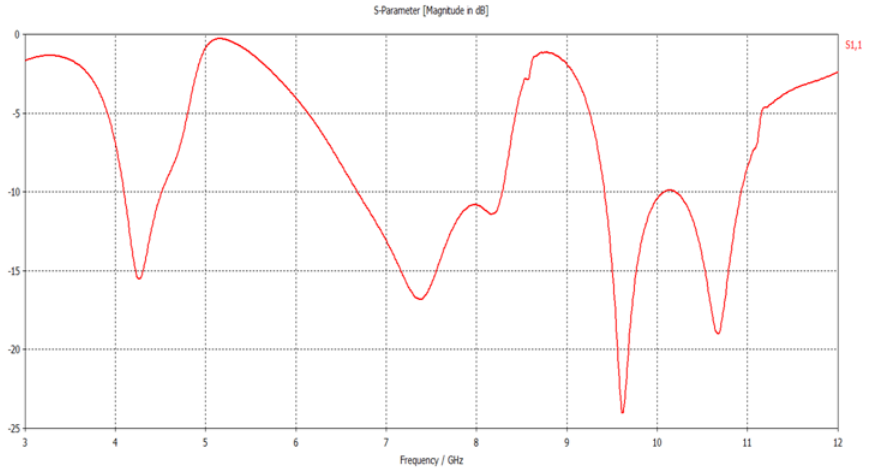

Figure 4.14: Frequency Response of The CPW UWB Antenna With Initial Dimensions

necessary to optimize all dimensions of the SIW structure and its distance from the antenna to get the best frequency response. After optimization, the total width of the structure becomes 70.5 mm. And its frequency response is shown in Figure 4.15. It can be observed that the optimized frequency response is smoother, the poles are more balanced, and even the first pass-band becomes wider.

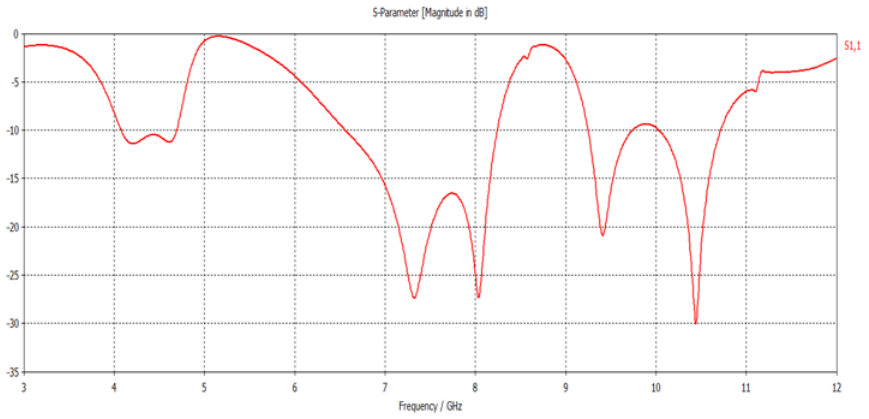

Figure 4.15: Frequency Response of The CPW UWB Antenna With Optimized Dimensions

The input signal applied to the CPW UWB antenna with band-stop filter (BSF)

is the same as that depicted in Figure 4.2 to Figure 4.4. After the input reflection coefficient (S_{11}) of this CPW UWB antenna with the BSF is simulated, it is necessary to verify the far-field performance of this antenna, including output signal response, gain, radiation pattern and group delay. As has been mentioned in the previous section, the minimum distance R in the far-field is given in Eqn 4.3. And since the largest dimension of this proposed antenna is 88.85 mm (diagonal distance of a 54.074 x 70.5 mm^2 PCB), R is 631 mm. Two probes are placed at this radius with $\theta = 90^o$ and $\phi = 90^o$. Hence, the output signal in the far-field for both θ and ϕ directions can be simulated. Figure 4.16 shows the output signal in the time domain. It can be observed that the signal in θ direction is much higher than the one in ϕ direction. That is because the θ direction is the co-polarization direction, and ϕ direction is the cross-polarization direction.

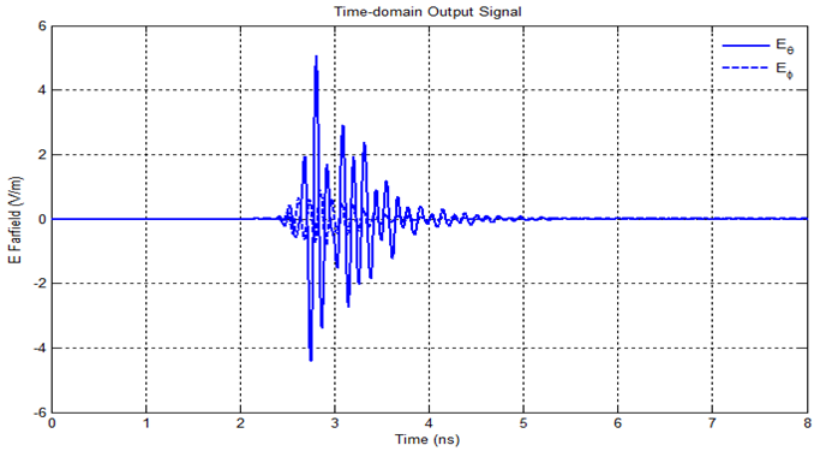

Figure 4.16: Output Signal of The CPW UWB Antenna With BSF

After the observation of the output signal in the time domain is completed, the output signal in the frequency domain can be observed. This will verify if the notch filter functions as expected. Figure 4.17 shows the amplitude of the output signal in the frequency domain and Figure 4.18 indicates its phase. It can be observed that

there are two notch points shown in Figure 4.17. One is between 5 and 6 GHz and the other is between 8 and 9 GHz. Moreover, the amplitude in the cross-polarization direction is much lower than that in the co-polarization direction.

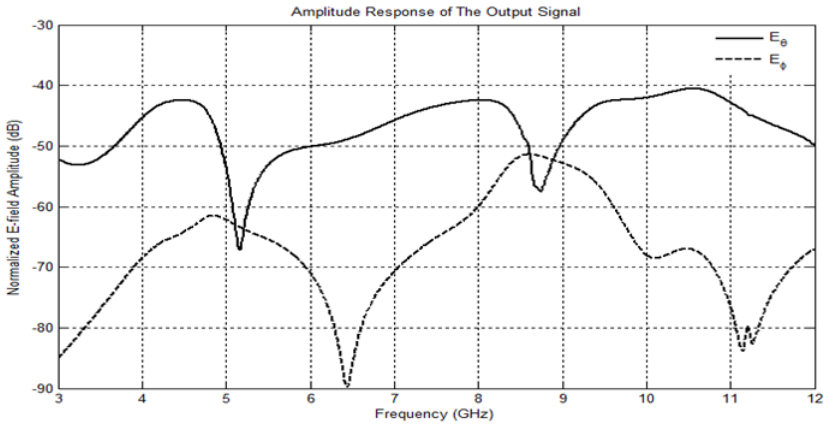

Figure 4.17: Amplitude of The Output Signal for The CPW UWB Antenna With BSF

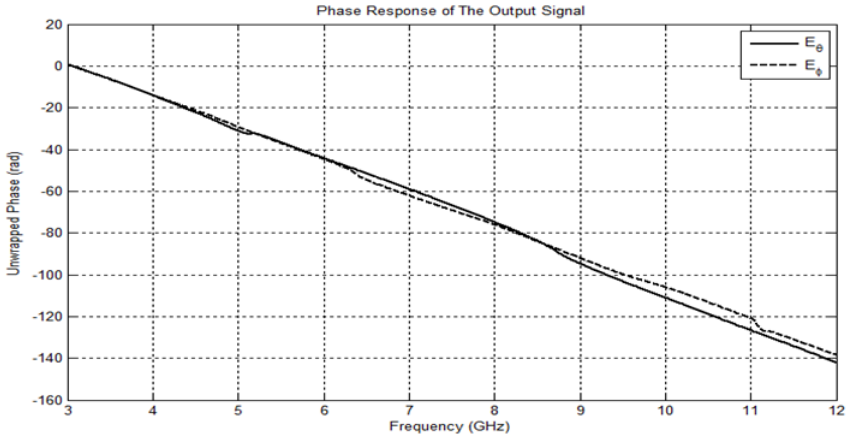

Figure 4.18: Phase of The Output Signal for The CPW UWB Antenna With BSF

Next, the farfield gain (Figure 4.19) will be examined. It can be observed that the realized gain (at $\theta = 90^o$ and $\phi = 90^o$) decreases to below 0 dB at 6 and 9 GHz, which are two frequencies in the stop band range. And the shapes of the gain in the

E-plane ($\phi = 90^o$ and varying θ) and in the H-plane ($\theta = 90^o$ and varying ϕ) agree with that of the realized gain across frequencies. The only difference is that the first notch point moves from 6 GHz to 5 GHz, but 5 GHz is still in the stop band range. It verifies that the notch filter functions properly.

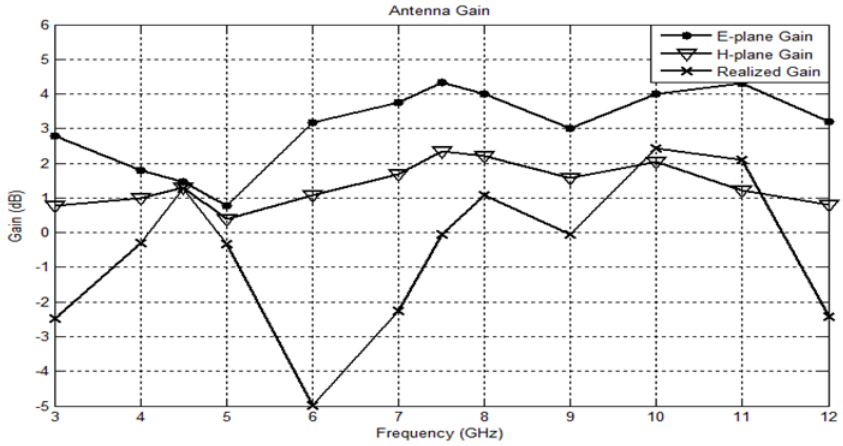

Figure 4.19: Gain of This CPW UWB Antenna

After that, the radiation patterns in both E-plane and H-plane need to be examined. Table 4.3 shows the frequencies to be simulated. The reason to choose these frequencies is that they individually represent different pass bands and stop bands.

Name	**Frequency (GHz)**	**Name**	**Frequency (GHz)**
f_1	4.3	f_2	5
f_3	7	f_4	9
f_5	10		

Table 4.3: Simulated Frequencies

Figure 4.20 (a) and Figure 4.20 (b) indicate the radiation patterns in the H-plane for both the co-polarization and the cross-polarization. And Figure 4.21 (a) and Figure 4.21 (b) illustrate the radiation patterns in the E-plane for both the polarizations. It can be observed that regardless of the principal plane (E-plane or H-

plane), the radiation patterns in the pass band frequencies have much higher power levels than those in the stop band frequencies. It indicates that the BSF in the antenna works well to block the signals from the stop band. Moreover, the radiation patterns of the co-polarization plots (Figure 4.20 (a) and Figure 4.21 (a)) show that this antenna is nearly omni-directional for those pass band frequencies. In addition, the radiation patterns of the cross-polarization plots (Figure 4.20 (b) and Figure 4.21 (b)) for those pass band frequencies have much lower power levels than those of the co-polarization plots. This indicates that the antenna radiates mainly in co-polarization direction. Over the pass band frequencies, the cross-polarized signal is at least 10 dB below the co-polarized one.

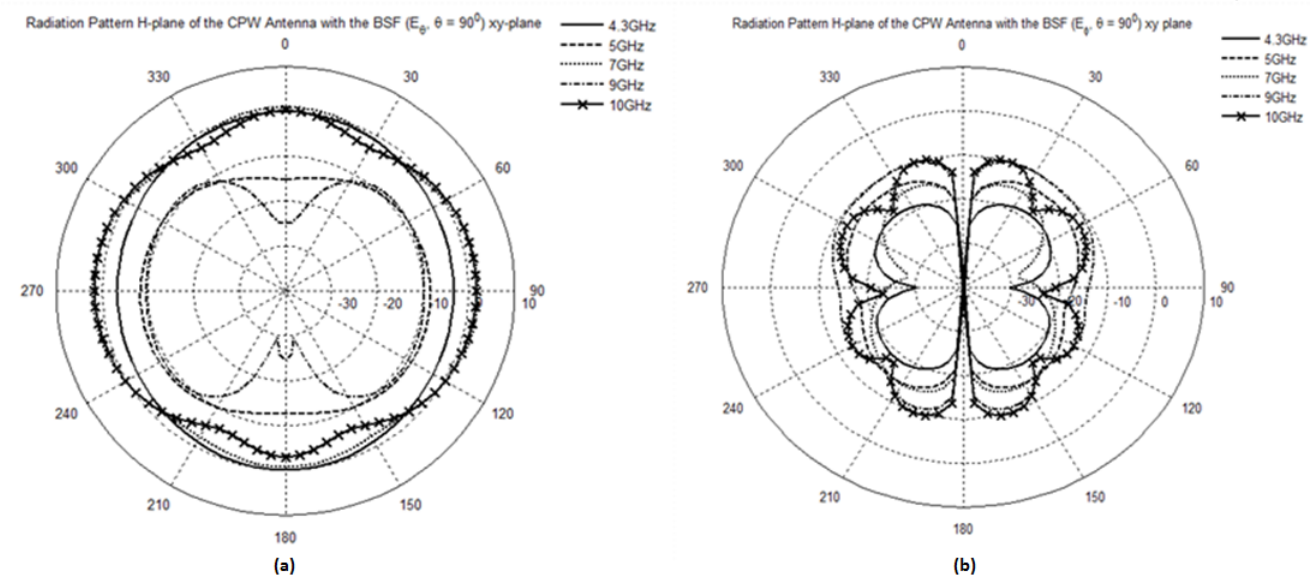

Figure 4.20: H-plane Radiation Patterns of The UWB Antenna With Band-stop Filter; (a) Co-polarization, (b) Cross-polarization

The group delay in Figure 4.22 is another important attribute in the performance evaluation of this CPW UWB antenna with the BSF. This figure illustrates the group delay in both the co-polarization and the cross-polarization directions. The variations of the group delay in both directions are less than 80 ps in the pass bands, and the

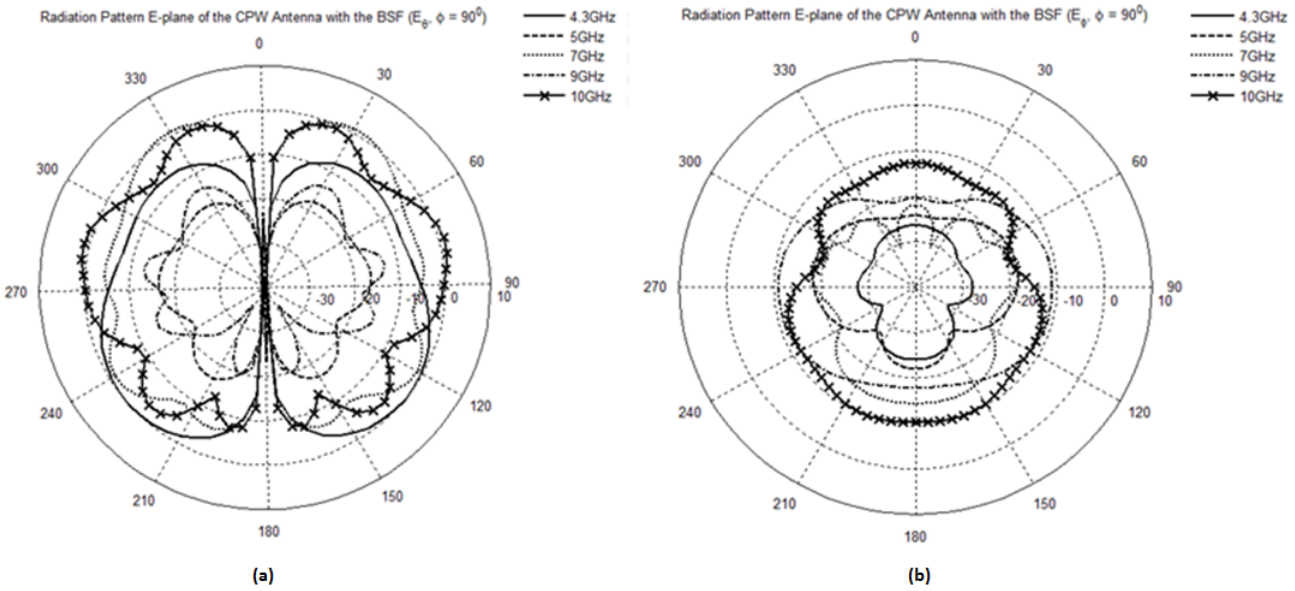

Figure 4.21: E-plane Radiation Patterns of The UWB Antenna With Band-stop Filter, (a) Co-polarization, (b) Cross-polarization

variations in the stop band are quite large. It demonstrates that this antenna has an acceptable group delay in the three pass bands.

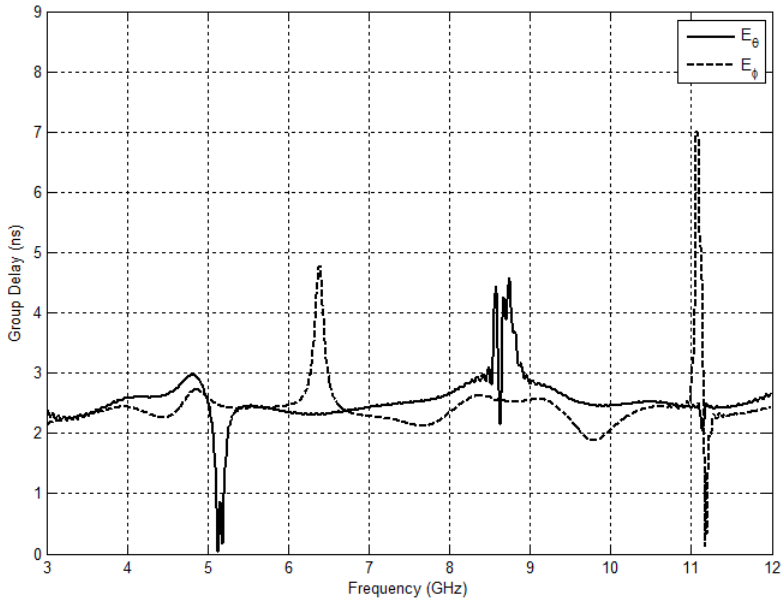

Figure 4.22: Group Delay for The CWP UWB Antenna with BSF

4.2.2 Measurement of CPW UWB Antenna With Band-stop Filter

After the design of this CPW UWB antenna with band-stop filter is completed, its prototype is fabricated. Figure 4.23 shows the front and back views of this antenna. It is necessary to measure the input reflection coefficient and the radiation patterns of this antenna and compare them with simulation results. This will verify the antenna design process.

Figure 4.23: (a) Antenna's Front View (b) Antenna's Back View

The first measurement is the input reflection coefficient. Figure 4.24 shows the measurement setup. The Network Analyzer in Figure 4.24 (a) represents the HP 8720C 50 MHz-20 GHz Network Analyzer, and the AUT is the designed antenna under test. Figure 4.24 (b) shows this CPW UWB antenna connected to Port1 of the Network Analyzer with a coaxial cable. The input reflection coefficient of the antenna is measured with an output signal of 0 dBm from the network analyzer. Figure 4.25 shows the measured input reflection cofficient in comparison with its simulation results. The red curve is the simulation result without Adaptive Mesh, whereas the blue curve is the simulation with Adaptive Mesh. Adaptive Mesh means

that when the CST software does the wave calculation, it uses different mesh steps to do the calculation. The simulation with Adaptive Mesh is more accurate. As can be seen, the measured curve is in agreement with the simulated ones. Furthermore, the simulation with Adaptive Mesh agrees better with measured results. It displays three pass bands and two stop bands, which proves that the BSF rejects the signals in the two stop bands.

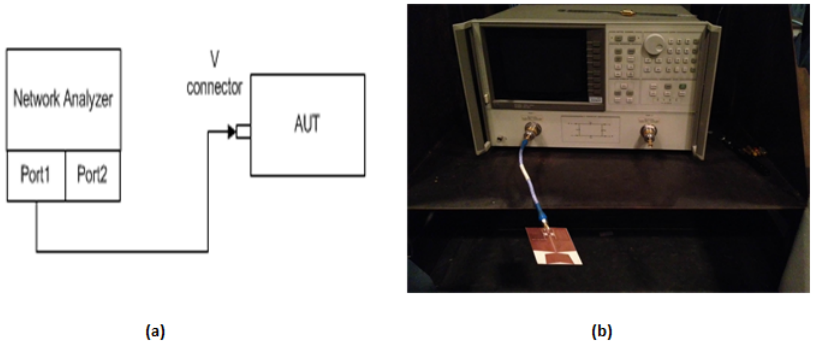

Figure 4.24: (a) Schematic View (b) Measurement Setup

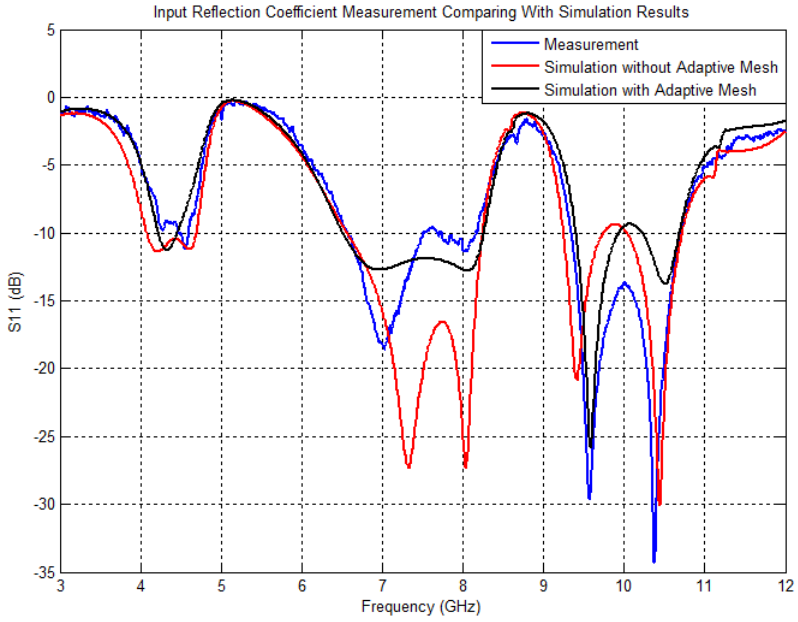

Figure 4.25: S_{11} Comparison between Measurement and Simulation

The second measurement is the antenna radiation pattern in the far-field. This measurement is performed in an anechoic chamber shown in Figure 4.26. This chamber is fully covered with pyramidal and walk-on absorbers which are made of radio absorbent material. The measurement contains only the direct path since reflected signal are absorbed. Figure 4.27 shows the setup for this radiation pattern measurement. The output signal power from the network analyzer is maintained at 0dBm.

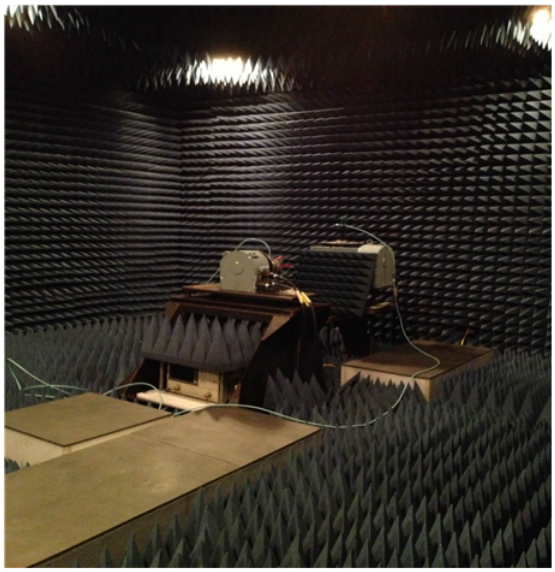

Figure 4.26: Anechoic Chamber View

The radiation patterns are measured by receiving the transmitted signal at different angles for the frequencies which are the same as those in the antenna simulation. This measurement will indicate the radiation direction of this antenna across frequencies in a test environment. The following figures (Figure 4.28, Figure 4.29, Figure 4.30, Figure 4.31 and Figure 4.32) illustrate the measured radiation patterns in comparison with the simulated ones.

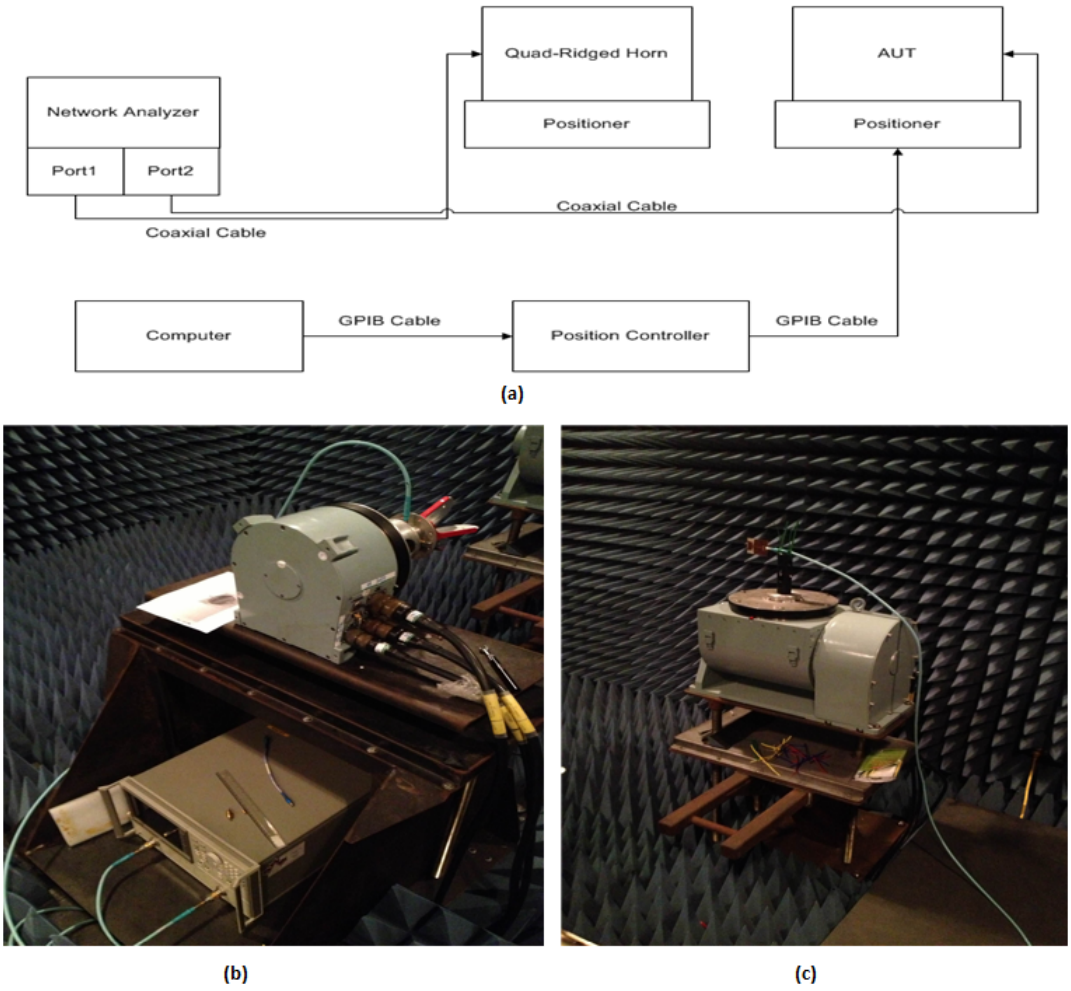

Figure 4.27: (a) Schematic View (b) Measurement Setup (c) AUT Setup

It can be observed that regardless of the principal plane (E-plane or H-plane), the measured radiation patterns agree well with the simulated ones. It demonstrates that the farfield of this antenna performs according to theoretical assumption. Since this antenna is omni-directional, the antenna gain was not measured at this point.

After both this antenna's input reflection coefficient and radiation patterns are measured, they all agree well with the simulation results. It proves that the design of this Co-planar UWB is valid.

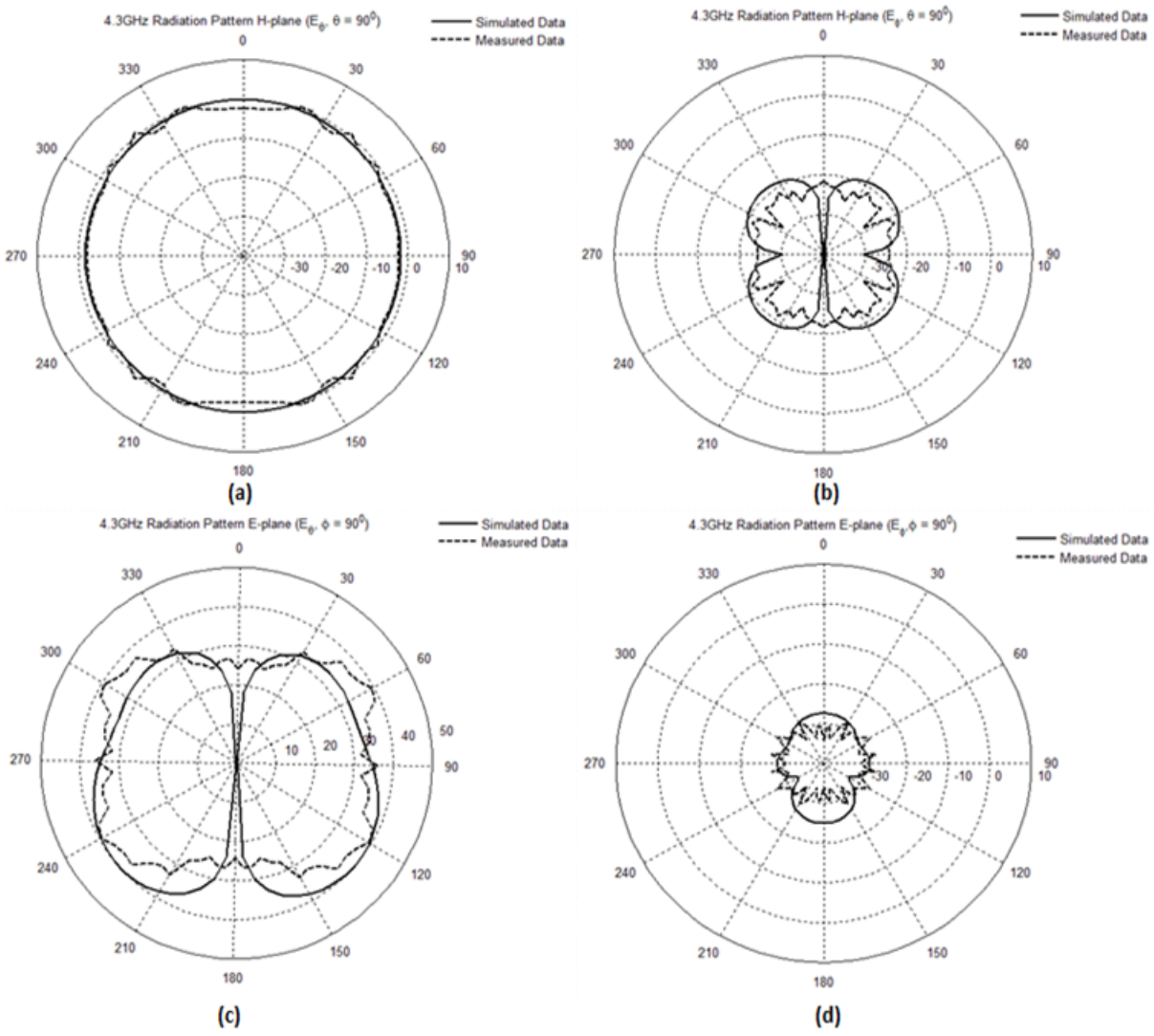

Figure 4.28: H-plane and E-plane Radiation Patterns Measurement of The UWB Antenna With Band-stop Filter at 4.3GHz; (a) H-plane Co-polarization, (b) H-plane Cross-polarization, (c) E-plane Co-polarization, (d) E-plane Cross-polarization

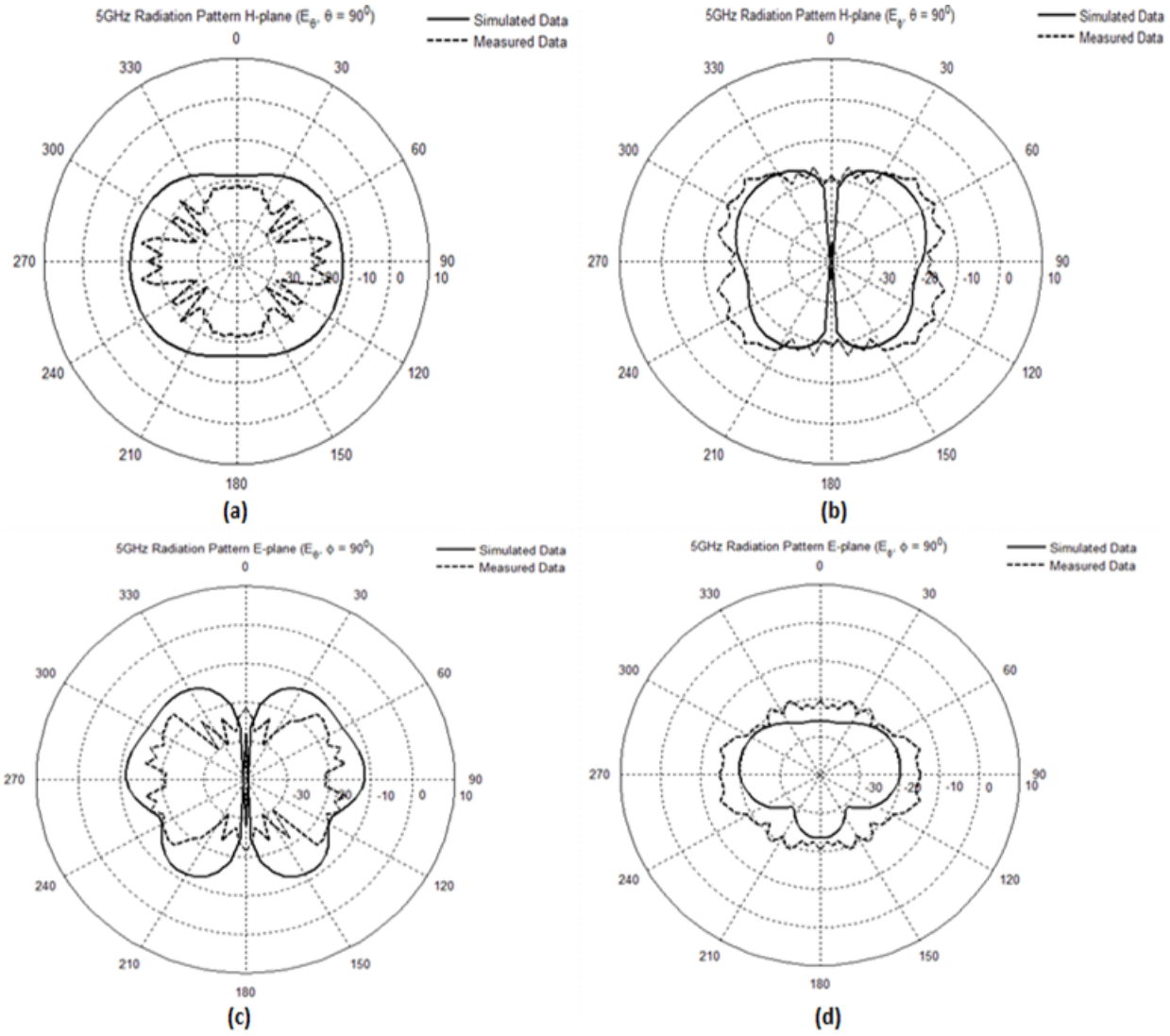

Figure 4.29: H-plane and E-plane Radiation Patterns Measurement of The UWB Antenna With Band-stop Filter at 5GHz; (a) H-plane Co-polarization, (b) H-plane Cross-polarization, (c) E-plane Co-polarization, (d) E-plane Cross-polarization

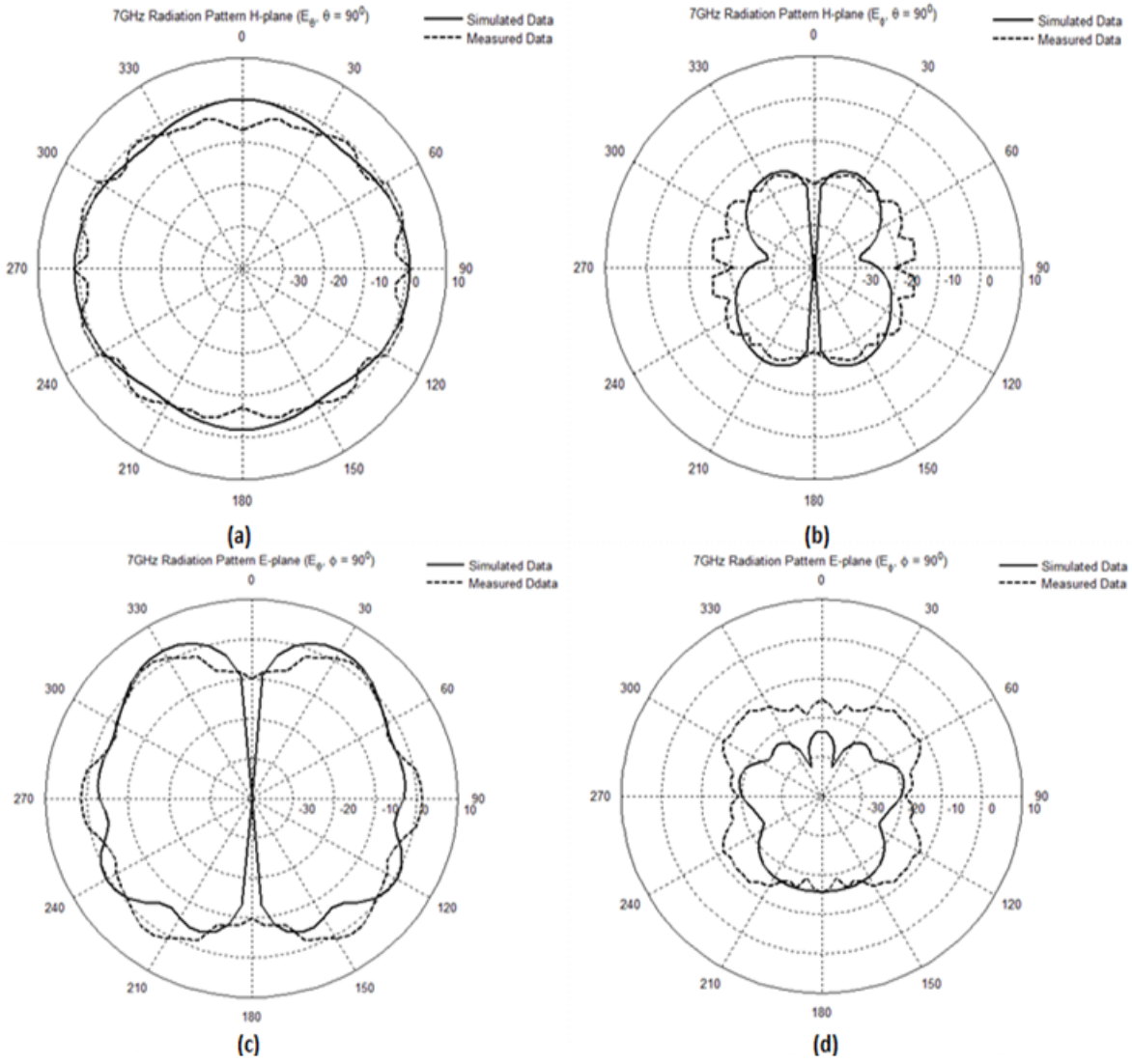

Figure 4.30: H-plane and E-plane Radiation Patterns Measurement of The UWB Antenna With Band-stop Filter at 7GHz; (a) H-plane Co-polarization, (b) H-plane Cross-polarization, (c) E-plane Co-polarization, (d) E-plane Cross-polarization

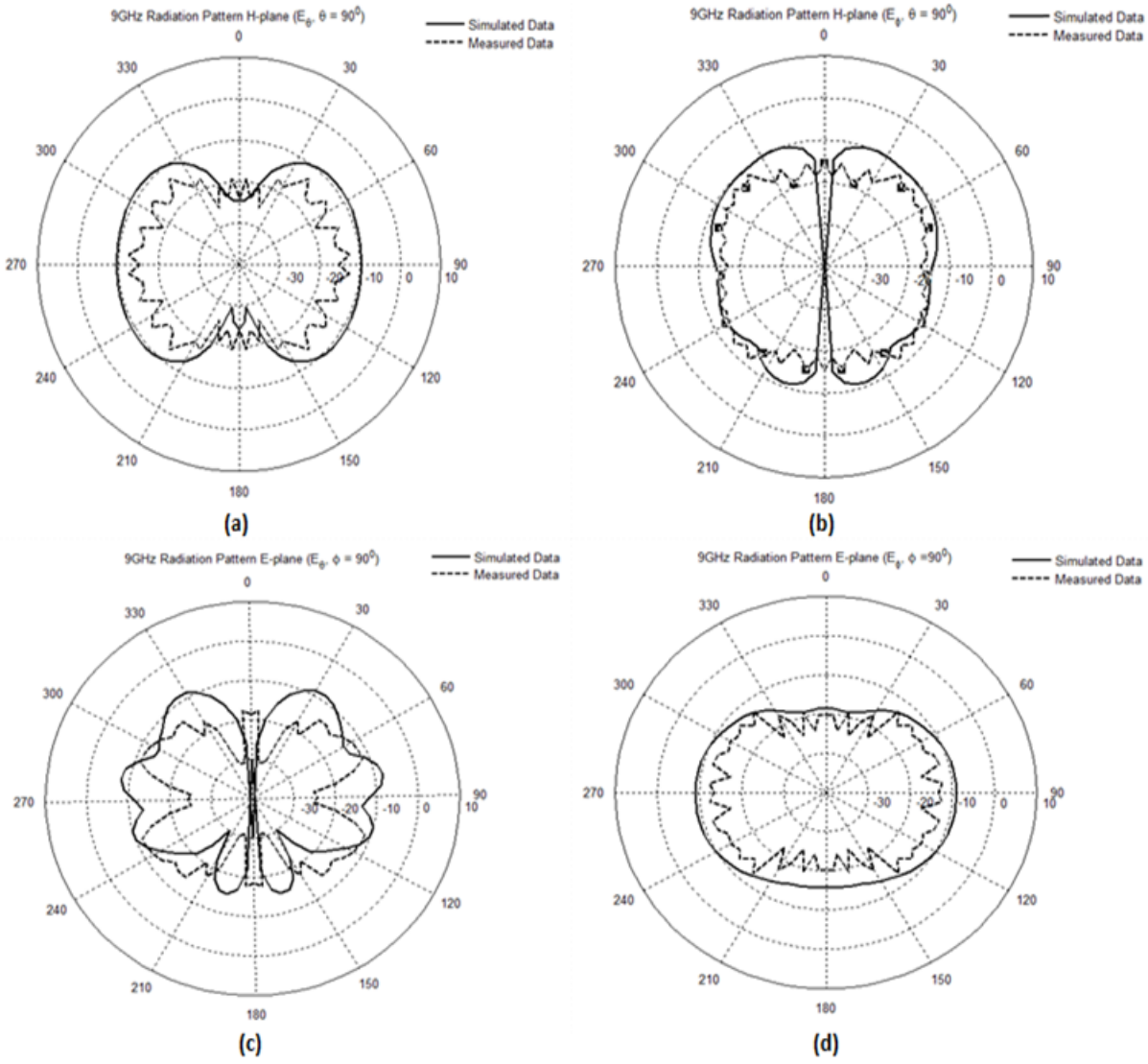

Figure 4.31: H-plane and E-plane Radiation Patterns Measurement of The UWB Antenna With Band-stop Filter at 9GHz; (a) H-plane Co-polarization, (b) H-plane Cross-polarization, (c) E-plane Co-polarization, (d) E-plane Cross-polarization

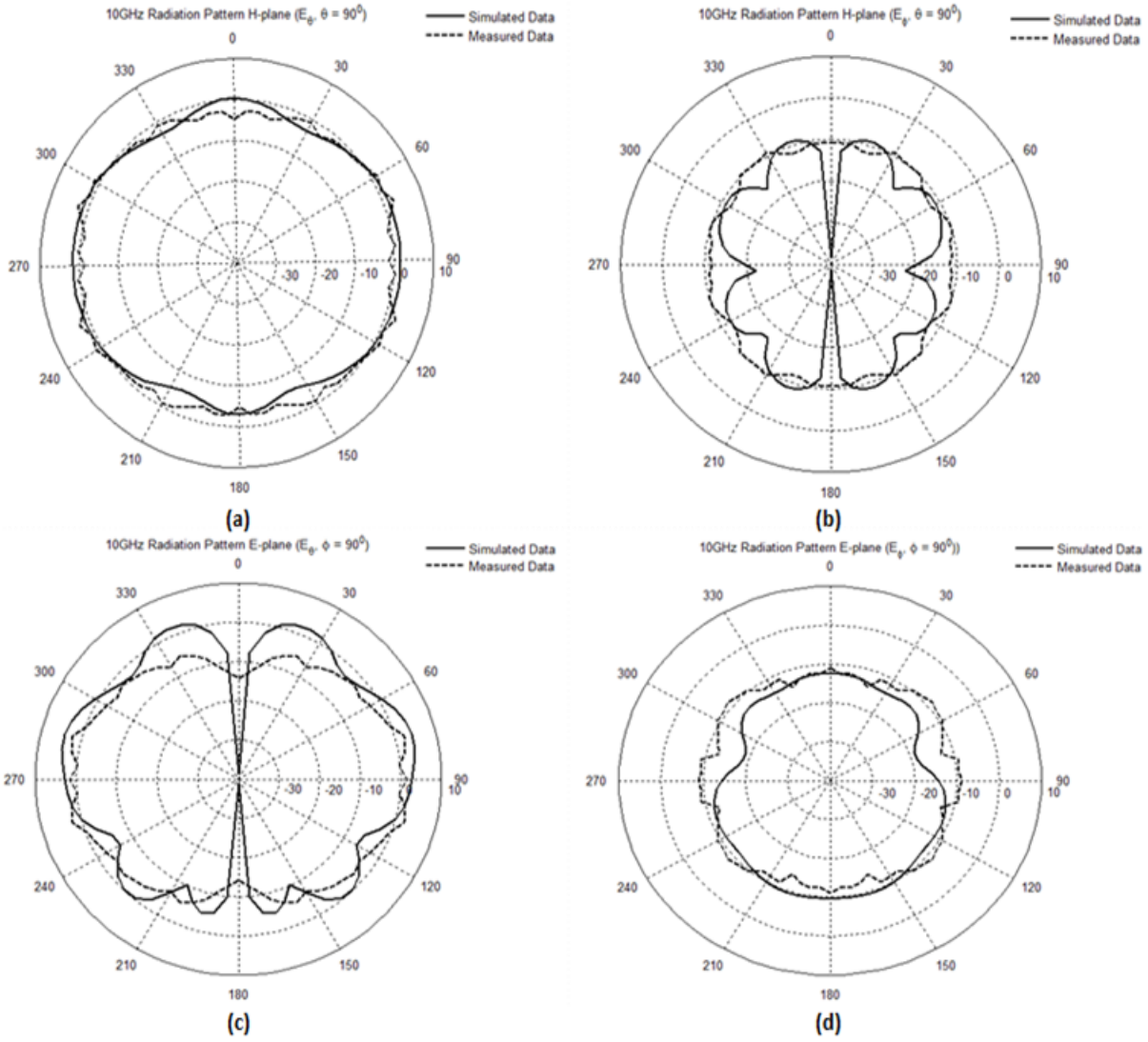

Figure 4.32: H-plane and E-plane Radiation Patterns Measurement of The UWB Antenna With Band-stop Filter at 10GHz; (a) H-plane Co-polarization, (b) H-plane Cross-polarization, (c) E-plane Co-polarization, (d) E-plane Cross-polarization

Chapter 5

Conclusions

UWB technology presents a viable solution for future telecommunication, radar and WPAN systems due to its extremely high data transmission rate. This high data rate is attributed to the large frequency spectrum. Since the FCC released the 3.1-10.6 GHz band for UWB communications, a large number of UWB applications have been developed. However, the existing wireless networks such as IEEE 802.11a and HIPERLAN/2 in Europe have occupied a band between 5 GHz and 6 GHz. It is necessary to design a UWB antenna with a band-rejection filter to avoid this interference. The research of such a filter is carried out and the design of a UWB antenna with this band-reject filter is achieved in this thesis.

Since there is a trend towards miniaturization of printed circuits, the development of an UWB antenna with both microstrip technology and co-planar technology has attracted more interest. Comparing with microstrip technology, co-planar technology is easier to fabricate, has wider impedance match and better S parameters. The UWB antenna with the band-reject filter in this thesis is prototyped in co-planar technology.

The research of this band-reject filter includes bent resonators in the ground plane,

DBRs in the ground plane, loaded EBGs in the ground plane, short-ended stubs in the main patch, periodically loaded slot resonators in the ground plane, DGS structures, and SIW structures. These circuits are modeled and simulated with CST Microwave Studio. The frequency responses of the first six models have different defects so that they are not practical enough to be exploited as a band-reject filter for this UWB antenna. However, the SIW structure has provided highest insertion loss in the stop band and the narrowest 3 dB bandwidth for the stop band. This SIW structure is chosen as the band-reject filter.

After the research of the band-reject filter is completed, a UWB antenna in CPW technology is modeled and simulated with CST Microwave Studio. According to this antenna's frequency response, gain, radiation pattern and group delay, it performs well as a UWB antenna. Then, the final design is to combine this antenna with the band-reject filter in order to separate the entire band into multiple sub-bands. Thus, it can avoid interference from other existing wireless communications between 5 GHz and 6 GHz. The final design is validated by its frequency response, gain, radiation pattern and group delay. At this point, the design of this CPW UWB antenna with the band-reject filter is accomplished. According to its tested performances, it can be exploited as a practical UWB antenna.

Bibliography

[1] H.G. Schantz. A brief history of UWB antennas. *IEEE Aerospace and Electronic Systems Magazine*, 19(4):22 – 26, April 2004.

[2] K. Kiminami, A. Hirata, and T. Shiozawa. Double-sided printed bow-tie antenna for UWB communications. *IEEE Antennas and Wireless Propagation Letters*, 3(1):152 – 153, 2004.

[3] J. Liang, C.C. Chiau, X. Chen, and C.G. Parini. Printed circular disc monopole antenna for ultra-wideband applications. *IET Electronics Letters*, 40(20):1246 – 1247, Sep. 2004.

[4] S.H. Choi, J.K. Park, S.K. Kim, and J.Y. Park. A new ultra-wideband antenna for UWB applications. *Microwave and Optical Technology Letters*, 40(5):399 – 401, Mar. 2004.

[5] Jianxin Liang, C.C. Chiau, Xiaodong Chen, and C.G. Parini. Study of a printed circular disc monopole antenna for UWB systems. *IEEE Transactions on Antennas and Propagation*, 53(11):3500 – 3504, Nov. 2005.

[6] Z.N. Low, J.H. Cheong, and C.L. Law. Low-cost PCB antenna for UWB applications. *IEEE Antennas and Wireless Propagation Letters*, 4:237 – 239, 2005.

[7] C.-C. Lin, Y.-C. Kan, L.-C. Kuo, and H.-R. Chuang. A planar triangular monopole antenna for UWB communication. *IEEE Microwave and Wireless Components Letters*, 15(10):624 – 626, 2005.

[8] H.R. Chuang, C.C. Lin, and Y.C. Kan. A printed UWB triangular monopole antenna. *Microwave Journal*, 49:108 – 120, Jan. 2006.

[9] K. Rambabu, M.Z. Alam, and J. Bornemann. Design of compact dual-polarized printed-circuit antenna for ultra-wideband applications. In *36th European Microwave Conference, Proceedings*, pages 626 –629, Sep. 2006.

[10] D.-C. Chang, J.-C. Liu, and M.-Y. Liu. A novel tulip-shaped monopole antenna for UWB applications. *Microwave and Optical Technology Letters*, 48(2):307 – 312, Feb. 2006.

[11] S.-F. Tseng and C.-L. Huang. Ultrawideband planar microstrip-fed monopole antenna. *Microwave and Optical Technology Letters*, 49(1):183 – 185, Jan. 2007.

[12] J. Liang, C.C. Chiau, X. Chen, and C.G. Parini. CPW-fed circular ring monopole antenna. In *IEEE Antennas and Propagation Society International Symposium Digest*, volume 2A, pages 500 – 503, July. 2005.

[13] A.M. Abbosh, M.E. Bialkowski, M.V. Jacob, and J. Mazierska. Investigations into an LTCC based ultra wideband antenna. In *Asia-Pacific Microwave Conference, Proceedings*, volume 3, pages 1 – 4, Dec. 2005.

[14] C.T.H. Lim. A GCPW-fed printed antenna for UWB applications. In *Asia-Pacific Microwave Conference, Proceedings*, volume 4, pages 1 – 3, Dec. 2005.

[15] X. Chen, J. Liang, P. Li, L. Guo, C.C. Chiau, and C.G. Parini. Planar UWB monopole antennas. In *Asia-Pacific Microwave Conference, Proceedings*, volume 1, pages 1 – 4, Dec. 2005.

[16] H.K. Lee, J.K. Park, and J.N Lee. Design of a planar half-circle shaped UWB notch antenna. *Microwave and Optical Technology Letters*, 47(1):9 – 11, Oct. 2005.

[17] Tzyh-Ghuang Ma and Chao-Hsiung Tseng. An ultrawideband coplanar waveguide-fed tapered ring slot antenna. *IEEE Transactions on Antennas and Propagation*, 54(4):1105 – 1110, Apr. 2006.

[18] Yi-Chieh Lee, Syuan-Ci Lin, and Jwo-Shiun Sun. CPW-fed UWB slot antenna. In *Asia-Pacific Microwave Conference, Proceedings*, pages 1636 –1639, Dec. 2006.

[19] S. Nikolaou, D.E. Anagnostou, G.E. Ponchak, M.M. Tentzeris, and J. Papapolymerou. Compact ultra wide-band (UWB) CPW-fed elliptical monopole on liquid crystal polymer (LCP). In *IEEE Antennas and Propagation Society International Symposium Digest*, pages 4657 –4660, July. 2006.

[20] E.S. Angelopoulos, A.Z. Anastopoulos, C.E. Githonas, and D.I. Kaklamani. A modified bow-tie slot antenna fed by a CPW-to-CPW transition loaded with inductively coupled slots for ultra wide-band applications. In *IEEE International Workshop on Antenna Technology: Small Antennas and Novel Metamaterials, IWAT 2005*, pages 513 – 516, Mar. 2005.

[21] X.-L. Liang, S.-S. Zhong, and W. Wang. UWB printed circular monopole antenna. *Microwave and Optical Technology Letters*, 48(8):1532 – 1534, Aug. 2006.

[22] J.-S. Sun, Y.-C. Lee, and S.-C. Lin. New design of a CPW-fed ultrawideband slot antenna. *Microwave and Optical Technology Letters*, 49(3):561 – 564, Mar. 2007.

[23] D.-B. Lin, I.-T. Tang, and M.-Y. Tsou. A compact UWB antenna with CPW-feed. *Microwave and Optical Technology Letters*, 49(3):564 – 567, Mar. 2007.

[24] R. Chair, A.A. Kishk, and K.F. Lee. Ultrawide-band coplanar waveguide-fed rectangular slot antenna. *IEEE Antennas and Wireless Propagation Letters*, 3(1):227 –229, 2004.

[25] N. Fortino, G. Kossiavas, J.Y. Dauvignac, and R. Staraj. Novel antenna for ultra-wideband communications. *Microwave and Optical Technology Letters*, 41(3):166 – 169, May. 2004.

[26] W. Wang, S.S. Zhong, and S.-B. Chen. A novel wideband coplanar-fed monopole antenna. *Microwave and Optical Technology Letters*, 43(1):50 – 52, Oct. 2004.

[27] Joon Il Kim and Yong Jee. Design of ultrawideband coplanar waveguide-fed LI-shape planar monopole antennas. *IEEE Antennas and Wireless Propagation Letters*, 6:383 – 387, 2007.

[28] Zhi Ning Chen and Xianming Qing. Research and development of planar UWB antennas. In *Asia-Pacific Microwave Conference, Proceedings*, volume 1, pages 1 – 4, Dec. 2005.

[29] B.L. Ooi, G. Zhao, M.S. Leong, K.M. Chua, and C.W.L. Albert. Wide-band LTCC CPW-fed two-layered monopole antenna. *IET Electronics Letters*, 41(16):9 – 10, Aug. 2005.

[30] K. Rambabu, H.A. Thiart, J. Bornemann, and S.Y. Yu. Ultrawideband printed-circuit antenna. *IEEE Transactions on Antennas and Propagation*, 54(12):3908 –3911, Dec. 2006.

[31] Z. Ying and J. Andersson. An ultra wideband "cobra" patch antenna. *IEE Proceedings Microwaves, Antennas and Propagation*, 151(6):486 – 490, Dec. 2004.

[32] H.M. Zamel, A.M. Attiya, and E.A. Hashish. Design of a compact UWB planar antenna with band-notch characterization. In *National Radio Science Conference, Proceedings*, pages 1 – 8, Mar. 2007.

[33] Qing-Xin Chu and Ying-Ying Yang. A compact CPW-fed planar ultra-wideband antenna with a frequency notch characteristic. In *Asia-Pacific Microwave Conference, Proceedings*, pages 1 – 4, Dec. 2007.

[34] Se-Hwan Choi, Ho-Jun Lee, and Jong-Kyu Kim. Design of a ultra-wideband antenna with band notch characteristic. In *IEEE Antennas and Propagation Society International Symposium Digest*, pages 1 – 4, July. 2008.

[35] H.M. Jafari, M.J. Deen, S. Hranilovic, and N.K. Nikolova. Slot antenna for ultra-wideband applications. In *IEEE Antennas and Propagation Society International Symposium Digest*, pages 1107 – 1110, July. 2006.

[36] R.J. Fontana. A brief history of UWB communications. *Transmission Microwave Theory and Technology*, 14(11):528 – 547, 1966.

[37] H.-J. Lam. Ultra-wideband antenna in coplanar technology. M.A.Sc. Thesis, Dept. of ECE, University of Victoria, Victoria, B.C., Canada, 2007.

[38] H. Sheng, P. Orlik, A.M. Haimovich, L.J. Cimini, and J. Zhang. On the spectral and power requirements for ultra-wideband transmission. In *IEEE International Conference on Communications, Proceedings*, volume 1, pages 738 – 742, May. 2003.

[39] Faranak Nekoogar. *Ultra-Wideband Communications: Fundamentals and Applications*. Prentice Hall, 2005.

[40] G.F. Ross. The transient analysis of certain TEM mode four-port networks. *IEEE Transactions on Microwave Theory and Techniques*, 14(11):528 – 542, Nov. 1966.

[41] T.W. Barrett. History of ultrawideband (UWB) radar & communications: Pioneers and innovators. In *Progress In Electromagnetics Research Symposium, Proceedings*, July 2000.

[42] R.J. Fontana. Recent applications of ultra wideband radar and communications systems. In *Ultra-Wideband, Short-Pulse Electromagnetics 5*, volume 1, pages 225 – 234, 2002.

[43] O. Lodge. Electric telegraphy. U.S. Patent 609,154 (August 16, 1898).

[44] P.S. Carter. Short wave antenna. U.S. Patent 2,175,252 (October 10, 1939).

[45] P.S. Carter. Wide band, short wave antenna and transmission line system. U.S. Patent 2,181,870 (December 5, 1939).

[46] L.N. Brillouin. Broad band antenna. U.S. Patent 2,454,766 (November 30, 1948).

[47] A.P. King. Transmission, radiation, and reception of electromagnetic waves. U.S. Patent 2,283,935 (May 26, 1942).

[48] M. Katzin. Electromagnetic horn radiator. U.S. Patent 2,398,095 (April 9, 1946).

[49] R.W. Master. Antenna. U.S. Patent 2430353 (November 4, 1947).

[50] H.G. Schantz and L. Fullerton. The diamond dipole: A gaussian impulse antenna. In *IEEE Antennas and Propagation Society International Symposium Digest*, volume 4, pages 100 – 103, 2001.

[51] W. Stohr. Broadband ellipsoidal dipole antenna. U.S. Patent 3,364,491, (January 16, 1968).

[52] H. Harmuth. Frequency independent shielded loop antenna. U.S. Patent 4,506,267 (March 19, 1985).

[53] Jens Bornemann. Lecture notes on antennas and propagation. University of Victoria, Spring 2012.

[54] J. Liang. Antenna study and design for ultra wideband communication applications. Ph.D. Dissertation, Dept. of ECE, University of London, United Kingdom, London, England, 2006.

[55] H.G. Schantz. Introduction to ultra-wideband antennas. In *IEEE Conference on Ultra Wideband Systems and Technologies, Proceedings*, pages 1 – 9, Nov. 2003.

[56] Abdallah Alshehri. *Mobile and Wireless Communications Network Layer and Circuit Level Design*. NewYork: InTech, 2010.

[57] M. Ho, L. Taylor, and G.R. Aiello. UWB technology for wireless video networking. In *IEEE International Conference on Consumer Electronics, Proceedings*, pages 18 – 19, 2001.

[58] M. Welborn, T. Miller, J. Lynch, and J. McCorkle. Multi-user perspectives in UWB communications networks. In *IEEE Conference on Ultra Wideband Systems and Technologies, Proceedings*, pages 271 – 275, 2002.

[59] M.R. Mahfouz, Cemin Zhang, B.C. Merkl, M.J. Kuhn, and A.E. Fathy. Investigation of high-accuracy indoor 3-D positioning using UWB technology. *IEEE Transactions on Microwave Theory and Techniques*, 56(6):1316 – 1330, June 2008.

[60] C. Zhang and A.E. Fathy. Reconfigurable pico-pulse generator for UWB applications. In *IEEE MTT-S International Microwave Symposium Digest*, pages 407 – 410, June 2006.

[61] K. Thirumalaivasan and R. Nakkeeran. UWB bandpass filter with notched band for the rejection of 5 GHz WLAN using hexagonal multiple mode resonator. In *IEEE International Conference on Communication Control and Computing Technologies (ICCCCT), Proceedings*, pages 21 – 24, Oct. 2010.

[62] G.L. Matthaei, L. Young, and E.M.T. Jones. *Microwave filters, impedance-matching networks, and coupling structures.* Boston, MA: Artech House, 1980.

[63] K. Rambabu, M.Y.-W. Chia, Khee Meng Chan, and J. Bornemann. Design of multiple-stopband filters for interference suppression in UWB applications. *IEEE Transactions on Microwave Theory and Techniques*, 54(8):3333 – 3338, Aug. 2006.

[64] C. Quendo, E. Rius, and C. Person. Narrow bandpass filters using dual-behavior resonators. *IEEE Transactions on Microwave Theory and Techniques*, 51(3):734 – 743, Mar. 2003.

[65] K.C. Gupta, Ramesh. Garg, I. Bahl, and Prakash Bhartia. *Microstrip Lines and SlotLines*. Boston, MA: Artech House, 1996.

[66] M.F. Karim, A.-Q. Liu, A. Alphones, X.J. Zhang, and A.B. Yu. CPW band-stop filter using unloaded and loaded EBG structures. *IEE Proceedings Microwaves, Antennas and Propagation*, 4:434 – 440, Dec. 2005.

[67] H.W. Liu, T. Yoshimasu, and L.L. Sun. CPW bandstop filter using periodically loaded slot resonators. *IET Electronics Letters*, 42(6):352 – 353, Mar. 2006.

[68] H.B. El-Shaarawy, F. Coccetti, R. Plana, M. El-Said, and E.A. Hashish. A novel reconfigurable DGS cell for multi-stopband filter on CPW technology. In *Asia-Pacific Microwave Conference, Proceedings*, pages 1 – 4, Dec. 2008.

[69] F. Taringou and J. Bornemann. Return-loss investigation of the equivalent width of substrate-integrated waveguide circuits. In *IEEE MTT-S International Microwave Workshop Series on Millimeter Wave Integration Technologies (IMWS)*, pages 140 – 143, Sep. 2011.

[70] Ke Wu. Substrate integrated circuits (SICs) for GHz and THz electronics and photonics: Current status and future outlook. In *2010 German Microwave Conference, Proceedings*, pages 292 – 295, Mar. 2010.

[71] Jens Bornemann. Lecture notes on waveguide technology. University of Victoria, Summer 2012.

[72] M. Mokhtaari and J. Bornemann. Printed-circuit antennas for 3-30 GHz and 3-60 GHz UWB applications. In *2010 Asia-Pacific Microwave Conference, Proceedings*, pages 1922 – 1925, Dec. 2010.

Appendix A

Ultra-Wideband (UWB Technology) Enabling High-speed Wireless Personal Area Networks

Ultra-Wideband (UWB Technology)

Enabling high-speed wireless personal area networks.

Contents

Executive Summary

Wireless connectivity has enabled a new mobile lifestyle filled with conveniences for mobile computing users. Consumers will soon demand the same conveniences throughout their digital home, connecting their PCs, personal digital recorders, MP3 recorders and players, digital camcorders and digital cameras, high-definition TVs (HDTVs), set-top boxes (STBs), gaming systems, personal digital assistants (PDAs), and cell phones, to connect to each other in a wireless personal area network (WPAN) in the home. But today's wireless LAN and WPAN technologies cannot meet the needs of tomorrow's connectivity of such a host of emerging consumer electronic devices that require high bandwidth. A new technology is needed to meet the needs of high-speed WPANs.

Ultra-wideband (UWB) technology offers a solution for the bandwidth, cost, power consumption, and physical size requirements of next-generation consumer electronic devices. UWB enables wireless connectivity with consistent high data rates across multiple devices and PCs within the digital home and the office. This emerging technology provides the high bandwidth that multiple digital video and audio streams require throughout the home.

With the support of industry workgroups, such as the wireless universal serial bus (USB) workgroup, and technology leaders, like Intel, UWB technology promises to make it easy to create high-speed WPANs that can connect devices throughout the home.

Introduction

The benefits of an increasingly mobile lifestyle introduced by wireless technologies in cell phones and home PCs have resulted in greater demand for the same benefits in other consumer devices. Consumers enjoy the increased convenience of wireless connectivity. They will soon demand it for their video recording and storage devices, for real-time audio and video (AV) streaming, interactive gaming, and AV conferencing services as the need for digital media becomes more predominate in the home.

Many technologies used in the digital home, such as digital video and audio streaming, require high-bandwidth connections to communicate. Considering the number of devices used throughout the digital home, the bandwidth demand for wireless connectivity among these devices becomes very large indeed. The wireless networking technologies developed for wirelessly connecting PCs, such as Wi-Fi* and Bluetooth* Technology, are not optimized

for multiple high-bandwidth usage models of the digital home. Although data rates can reach 54 Mbps for Wi-Fi, for example, the technology has limitations in a consumer electronics environment, including power consumption and bandwidth. When it comes to connecting multiple consumer electronics (CE) devices in a short-range network, or WPAN, a wireless technology needs to support multiple high data rate streams, consume very little power, and maintain low cost, while sometimes fitting into a very small physical package, such as PDA or cell phone. The emerging UWB wireless technology and silicon developed for UWB applications offer a compelling solution.

This document describes UWB technology and presents potential applications for UWB technology for use in WPANs in the digital home.

The Case for UWB

The emerging digital home environment is made up of many different CE devices (e.g., digital video and audio players), mobile devices (e.g., cellular phones and PDAs), and personal computing devices (e.g., mobile notebook PCs) that will support a multitude of applications. These devices fall into three general overlapping categories (Figure 1):

- PC and the Internet
- Consumer electronics and the broadcast system
- Mobile and handheld devices

These devices have traditionally been kept in different rooms and used for different functions. Increasingly, however, owners expect them to interact – MP3 players exchanging files with PCs, digital video recorders communicating with STBs, etc. This convergence of device segments calls for a common wireless technology and radio that allows them to easily interoperate and delivers high throughput to accommodate multiple, high-speed applications. Currently, these segments utilize different interfaces and content formats.

The next generation of PC, consumer electronics, and mobile applications demand connectivity speeds beyond the 1 Mbps peak data rate of Bluetooth Technology, which is used by many devices to create WPANs today. But many CE devices cannot support the cost and power required by the higher speed 802.11a/b/g radios for Wi-Fi networking.

While Wi-Fi is much faster than Bluetooth Technology, it still does not deliver sufficient performance to effectively allow streaming of multiple simultaneous high-quality video streams. UWB technology provides the throughput required by the next generation of converged devices. Plus, the support of industry initiatives, such as the WiMedia* Alliance, will help ensure interoperability across multiple protocols, including IEEE 1394, USB, and Universal Plug and Play (UPnP*), making UWB a broad technology solution for creating high-speed, low-cost, and low-power WPANs.

Figure 1. Convergence of device segments

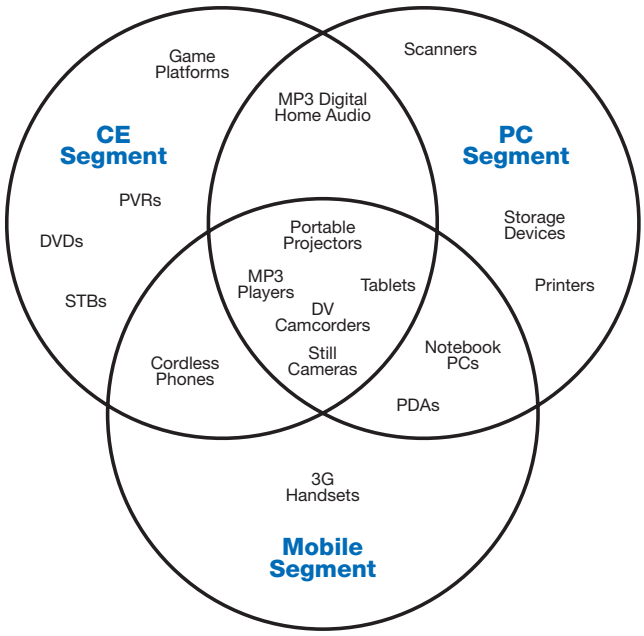

UWB Technology

UWB differs substantially from conventional narrowband radio frequency (RF) and spread spectrum technologies (SS), such as Bluetooth Technology and 802.11a/b/g. UWB uses an extremely wide band of RF spectrum to transmit data (Figure 2). In so doing, UWB is able to transmit more data in a given period of time than the more traditional technologies.

The potential data rate over a given RF link is proportional to the bandwidth of the channel and the logarithm of the signal-to-noise ratio (Shannon's Law). RF design engineers typically have little control over the bandwidth parameter, because this is dictated by FCC regulations that stipulate the allowable bandwidth of the signal for a given radio type and application. Bluetooth Technology, 802.11a/b/g Wi-Fi, cordless phones, and numerous other devices are relegated to the unlicensed frequency bands that are provided at 900 MHz, 2.4 GHz, and 5.1 GHz. Each radio channel is constrained to occupy only a narrow band of frequencies, relative to what is allowed for UWB.

UWB is a unique and new usage of a recently legalized frequency spectrum. UWB radios can use frequencies from 3.1 GHz to 10.6 GHz – a band more than 7 GHz wide. Each radio channel can have a bandwidth of more than 500 MHz, depending on its center frequency. To allow for such a large signal bandwidth, the FCC put in place severe broadcast power restrictions. By doing so, UWB devices can make use of an extremely wide frequency band while not emitting enough energy to be noticed by narrower band devices nearby, such as 802.11a/b/g radios. This sharing of spectrum allows devices to obtain very high data throughput, but they must be within close proximity.

UWB's low power requirements make it feasible to develop cost-effective CMOS implementations of UWB radios. With the characteristics of low power, low cost, and very high data rates at limited range, UWB is positioned to address the market for a high-speed WPAN.

UWB technology also allows spectrum reuse. A cluster of devices in proximity (for example, an entertainment system in a living area) can communicate on the same channel as another cluster of devices in another room (for example, a gaming system in a bedroom). UWB-based WPANs have such a short range that nearby clusters can use the same channel without causing interference. An 802.11g WLAN solution, however, would quickly use up the available data bandwidth in a single device cluster, and that radio channel would be unavailable for reuse anywhere else in the home. Because of UWB technology's limited range, 802.11 WLAN solutions are an excellent complement to a WPAN, serving as a backbone for data transmission between home clusters.

UWB Applications

UWB technology can enable a wide variety of WPAN applications. Examples include:

- Replacing cables between portable multimedia CE devices, such as camcorders, digital cameras, and portable MP3 players, with wireless connectivity
- Enabling high-speed wireless universal serial bus (WUSB) connectivity for PCs and PC peripherals, including printers, scanners, and external storage devices
- Replacing cables in next-generation Bluetooth Technology devices, such as 3G cell phones, as well as IP/UPnP-based

Figure 2. Comparison of narrowband (NB), spread spectrum (SS), and ultra-wideband (UWB) signal concepts

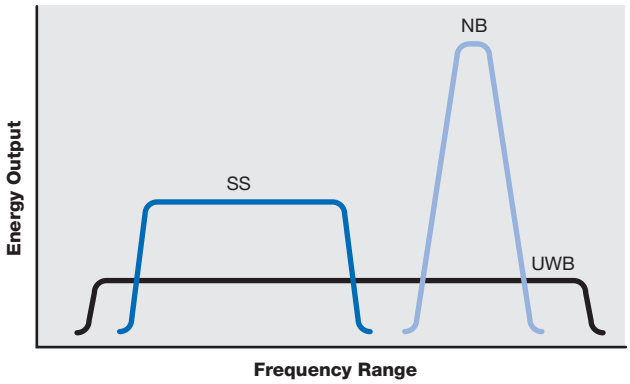

SS = Spread Spectrum
NB = Narrowband
UWB = Ultra-Wideband

connectivity for the next generation of IP-based PC/CE/mobile devices

- Creating ad-hoc high-bit-rate wireless connectivity for CE, PC, and mobile devices

Wireless PC peripheral connectivity

For wireless PC peripheral connectivity, UWB Technology can take the performance and ease-of-use found in USB to the next level. Presently, wired USB has significant market segment share as the cable interconnect of choice for the PC platform (Figure 3). But the cable can get in the way. Bluetooth Technology has resolved this issue to some degree, but has performance limitations and interoperability problems. A UWB-enabled WUSB solution provides the performance users have come to expect from wired USB without the cable. Enabling untethered USB connectivity, UWB has the possibility of gaining significant volume in the PC peripheral interconnect market segment. The Wireless USB Working Group will define a specification that delivers on this promise by providing speeds up to 480 Mbps (equivalent to wired USB 2.0) within a 10-meter range.

With WUSB, a user can bring a mobile device, such as a portable media player (PMP), in proximity to a content source, like a PC, laptop, or external hard disk drive, and, once authentication and authorization are complete, video files can be streamed onto the PMP for later viewing.

Wireless multimedia connectivity for CE devices

Closely related to PC peripheral connectivity is wireless multimedia connectivity for audio and video consumer electronics (CE) devices. The benefits are similar to those of PCs and peripherals; wireless ease-of-use and data transfer performance are key advantages. The variety of devices within the entertainment cluster (Figure 4) is wide: digital video disc players (DVDs), HDTVs, STBs, personal video recorders (PVRs), MP3 players and stereos, digital camcorders and digital cameras, and other CE devices found throughout the home. For example, UWB could connect a wall-mounted plasma display or HDTV to an STB or DVD player, without annoying and unaesthetic cables. UWB can also enable multiple streams to multiple devices, simultaneously. This would allow picture-in-picture functionality or the ability to view the same or different content on multiple devices throughout the home.

UWB can also connect devices between the PC and entertainment clusters, such as a digital camcorder to a media PC for digital video editing or to a large LCD for viewing. Connect a digital camera to a mobile notebook PC for editing, compiling, and sending pictures via e-mail to a family member while sitting at a public hotspot. UWB offers key benefits for these kinds of uses (Table 1, on the next page). With UWB-enabled WPANs, once the devices are within proximity, they recognize each other, and streaming occurs when the user presses the Play button.

Figure 3. PC clusters interconnected through USB

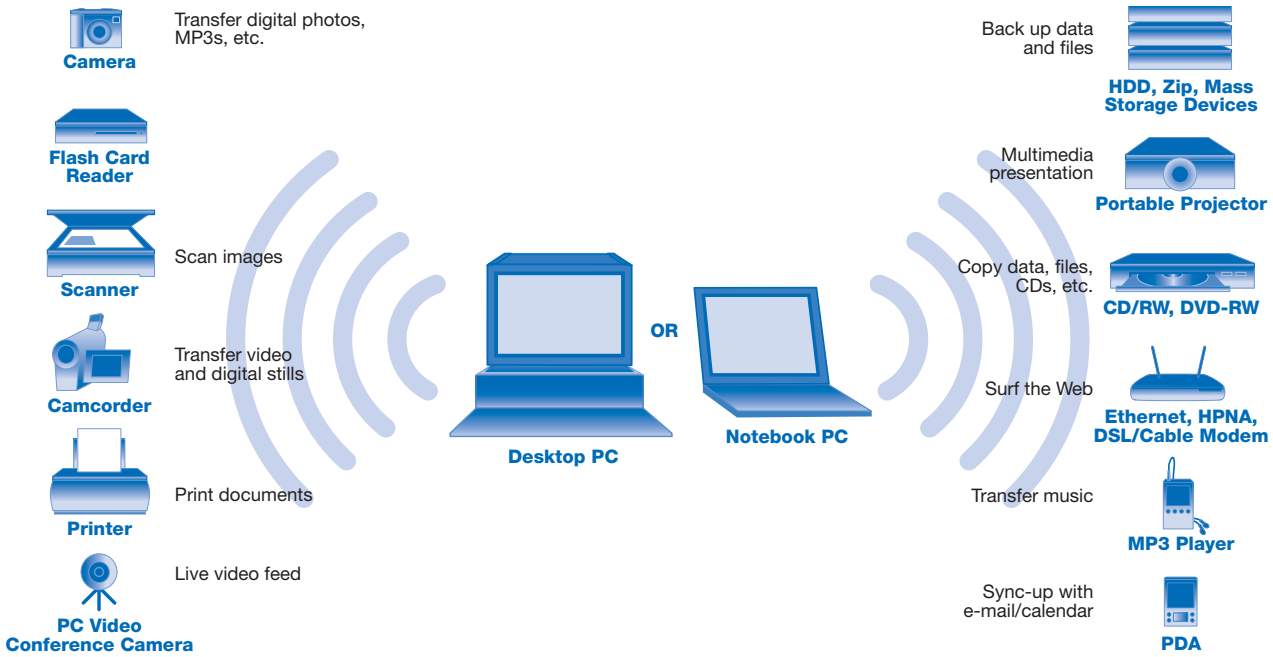

Table 1. Features and benefits of UWB in entertainment and PC environments

Feature	Benefit
High-speed throughput	Fast, high-quality transfers
Low power consumption	Long battery life of portable devices
Silicon-based, standards-based radios	Low cost
Wired connectivity options	Convenience and flexibility

Portable CE devices, such as digital camcorders, digital still cameras, portable MP3 players, and emerging personal video players are expected to create a sweet spot of the early UWB mainstream market.

Cable replacement and network access for mobile computing devices

For users of multiple mobile devices, cable management can be a large inconvenience when devices need to communicate with each other. Many devices, such as personal digital assistants, connect through USB ports, but others, like 3G cellular phones, might require a special connector or adapter for a USB cable. UWB technology allows these devices to interoperate – without cables – as soon as they are in proximity. UWB could also be used to enable high-speed, low-power network access within hotspot locations.

Hotspot Internet coverage is generating a great deal of market interest for broadband Internet access for mobile computing devices at remote locations. Today, two technologies enable hotspots: 802.11a/b/g WLAN and Bluetooth Technology-based WPAN. Both have limitations for addressing the combined needs for high-bandwidth connectivity: high spatial capacity for serving many users in a given space and low power consumption. UWB will help overcome these challenges and could provide a significantly improved user experience once this segment matures.

Ad-hoc connections between UWB-enabled devices

Like with Bluetooth Technology, every UWB-enabled device can be both a content source and recipient. The device gains the value of all the devices that it can connect with in a cluster. Useful applications would include connecting a digital camera directly to a printer for printing pictures.

Figure 4. Entertainment cluster

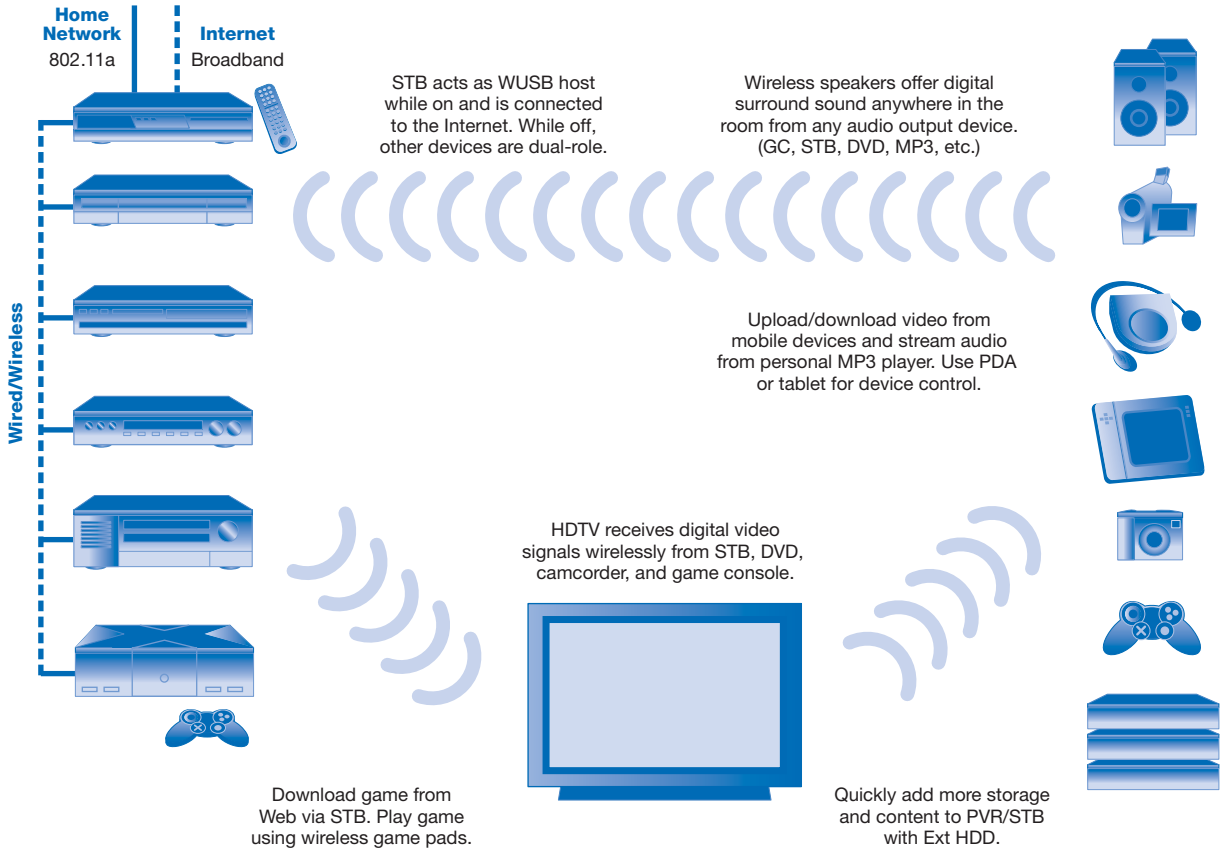

Technology Considerations

For UWB technology to become a widely adopted radio solution, a few key areas need to be resolved:

- Interoperability
- Ease of product integration and certification
- Overall solution cost (to the OEM)
- Global spectrum allocation

Intel is addressing a number of these issues through investment strategies, research, participation in wired and wireless communications initiatives, and product development. Intel is also developing protocols that will take full advantage of the strengths of UWB technology. The WUSB specification developed through the Wireless USB Working Group and the UPnP work done through the Digital Home Working Group (DHWG) are examples of Intel contributions.

The Future: Radio Free Intel

Intel is committed to wireless technologies. The company envisions a future in which all devices are connected by smart radios. The vision is called Radio Free Intel, and it embodies the concept of a smart radio that can reprogram and reconfigure itself based on available spectrum, the desired application, and the device at hand. Configurations would include an 802.11 radio for communicating with a WLAN hotspot, a Bluetooth Technology radio for communication with a cell phone, or a UWB radio for participation in a WPAN. To promote this vision, Intel is involved in all areas of the RF space (Figure 5). In wireless wide area networks (WWAN), Intel is a supporter of WiMAX.* In the WLAN space, Intel continues to push forward with Intel® Centrino™ mobile technology. Now, with support of UWB technology for the WPAN space, the concept of Radio Free Intel is one step closer to reality.

Figure 5. RF data communications coverage range

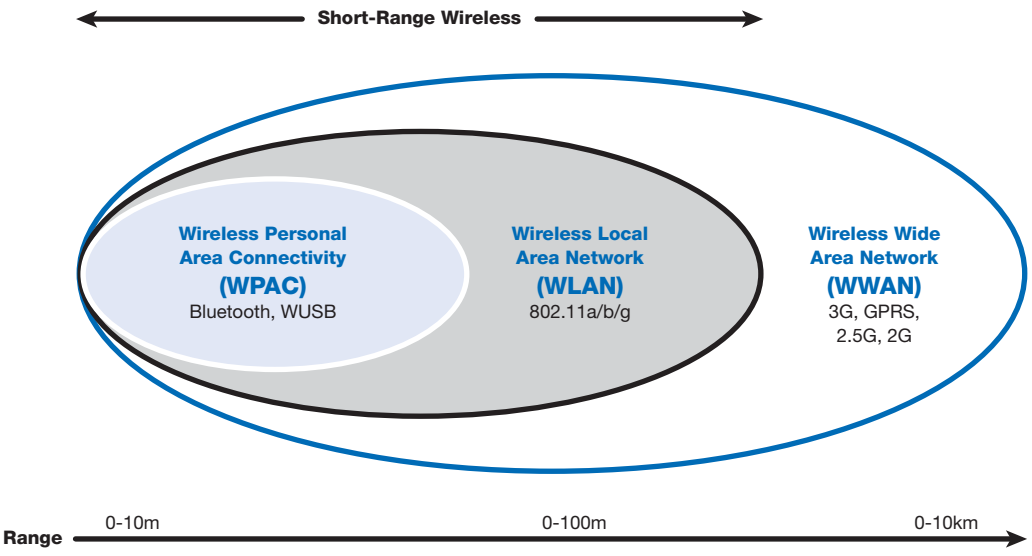

Conclusion

UWB and the associated networking protocol efforts are in the early stages of development, and several key deployment scenarios are being defined and evaluated. UWB complements currently deployed wireless networks in the WLAN environment, plus it extends high bit-rate, multimedia connectivity to WPANs supporting PC, CE and cellular devices. This combination will enable true convergence of computers, consumer electronics and mobile communications.

A common radio platform that connects seamlessly with the existing networking protocols and cost effectively enables connectivity solutions among CE peripherals will shift the home entertainment environment. It will enable multiple usage models from cable replacement to the streaming of video, audio, and other entertainment media.

Many UWB components and systems are already in the testing and demonstration phases, with actual release dates for final consumer products expected in early 2005. Intel Corporation is working with the industry to enable this exciting technology and help ensure its success.

Printed in USA. 0205/MLG/HBD/PDF Please Recycle 300982-002 US